CIO-CIO-SAN NO YŪUTSU: MEMOIRS OF MAGNETOGENESIS AND TURBULENT DYNAMO THEORY

A MINOR DISCOURSE ON MAGNETOGENESIS, (NON-)LINEAR, TURBULENT DYNAMO THEORY AND THE MHD SIMULATION OF KINEMATIC AND SMALL-SCALE, NONHELICAL, TURBULENT DYNAMO ACTION ON MAGNETIC FIELDS

DISSERTATION PRESENTED IN FULFILLMENT OF THE REQUIREMENTS FOR THE DEGREE OF MASTER OF SCIENCE IN APPLIED MATHEMATICS

PATRICK WILLIAM ADAMS
B.SC. (IT), B.SC. (HONS)

OCTOBER 2013

SUPERVISOR:
DR B. OSANO

UNIVERSITY OF CAPE TOWN
FACULTY OF SCIENCE
DEPARTMENT OF MATHEMATICS AND APPLIED MATHEMATICS

The financial assistance of the National Research Foundation (NRF) towards this research is hereby acknowledged. Opinions expressed and conclusions arrived at, are those of the author and are not necessarily to be attributed to the NRF.

Abstract

The origins of cosmic magnetic fields are not as yet well understood. In this dissertation we investigate, via direct numerical simulation, the temporal evolution and behaviour of magnetic fields that are generated from absolute zero initial conditions via a thermal battery term in the Induction Equations (i.e. the Magnetogenesis problem), whilst making use of the Ideal- and Chaplygin Gas equations of state, in turn, to model the relationship between pressure and density. The dependence of the onset of dynamo action on various values of the magnetic Reynolds- and Prandtl numbers for the cases of the Roberts Flow kinematic dynamo and a flow that, in turn, incorporates both a non-helical and helical forcing function that introduces turbulence into the system is also considered via direct numerical simulation. For the purposes of the simulation work conducted, we make use of the PENCIL CODE, which is a high-order finite-difference Magnetohydrodynamical code capable of performing simulation runs in parallel using the Message Passing Interface (MPI) system for parallel processing.

Theoretical results relevant to the simulations conducted are partially recovered and discussed in detail. These include, and are not limited to, the emergence of the thermal battery term in the General Ohm's Law as a consequence of the two-fluid approximation of a plasma, derivation of the Induction Equations incorporating the aforementioned battery term, introduction and discussion of the Chaplygin Gas and its place in the field of Cosmology, energetics governing the flow of kinetic- and magnetic energy during the dynamo process, the Zel'dovich stretch-twist-fold dynamo as an example of both a fast dynamo and a cornerstone underlying the operation of all dynamos and, finally, the Kazantsev Theory for small-scale, turbulent dynamos.

For our magnetogenesis simulations, it is found that the magnetic fields produced undergo two distinct growth phases (the first, classified as an initial "upshoot" that is possibly due to the battery term and the second, classified as an exponential growth phase), as well as two distinct phases of decay in strength, which is attributed to the effects of magnetic diffusion. This behaviour is observed for fields generated using both the Ideal- and Chaplygin Gas equations of state in turn and it is noted that the Chaplygin Gas equation of state produces magnetic fields that are of comparable strength to those produced by the Ideal Gas equation of state. Dynamo action simulations confirm the existence of a critical magnetic Reynolds number, beyond which, an initial prescribed magnetic field will grow exponentially in strength. In the case of the forced turbulence simulations, it is noted that the use of a helical forcing function greatly lowers the value of the critical magnetic Reynolds number required for the onset of guaranteed dynamo action and also produces stronger magnetic fields when compared to

the cases that used a non-helical forcing function. In both cases of the forced turbulence, the magnetic field is observed to saturate when its kinematic (i.e. exponential growth) phase is complete, provided that the magnetic Reynolds number is above the aforementioned critical threshold. Results of the magnetogenesis simulations are also investigated for dynamo action, and it is concluded that a type of "kinematic dynamo" phase was most probably present when these fields underwent the observed phase of exponential growth.

DECLARATION

I know the meaning of plagiarism and declare that all of the work in the dissertation, save for that which is properly acknowledged, is my own.

PATRICK WILLIAM ADAMS

In loving memory of my late aunt,

Miss Magdalene Mathilda Rachael Adams:

After all they've stolen from me, no matter how they choose to justify it, this shall be a work of progress, but not solely for the sake of progress. . .

★

Prologue

If you'd have told me back in 2007 that I'd be completing a dissertation for an M.Sc., I'd most probably have laughed at you. Well, not really. I may just have believed you. The past 18 months have been nothing short of a whirlwind of so many different experiences, transmuted and culminating in the gestation of this work. Perhaps the most important lesson that I have learned from my studies is that no man is an island – we must all work together and help carry each other's weight where necessary to ultimately better ourselves and the world around us.

For this reason, I, too, have many people who deserve to be thanked for their gracious help in carrying me through the past time. From the academic side, I was most fortunate to be under the excellent guidance and mentorship of my supervisor, Dr B. Osano. I consider myself very lucky indeed! Along with this, I also wish to thank my other colleagues in the Department with whom I have interacted with on a weekly basis.

Outside of office hours, the thank-you list is even longer. I wish to thank my parents for their continued presence for the duration of my academic studies. My friends: Janel, Zandile, Mpheng, Gené, Michael, Sean and Jaco have all been immense pillars of support as well. Special mention must be made of Mpheng, who willingly volunteered to act as my muse and task mistress for this work. There are surely many others I have not named here, but to whom I am equally grateful to for any help that they have knowingly, or unknowingly, given me over the past time as well. To Amys Ræ and Lee: may both of you always be able to fit into anything your hearts desire, heaven knows that it's an ability I covet immensely.

And now, let us begin...

It's always about timing. If it's too soon, no one understands. If it's too late, everyone's forgotten.

— Anna Wintour (1949 –)

★

Notation and Symbols

Unless otherwise stated, the meanings for following notation and symbols apply:

$\mathbf{V}$ or V_i	Vector quantity
$\lvert\mathbf{V}\rvert$ or V	Magnitude of vector quantity
$\mathbf{V}^2 = \mathbf{V} \cdot \mathbf{V}$	Squared magnitude of vector quantity
$\tilde{\mathbf{V}}$, V_{ij} or $\mathbb{V}$	Tensor quantity
g_{ij}	Metric tensor
δ_{ij}	Krönecker Delta Symbol
ε_{ijk}	Levi-Civita Symbol
$\frac{\mathrm{d}*}{\mathrm{d}t}$	Total time derivative
$\frac{\mathrm{D}*}{\mathrm{D}t}$	Lagrangian derivative
EoS	Equation of State
FDM	Finite Difference Method
MoL	Method of Lines
SSD	Small-scale Dynamo
$\mathbf{A}$	Magnetic vector potential
$\mathbf{B}$	Magnetic flux density
$\mathbf{E}$	Electric field intensity
$\mathbf{v}$	Velocity field
$\tilde{\boldsymbol{\sigma}}$ or σ^{ij}	Stress tensor

Contents

Chapter 1

The Beginning...

Three Rings for the Elven-kings under the sky,
Seven for the Dwarf-lords in halls of stone,
Nine for Mortal Men, doomed to die,
One for the Dark Lord on his dark throne
In the Land of Mordor where the Shadows lie.
One Ring to rule them all, One Ring to find them,
One Ring to bring them all and in the darkness bind them.
In the Land of Mordor where the Shadows lie.

— J. R. R. Tolkein (1892 – 1973), *The Lord of the Rings*

Magnetic fields are of utmost importance in the universe and in our everyday lives; their applications are wide, ranging from Engineering, Physics and Medicine to Astronomy and Cosmology – the prime focus of this dissertation. We are first acquainted with them within our own solar system and on our own planet. It is the Earth's magnetic field that is responsible for the beautiful AuroræBorealis and Australis and also for protecting us from the sun's harmful radiation. In turn, the Sun's magnetic field also helps shield the solar system from the harmful radiation emanating from neighbouring stars as it races through the interstellar medium.

Much work has been done in the field of Cosmic Magnetism, ranging from vast theories describing the behaviour and temporal evolution of magnetic fields and their associated phenomena, to observation of physical magnetic fields in nearby stars and galaxies. In the following, we take some time to recount the work that has already been done in the fields of Magnetogenesis and Dynamo Theory, also considering the progress of numerical simulations in the aforementioned fields.

1.1 Literature Review

1.1.1 Magnetogenesis

It is often thought that the universe emerged in an originally unmagnetised state [10]. The problem of generating magnetic fields from a state of zero electrical currents [10] is called **magnetogenesis**. The magnetic fields observed today are thought to have originated in the very early universe, though the exact mechanism is not yet well understood. Many theories have attempted to explain this origin, the simplest of these being the so-called thermal, or Biermann, battery [5], which is a cosmic battery. Many other types of battery mechanisms have also been proposed [10, 13, 37, 55, 56, 58], though each of these, including the thermal battery, lead to magnetic fields that are much weaker than those observed today. Some method of amplification is thus needed to grow these fields to the strengths observed today; this is commonly referred to as a dynamo mechanism or, more simply, a dynamo.

1.1.2 Dynamo Theory

The study of dynamos originally started in an attempt to explain the processes by which magnetic fields are amplified. In Cosmology, this concerned attempts to describe the processes by which primordial magnetic fields were amplified to the strengths observed today and in Astrophysics, the main concern was explaining the 11-year solar cycle and its associated phenomena, which appear as a con-

sequence of the solar dynamo [10]. Many phenomenological observational models were proposed, such as those by Babcock (1961), Leighton (1969) and Parker (1955) [1, 33, 41], which ultimately led to one of the first the formal descriptions of a mathematical dynamo model, proposed by Herzenberg (1958) [23], which served to compliment the observational models of the time [10]. Work done by Vainshtein and Zel'dovich (1972) [57] outlined the dynamo algorithm of a simple stretch-twist-fold dynamo, which outlines the general mechanism by which most dynamos are thought to operate. Small-scale dynamos, the prime focus of this dissertation, have been studied intensively by Kazantsev, who first attempted to model the turbulent velocity field present in these dynamos via the statistical properties of turbulence [28], and then later on by others who recovered and extended these results in more sophisticated analyses (e.g. Kraichnan *et al.* (1967) [29], Kulsrud *et al.* (1992) [30], Molchanov *et al.* (1985, 1987) [39, 40] and Subramanian (1997, 1999) [52, 53]). Of particular interest in the turbulent small-scale dynamo is the effect of non-linearities introduced by the stochastic velocity field on the long-term behaviour of the dynamo and its ability to amplify magnetic fields; examples in the forms of ambipolar damping and hyperdiffusion were studied in detail by Kulsrud *et al.* (1992) [30] and Subramanian (2003) [54] respectively.

1.1.3 Simulation Work

Simulations of cosmological magnetogenesis via the thermal battery, such as those done by Gnedin *et al.* (2000) [17] and Kulsrud *et al.* (1997) [31], have mostly considered the generation of magnetic fields during the re-ionization of the intergalactic medium. Simulations, such as those done by Doi *et al.* (2011) [15] and Hanayama *et al.* (2006) [21] have also focussed on generation of primordial magnetic fields via the thermal battery, though these considered the generation of magnetic fields around the first stars during their lifetime and death, respectively. Contopoulos *et al.* (2006) [13] and Kahniashvili *et al.* (2012) [26] have also presented simulations of the growth of primordial magnetic fields, though these do not make use of the thermal battery, opting to generate the fields via the Poynting-Robertson drag and inflation of the universe, respectively.

Simulations of turbulent small-scale dynamo action focus mainly on studying the onset of dynamo action when the magnetic Prandtl number of the system under consideration is equal to, or less than, unity. Such situations may arise physically in media where the magnetic diffusivity and kinematic viscosities are equal, or where the medium itself is highly viscous. These are thought to be most common in stellar convection zones and laboratory experiments. Examples of this are the works done by Haugen *et al.* (2004) [22] and Schekochihin *et al.* (2005) [47]. Study of the onset of dynamo action in cases of a high magnetic Prandtl number are also highly favoured, and has been covered again by Haugen *et al.* (2004) [22] and Schekochihin *et al.* (2002, 2002, 2002) [45, 46, 48]. Examples of such

systems are the interstellar medium and the early universe [45]. In all of these simulations, the effects of turbulence on the operation of the dynamo are most often investigated and quantified by examining the evolution of the kinetic- and magnetic energy spectra associated with the velocity- and magnetic fields under consideration. In more recent work, such as Schleicher *et al.* (2012) [49] and Schober *et al.* (2012) [50] the amplification of primordial magnetic fields (i.e. at high redshifts) via small-scale dynamo action has also been simulated.

★

Magnetogenesis and dynamo theory are both fields which still have much more potential in terms of research, in part due to the many subtle mechanisms employed by nature to amplify magnetic fields to the strengths observed today. Much is still left to be understood. As technology becomes increasingly more advanced, more models may be able to be formulated for simulation purposes, allowing better understanding of these subtle, yet complicated, mechanisms.

1.2 Statement of the Research Problem

This dissertation addresses problems in the fields of Magnetogenesis and Dynamo Theory, primarily via direct numerical simulation. In each of the aforementioned fields, the necessary theory is first developed discussed, after which the numerical simulations commence.

In Magnetogenesis, we address the problem of generating magnetic fields from absolute zero initial conditions via the use of a thermal battery term in the Induction Equations, also making use of two different equations of state (i.e. the Ideal Gas and the Chaplygin Gas) to model the pressure, and then assess the temporal evolution behaviour and resulting strengths of the magnetic fields that are generated.

In Dynamo theory, we study the dependence of the onset of dynamo action on the value of the magnetic Reynolds- and Prandtl numbers for the cases of a kinematic dynamo and a small-scale, turbulent dynamo. Temporal evolution behaviour and strengths of the resulting magnetic fields are once more assessed. Together with this, we also attempt to use the aforementioned results that have been developed and discussed in order to determine whether dynamo action is present in the simulations conducted in the Magnetogenesis portion of this dissertation, in order to make predictions on the long-term temporal behaviour of the magnetic fields that are generated.

To perform our numerical simulations, we make use of an open-source, high-order finite difference Magnetohydrodynamics code called the PENCIL CODE.

1.3 Dissertation Roadmap

The layout of the remainder of this dissertation is organised as follows:

- In Chapter 2, we develop basic results from the theories of Fluid Dynamics, Electrodynamics, Magnetohydrodynamics and Turbulence that will be used for later work.
- In Chapter 3, we introduce the aforementioned Magnetohydrodynamical code that we use to perform all of our numerical simulations. Some initial validatory simulations are done and presented.
- In Chapter 4, we develop the multi-fluid approximation equations of motion for a fluid consisting of two particle species and show how the thermal battery term arises as a consequence thereof. The Chaplygin Gas is also introduced and motivation for its use in our simulations is stated. Results of simulations involving the battery term and the Ideal- and Chaplygin Gas equations of state are presented and discussed.
- In Chapter 5, we develop some of the basic results of Dynamo Theory such as energetics, the important limits of the Induction Equations and the magnetic Reynolds number. These are then used to discuss other results, such as the antidynamo theorems, the Kinematic Dynamo and small-scale, turbulent dynamos. Results of simulations concentrating on the onset of dynamo action for the kinematic and small-scale, turbulent dynamos are then presented, which are then used to discuss the possibility of dynamo action in the Magnetogenesis simulations.
- In Chapter 6, we re-iterate some of the important closing points made in the preceding chapters and end off by making some final recommendations for the work done in this dissertation.

Chapter 2

Some Previous Results, Revisited

ALL THIS IS A DREAM. Still examine it by a few experiments. Nothing is too wonderful to be true, if it be consistent with the laws of nature; and in such things as these experiment is the best test of such consistency.

— Michael Faraday (1791 – 1867)

Before attempting to answer the research question, we first consider some of the key results of the theories of Fluid Dynamics, Electromagnetism, Magnetohydrodynamics and Turbulence. From the nature of the work conducted, it is clear that these theories are related to each other, which warrants an understanding of *why* and *how* this relationship occurs. Only key results that are of greatest importance in this work are considered in the following sections, whilst any other complementary results may be found in any good textbook on the subject in question.

2.1 Fluid Dynamics, Redux

In this section we introduce some results from the theory of Fluid Dynamics that are central to the study of this work. Derivations of the Continuity Equation, the Momentum Equations and the Navier-Stokes Equations are presented. Some complimentary results may also be found in Appendix A, as well as in any good textbook on Fluid Dynamics (e.g. [32]). The reader is reminded that **all derivations done here consider a non-relativistic frame-of-reference**. Note also that results presented in this section have been based partially on references [16] and [32].

2.1.1 The Continuity Equation

Consider some region in space that is occupied by a volume, $\mathcal{V}$, and filled with a non-relativistic, neutral fluid of density, ϱ, which flows with a velocity, $\mathbf{v}$. Taking into account the volume as a whole, the mass of the fluid contained within may be expressed as:

$$m = \int_{\mathcal{V}} \varrho \mathrm{d}\mathcal{V}. \tag{2.1}$$

Consider also the mass flux, Φ_m, through an element of the surface, S, bounding the aforementioned volume; this is given by:

$$\Phi_m = \oint_{\partial\mathcal{V}} \varrho \mathbf{v} \cdot \mathrm{d}\mathbf{S}, \tag{2.2}$$

where $\mathrm{d}S$ is equal to the area of the surface element and its direction is in that of the outward normal to the element.

Equating the flux- and mass-decrease rates gives:

$$-\frac{\partial}{\partial t}\int_{\mathcal{V}} \varrho \mathrm{d}\mathcal{V} = \oint_{\partial\mathcal{V}} \varrho \mathbf{v}\cdot \mathrm{d}\mathbf{S}. \tag{2.3}$$

The Divergence Theorem may be invoked on the right-hand side (RHS), giving:

$$\oint_{\partial\mathcal{V}} \varrho \mathbf{v}\cdot \mathrm{d}\mathbf{S} = \int_{\mathcal{V}} \nabla\cdot(\varrho\mathbf{v})\,\mathrm{d}\mathcal{V}. \tag{2.4}$$

If the volume, $\mathcal{V}$, is regarded as time-independent, the temporal derivative operator may be moved inside the integrand and equated to the result above, giving:

$$\int_{\mathcal{V}} -\frac{\partial \varrho}{\partial t}\mathrm{d}\mathcal{V} = \int_{\mathcal{V}} \nabla\cdot(\varrho\mathbf{v})\,\mathrm{d}\mathcal{V}. \tag{2.5}$$

As the integrals are clearly equal, we may demand that the result should hold for *all* volumes, $\mathcal{V}$. This yields the first result:

$$\frac{\partial \varrho}{\partial t} = -\nabla\cdot(\varrho\mathbf{v}), \tag{2.6}$$

which is the **Continuity Equation**. In order to obtain a slightly more general statement, we expand the divergence term and rearrange to give:

$$\frac{\partial \varrho}{\partial t} + \mathbf{v}\cdot\nabla\varrho + \varrho(\nabla\cdot\mathbf{v}) = 0, \tag{2.7}$$

or alternatively,

$$\boxed{\frac{\mathrm{D}\varrho}{\mathrm{D}t} + \varrho(\nabla\cdot\mathbf{v}) = 0,} \tag{2.8}$$

where we have recognised the definition of the Lagrangian derivative, $\mathrm{D}/\mathrm{D}t$.

2.1.2 The Momentum Equation

We now turn our attention to deriving a momentum-conservation equation for a fluid of density ϱ, flowing with a velocity $\mathbf{v}$.

If we consider a unitary volume within this fluid, we find that it has momentum $\varrho\mathbf{v}$. To see how this quantity changes with time, we apply the temporal derivative as follows:

$$\frac{\partial \varrho \mathbf{v}}{\partial t} = \mathbf{v}\frac{\partial \varrho}{\partial t} + \varrho\frac{\partial \mathbf{v}}{\partial t} \tag{2.9}$$

$$\Leftrightarrow \frac{\partial \varrho v_i}{\partial t} = v_i\frac{\partial \varrho}{\partial t} + \varrho\frac{\partial v_i}{\partial t}. \tag{2.10}$$

The Continuity Equation, expanded and expressed in tensor form, is given by:

$$\frac{\partial \varrho}{\partial t} = -v_i\partial_i\varrho - \varrho\partial_i v_i. \tag{2.11}$$

Along with this, we also make use of Euler's Equations (Section A.1 of Appendix A). Expressed in tensor form, they are given by:

$$\frac{\partial v_i}{\partial t} = -v_k\partial_k v_i - \frac{1}{\varrho}\partial_i p + g_i + f_i, \tag{2.12}$$

where the term g_i represents the gravitational body force acting on the fluid and f_i subsumes all other unaccounted-for body forces acting on the fluid[1]. Substituting the expressions for $\partial\varrho/\partial t$ and $\partial v_i/\partial t$ into Equations (2.10), we are left with:

$$\boxed{\frac{\partial \varrho v_i}{\partial t} = -\partial_k(\varrho v_i v_k) - \partial_k\delta_{ik}p + \varrho g_i + \varrho f_i,} \tag{2.13}$$

which is a version of the **Conservation of Momentum Equations** for the fluid under consideration. Note that other stresses (e.g. viscous stresses) may also be included in the derivation. For our purposes, only the pressure was considered.

2.1.3 The Navier-Stokes Equations

When assumptions are made on the nature of a fluid flow, they are often reflected in the form of the **stress tensor**, σ^{ij}. This tensor is usually written as the sum of two constituent tensors:

$$\sigma^{ij} = -p\delta^{ij} + \tau^{ij}. \tag{2.14}$$

[1]Here, $\partial_k \equiv \partial/\partial x_k$.

Here, the first term (a simple tensor) involves the scalar pressure, p, together with the **Krönecker Delta Symbol**, δ^{ij}, and represents the effects of hydrostatic pressure and the perpetual thermal motion of the particles in the fluid. The second tensor, τ^{ij} is known as the **viscous stress tensor** and is usually not considered in many applications, as fluid flow is mostly assumed to be inviscid. Real fluids, however, are not truly inviscid. It may be shown that the most general form of the viscous stress tensor is given by:

$$\tau^{ij} = \mu\left[\partial^i v^j + \partial^j v^i - \frac{2}{3}\delta^{ij}\left(\nabla\cdot\mathbf{v}\right)\right] + \lambda\delta^{ij}\left(\nabla\cdot\mathbf{v}\right), \tag{2.15}$$

where λ is known as the **coefficient of bulk viscosity** and μ as the **coefficient of dynamic viscosity**. Alternatively, expanding the stress tensor in its Taylor Series and stopping at the first order term (this is explained in Section A.2.1 of Appendix A) yields a more simple form:

$$\tau^{ij} = \mu\left(\partial^i v^j + \partial^j v^i\right) + \lambda g^{ij}\left(\nabla\cdot\mathbf{v}\right), \tag{2.16}$$

where g^{ij} is the metric tensor (which is simply δ^{ij} in the Cartesian co-ordinate system) and all symbols retain their original meaning. Substituting this form of the viscous stress tensor into Expression (2.14) allows the stress tensor to be expressed as:

$$\sigma^{ij} = -p\delta^{ij} + \mu\left(\partial^i v^j + \partial^j v^i\right) + \lambda g^{ij}\left(\nabla\cdot\mathbf{v}\right). \tag{2.17}$$

Identification of the term representing the hydrostatic pressure is an issue of importance in Fluid Dynamics and it is thought that it may be determined from the components of the stress tensor, σ^{ij} [16]. George Stokes assumed in his work that λ, the coefficient of bulk viscosity, could be set to zero if one assumed uniform dilatation of a fluid element [16]. A consequence of this is that the pressure, p, depends only on the density, ϱ, and the temperature, T, implying that the pressure is not dependent on $\nabla\cdot\mathbf{v}$.

Before proceeding further, we note the following assumptions made by Navier and Stokes in their original work [16]:

1. The fluid density, ϱ, is *constant* in space and time (this is usually assumed when considering liquids).

2. The fluid viscosity, μ, is constant.

3. The coefficient of bulk viscosity, λ, is zero.

A consequence of the first assumption is that the velocity field, $\mathbf{v}$, becomes divergenceless. Recalling the form of the stress tensor from Expression (2.17), applying the assumptions made by Navier and Stokes yields a stress tensor of the form:

$$\sigma^{ij} = -p\delta^{ij} + \mu\left(\partial^i v^j + \partial^j v^i\right). \tag{2.18}$$

Note that Stokes' assumption of zero bulk viscosity is a special case and does *not* always hold in general – an example of where this breaks down is **ultrasonic absorption**.

It may be shown that the Equations of Motion for a general fluid (Section A.1.1 of Appendix A) are given (in tensor form) by:

$$\boxed{\frac{\mathrm{D}v^i}{\mathrm{D}t} = \frac{1}{\varrho}\partial_j\sigma^{ij} + g^i + f^i,} \tag{2.19}$$

where all terms hold their original meanings. Substituting the form of the stress tensor given by Expression (2.18) into Equations (2.19) then yields the final result for this section:

$$\boxed{\frac{\mathrm{D}\mathbf{v}}{\mathrm{D}t} = -\frac{\nabla p}{\varrho} + \nu\nabla^2\mathbf{v} + \frac{\mathbf{g}}{\varrho} + \frac{\mathbf{f}}{\varrho}.} \tag{2.20}$$

These are the famous **Navier-Stokes Equations**. Here, we have made the identification of the ratio $\nu := \mu/\varrho$, which is called the **kinematic viscosity** of the fluid and is also a constant. These equations, non-linear in nature, describe the evolution of the velocity field as time progresses. A key difference to note between these and the Euler Equation is the addition of the Laplacian term, $\nabla^2\mathbf{v}$. These equations require very different boundary conditions in order to define a unique solution, as compared to the Euler Equation, and also a very different method of solving them numerically. Later on, we introduce additional modifications to these equations in order to obtain the final set that we shall solve in our work.

2.2 Electrodynamics, Redux

We now leave the field of Fluid Dynamics behind and turn our attention to some results from Electrodynamics, staying in line with the eventual aim of building up a set of MHD equations. In this section,

we only briefly consider the Lorentz Force, Ohm's Law and Maxwell's Equations. The reader is to note that results presented here are once more available in any good textbook on Electrodynamics and have been largely based on the work presented in references [2], [20] and [24].

2.2.1 The Lorentz Force

The existence of the magnetic force was established in experiments conducted by Jean-Marie Ampère on electrical current-carrying wires. During these experiments, he observed that if two wires carried current moving in the same direction, they would attract each other, but would repel otherwise. Today, it is clear from the context that some magnetic force had to be responsible for this phenomenon. If we consider some test-charge q moving with velocity $\mathbf{v}$, in some magnetic field $\mathbf{B}$, then the force on the charge due to the magnetic field would be

$$\mathbf{F}_{\text{mag}} = q(\mathbf{v} \times \mathbf{B}). \tag{2.21}$$

If an electric field is also present, the total force on the test-charge would be the sum of the forces due to the two fields acting on it. This gives the first result:

$$\boxed{\mathbf{F} = q(\mathbf{E} + \mathbf{v} \times \mathbf{B}),} \tag{2.22}$$

which is simply referred to as the **Lorentz Force Law**.

2.2.2 Ohm's Law

For a wide range of materials, it has been shown empirically that the **current density**, $\mathbf{J}$, and the **force per unit charge**, $\mathbf{f}$, obey a linear relationship through the proportionality constant, σ, called the **conductivity** of the material. Most often, some would also take the reciprocal of this constant, ρ, called the **resistivity** of the material. It is clear that for insulating materials, σ is very small (implying a large ρ), and vice-versa for metals. From this it can be concluded that most metals are "perfect" conductors. In symbols, this relationship between $\mathbf{J}$ and $\mathbf{f}$ is stated as:

$$\mathbf{J} = \sigma \mathbf{f}. \tag{2.23}$$

For our purposes, the force driving the charges would be the Lorentz Force, causing the above relationship to become:

$$\boxed{\mathbf{J} = \sigma(\mathbf{E} + \mathbf{v} \times \mathbf{B}).} \tag{2.24}$$

In the special case of a stationary conductor, or where the contribution of the magnetic force can be regarded as negligible, this reduces to the familiar form:

$$\mathbf{J} = \sigma \mathbf{E}, \tag{2.25}$$

seen often in Electrostatics. Equations (2.24) and (2.25) are both referred to as **Ohm's Law**, with the former sometimes being referred to as the **Generalised Ohm's Law**[2]. These forms are often attributed to Gustav Kirchhoff.

As our primary concerns in this work shall often be within plasma environments, where the magnetic forces *do* play a significant role, we shall make use of the form given by equation (2.24).

2.2.3 Maxwell's Equations

Gauss' Law for Electric Fields, Gauss' Law for Magnetic Fields, Faraday's Law of Induction and the Ampère-Maxwell Law together constitute **Maxwell's Equations**, first written down by James Clerk Maxwell. Together with the Lorentz Force Law, these five equations describe all of Classical Electrodynamics. Expressed in differential form, and in natural units of $c = \mu_0 = \epsilon_0 = 1$, they are:

$$\nabla \cdot \mathbf{E} = \varrho_{\mathrm{e}} \tag{2.26}$$

$$\nabla \cdot \mathbf{B} = 0 \tag{2.27}$$

$$\nabla \times \mathbf{E} = -\frac{\partial \mathbf{B}}{\partial t} \tag{2.28}$$

$$\nabla \times \mathbf{B} = \mathbf{J} + \frac{\partial \mathbf{E}}{\partial t}. \tag{2.29}$$

Here, ϱ_{e} is the **electric charge density**, $\mathbf{E}$ the **electric field intensity** and $\mathbf{B}$ the **magnetic flux density**. In simpler terms, $\mathbf{E}$ and $\mathbf{B}$ are more commonly referred to as the **electric-** and **magnetic fields** respectively; this is also the convention that we shall be using throughout this work.

[2] Later, we define an extended version of this law.

These equations can be derived in a unified manner from the Lagrangian Density [2]:

$$\boxed{\mathcal{L} = -\frac{1}{4}F^{\alpha\beta}F_{\alpha\beta} - 4J^{\alpha}A_{\alpha},} \tag{2.30}$$

and then using this to solve the Euler-Lagrange Equations,

$$\boxed{\frac{\partial\mathcal{L}}{\partial A_{\nu}} - \partial_{\nu}\frac{\partial\mathcal{L}}{\partial(\partial_{\mu}A_{\nu})} = 0.} \tag{2.31}$$

Here, $F^{\alpha\beta}$ is the **Electromagnetic Field Tensor**, which has components

$$F^{\alpha\beta} = \begin{pmatrix} 0 & E_x & E_y & E_z \\ -E_x & 0 & -B_z & B_y \\ -E_y & -B_z & 0 & B_x \\ -E_z & B_y & -B_x & 0 \end{pmatrix}, \tag{2.32}$$

where subscripts indicate the field components, J^{α} the **current density 4-vector**, which has components

$$J^{\alpha} = (\varrho_{\mathrm{e}}, \mathbf{J}), \tag{2.33}$$

and A_{α}, the so-called **4-vector potential**, which has components

$$A_{\alpha} = (\phi, -\mathbf{A}), \tag{2.34}$$

with $\mathbf{A}$ and ϕ themselves being the familiar **vector potential** and **scalar potential** seen in Electrodynamics, and defined via the relations

$$\mathbf{E} = -\nabla\phi - \frac{\partial\mathbf{A}}{\partial t} \tag{2.35}$$

$$\mathbf{B} = \nabla\times\mathbf{A}. \tag{2.36}$$

Substituting Expression (2.30) into Equations (2.31), and solving, will yield the Maxwell Equations in their unified form:

$$\boxed{\partial_\nu F^{\mu\nu} = J^\mu, \quad \varepsilon_{\mu\nu\varpi\varsigma}\partial^\varpi F^{\mu\nu} = 0,} \tag{2.37}$$

where $\varepsilon_{\mu\nu\varpi\varsigma}$ is the Levi-Civita symbol.

2.3 Rudimentary Magnetohydrodynamics

With discussions of the salient points of Fluid Dynamics and Electrodynamics complete, we now discuss the basic results of Magnetohydrodynamics (MHD). Here, we first look at why we may justify using the MHD approximation and then give a brief discussion on the Induction and Navier-Stokes Equations and their purpose in this work. Two quantities important to the study of Dynamo Theory and MHD, magnetic- and kinetic helicity, are also introduced and discussed in brief. Finally, we make some brief comments on the theory of turbulence and its significance in MHD.

2.3.1 Justifying the MHD Approximation

As its predecessor, Fluid Dynamics, MHD is a macroscopic theory. As these theories can often be seen as approximations to microscopic theories, it is reasonable to expect that there exist limits, beyond which, the approximation no longer holds.

MHD assumes that a plasma may be treated as a type of charged fluid; hence, its governing equations *may* simply be derived by marrying the equations of Fluid Dynamics to Maxwell's Equations of Electrodynamics. This isn't always the case, though, as the governing equations of MHD are most usually derived as a set of equations describing the microscopic dynamics of a multi-fluid plasma (i.e. a **multi-fluid approximation**), which are obtained by expanding a number of moments of the Boltzmann Equation from Kinetic Theory [18]:

$$\frac{\partial f_\alpha}{\partial t} + \mathbf{v}\cdot\frac{\partial f_\alpha}{\partial \mathbf{r}} + \frac{q_\alpha}{m_\alpha}(\mathbf{E}+\mathbf{v}\times\mathbf{B})\cdot\frac{\partial f_\alpha}{\partial \mathbf{v}} = C_\alpha, \tag{2.38}$$

where $f_\alpha = f_\alpha(\mathbf{r},\mathbf{v},t)$ is the so-called **distribution function**, $\mathbf{r}$ represents the spatial distance from the origin in the co-ordinate system under consideration, m_α represents the mass of a particular species of particle, α is a subscript that denotes the species of particle (ions or electrons in this case) in a unified manner and C_α represents the temporal rate-of-change of the distribution function due to particle collisions [18]; all other symbols retain their original meaning. The moment expansion is

done by multiplying Equations (2.38) by powers of $\mathbf{v}$ and then integrating the result over the entire velocity space.

In order to safely transition from the microscopic scales to the macroscopic scales, we must then be certain that any time- and length-scales under consideration greatly exceed those that are inherent to the dynamics of the constituent particle species comprising the plasma under consideration. In other words, any *individual* interactions between the particle species within the plasma must not be "visible" when the plasma is considered as a whole. This leads to the following restrictions on the MHD approximation of a plasma [18]:

- The MHD length scale, λ_{MHD}, must be much longer than the ion cyclotron radius, R_i. In symbols: $\lambda_{\mathrm{MHD}} \sim a \gg R_i$.
- The MHD time scale, τ_{MHD}, must be much longer than the reciprocal of the ion cyclotron frequency, Ω_i. In symbols: In symbols: $\tau_{\mathrm{MHD}} \sim a/v_A \gg \Omega_i^{-1}$.

Here, a is a typical length and v_A is a fundamental plasma quantity known as the **Alfvén velocity** which is defined via [18]:

$$v_A = \frac{B_0}{\sqrt{\mu_0 \varrho_0}}, \tag{2.39}$$

where B_0 and ϱ_0 are representative plasma magnetic field strengths and density respectively [18]; all other symbols once more retain their usual meanings.

As long as these restrictions are observed, the plasma may be treated as a single, charge-neutral, fluid. Along with this, three additional assumptions are implied [18]: the relative velocities of the particle species comprising the plasma are much smaller than the mean velocity of the plasma, the electron skin-depth must be very small (implied by the previous assumption) and, finally, the effects of relativity may be regarded as negligible (i.e. the mean velocity of the plasma is assumed to be much smaller than the speed of light). If all of these restrictions are met reasonably, then the MHD approximation may be regarded as valid.

★

Now that we have justified the use of the MHD approximation to model a plasma as a fluid, we turn to the fundamental set of equations that govern all of fluid flow: the Navier-Stokes Equations. As these have already been derived in Section 2.1.3, we briefly discuss their place in MHD.

2.3.2 The Navier-Stokes Equations, Charged

From the theory of Fluid Dynamics, we know that the Navier-Stokes Equations describe fluid flow. Recall that in Equations (2.20), a single term, $\mathbf{f}$, subsumed all other unaccounted-for body forces acting on the fluid was included.

The MHD approximation tells us that whilst the effects of the electric field intensity, $\mathbf{E}$, vanish everywhere (except, possibly, due to the effects of resistivity [18]), the remaining magnetic flux density, $\mathbf{B}$, and the resulting current density, $\mathbf{J}$, that arises due to $\mathbf{B}$'s spatial rate-of-change, begin to play an important role within the plasma. In fact, these two fields work together to produce an additional body force that acts on the plasma itself: the **Lorentz Force**[3], given by $\mathbf{J} \times \mathbf{B}$. In the Navier-Stokes equations, this new body force must now be brought forward and accounted for! The Navier-Stokes Equations then read as:

$$\boxed{\frac{\mathrm{D}\mathbf{v}}{\mathrm{D}t} = -\frac{\nabla p}{\varrho} + \nu\nabla^2\mathbf{v} + \frac{\mathbf{g}}{\varrho} + \frac{\mathbf{J}\times\mathbf{B}}{\varrho\mu_0} + \frac{\mathbf{f}}{\varrho}.} \tag{2.40}$$

Note that the form we supply here is still relatively simple due to the original assumptions that were made on the stress tensor, σ^{ij}. Thus, if a more general form of this tensor was used, the equations themselves would change accordingly. A simple example of this, disregarding any effects due to strain, would be the addition of a viscous force, $\mathbf{F}_{\mathrm{visc}} = \nu\left(\nabla^2\mathbf{v} + 1/3\nabla\nabla\cdot\mathbf{v}\right)$ [18], which would arise as a simple modification of the viscous part of the stress tensor. The Navier-Stokes Equations would then read as:

$$\boxed{\frac{\mathrm{D}\mathbf{v}}{\mathrm{D}t} = -\frac{\nabla p}{\varrho} - \nabla\Phi_{\mathrm{grav}} + \frac{\mathbf{J}\times\mathbf{B}}{\varrho\mu_0} + \nu\left(\nabla^2\mathbf{v} + \frac{1}{3}\nabla\nabla\cdot\mathbf{v}\right) + \frac{\mathbf{f}}{\varrho},} \tag{2.41}$$

where the body force due to gravity (previously identified by the term, $\mathbf{g}$, in Equations (2.40)) has also been re-expressed as the gradient of some scalar potential, Φ_{grav}. We recognise that in these forms, Equations (2.40) and (2.41) are more commonly referred to as the **Momentum Equations** for MHD; despite this, however, we shall continue to refer to them as the Navier-Stokes Equations.

★

With the inclusion of the Lorentz body force in the Navier-Stokes Equations, a set of equations

[3]The form for the Lorentz Force acting on a continuous charge distribution (which is what MHD considers) is given by $\mathbf{F} = \varrho_{\mathrm{e}}\mathbf{E} + \mathbf{J}\times\mathbf{B}$ and should not be confused with the form that describes the force acting on a single test charge, as given in Expression (2.22)

governing the temporal evolution of the magnetic flux density is now also required. We consider its derivation next.

2.3.3 The Induction Equations

When marrying Faraday's Law to Ohm's Law, a set of equations governing the temporal evolution of the magnetic flux density is obtained. These are the **Induction Equations**. Recall Ohm's Law, given by Expression (2.24) and now rearranged for the electric field intensity, may be stated as:

$$\mathbf{E} = \frac{\mathbf{J}}{\sigma} - \mathbf{v} \times \mathbf{B}.$$

Recalling the statement of Faraday's Law,

$$\nabla \times \mathbf{E} = -\frac{\partial \mathbf{B}}{\partial t},$$

we substitute for $\mathbf{E}$, yielding:

$$\frac{\partial \mathbf{B}}{\partial t} = \nabla \times \left(\mathbf{v} \times \mathbf{B} - \frac{\mathbf{J}}{\sigma} \right). \tag{2.42}$$

As mentioned before, the constant, σ, may be identified as the electrical conductivity, which may be related to the **magnetic diffusivity** via $1/\sigma = \eta\mu_0$, where η is the magnetic diffusivity. Invoking this relationship then yields the final form of the Induction Equations:

$$\boxed{\frac{\partial \mathbf{B}}{\partial t} = \nabla \times (\mathbf{v} \times \mathbf{B} - \mu_0 \eta \mathbf{J})\,.} \tag{2.43}$$

★

We are now finally in a position to state a set of MHD equations that can be solved. These are given as follows:

$$\begin{aligned}
\frac{\mathrm{D}\varrho}{\mathrm{D}t} &= -\varrho(\nabla \cdot \mathbf{v}) \\
\frac{\mathrm{D}\mathbf{v}}{\mathrm{D}t} &= -\frac{\nabla p}{\varrho} - \nabla \Phi_{\mathrm{grav}} + \frac{\mathbf{J} \times \mathbf{B}}{\varrho \mu_0} + \nu \left(\nabla^2 \mathbf{v} + \frac{1}{3} \nabla \nabla \cdot \mathbf{v} \right) + \frac{\mathbf{f}}{\varrho} \\
\frac{\partial \mathbf{B}}{\partial t} &= \nabla \times (\mathbf{v} \times \mathbf{B} - \mu_0 \eta \mathbf{J}),
\end{aligned}$$

which are the Continuity, Navier-Stokes and Induction Equations respectively. There are three equations missing from this set, however: the first describes the evolution of the **internal energy**, e, and is given without derivation as [18]:

$$\boxed{\frac{\mathrm{D}e}{\mathrm{D}t} = \frac{\eta}{\varrho}\mathbf{J}^2 - (\gamma-1)e\nabla\cdot\mathbf{v}.} \tag{2.44}$$

The internal energy is defined as $e \equiv (\gamma-1)^{-1}(p/\varrho)$ with its governing equation arising as one of the moments of the Boltzmann Equation, and is modified by the Ohmic dissipation, $\eta\mathbf{J}^2$, when cast in its non-conservation form [18]. The constant, γ, is identified as the **ratio of specific heats**, and may be set to its usual theoretical values, depending on the type of thermodynamical process prevalent in the problem under consideration.

As the Internal Energy- and Navier-Stokes Equations both involve the scalar pressure, p, there is also the need for an **equation of state**, which relates the scalar pressure and the fluid density to each other. This is usually assumed to be the Ideal Gas equation of state, given by:

$$pV = Nk_BT, \tag{2.45}$$

where V is the volume, N the particle number density, k_B the Boltzmann constant and T the temperature.

Finally, the Gauss Law for Magnetism must also make its appearance, in order to ensure that the magnetic field remains divergenceless. Thus, the full set of MHD equations may be written as:

$$\begin{aligned}
\frac{\mathrm{D}\varrho}{\mathrm{D}t} &= -\varrho(\nabla\cdot\mathbf{v}) \\
\frac{\mathrm{D}\mathbf{v}}{\mathrm{D}t} &= -\frac{\nabla p}{\varrho} - \nabla\Phi_{\mathrm{grav}} + \frac{\mathbf{J}\times\mathbf{B}}{\varrho\mu_0} + \nu\left(\nabla^2\mathbf{v} + \frac{1}{3}\nabla\nabla\cdot\mathbf{v}\right) + \frac{\mathbf{f}}{\varrho} \\
\frac{\partial\mathbf{B}}{\partial t} &= \nabla\times(\mathbf{v}\times\mathbf{B} - \mu_0\eta\mathbf{J}) \\
\frac{\mathrm{D}e}{\mathrm{D}t} &= \frac{\eta}{\varrho}\mathbf{J}^2 - (\gamma-1)e\cdot\mathbf{v} \\
pV &= Nk_BT \\
\nabla\cdot\mathbf{B} &= 0.
\end{aligned}$$

★

A set of MHD equations defined on the scales mentioned in Section 2.3.1 is now finally on the table.

We now turn to consider the two important quantities in MHD: the magnetic- and kinetic helicities, and state their relevance in the understanding of the dynamo process.

2.3.4 Double Helicity: Magnetic and Kinetic

2.3.4.1 Magnetic Helicity

Consider some closed volume, $\mathcal{V}$, that is bounded by a surface, S. The quantity known as **magnetic helicity** may then be defined through an integral over the entire volume as [10]:

$$\boxed{\mathcal{H}_M = \int_{\mathcal{V}} \mathbf{A}\cdot\mathbf{B}\mathrm{d}\mathcal{V},} \tag{2.46}$$

where $\mathbf{A}$ is the familiar **magnetic vector potential** (i.e. $\mathbf{B} = \nabla\times\mathbf{A}$). In order to find out how this quantity evolves with time, we apply the temporal derivative to the dot product $\mathbf{A}\cdot\mathbf{B}$ [10] and expand the result:

$$\begin{aligned}
\frac{\partial(\mathbf{A}\cdot\mathbf{B})}{\partial t} &= \frac{\partial\mathbf{A}}{\partial t}\cdot\mathbf{B} + \mathbf{A}\cdot\frac{\partial\mathbf{B}}{\partial t} \qquad (2.47)\\
&= (-\mathbf{E}+\nabla\Phi)\cdot\mathbf{B} + \mathbf{A}\cdot(-\nabla\times\mathbf{E})\\
&= (-\mathbf{E}+\nabla\Phi)\cdot\mathbf{B} - [\mathbf{E}\cdot(\nabla\times\mathbf{A}) - \nabla\cdot(\mathbf{A}\times\mathbf{E})]\\
&= -2\mathbf{E}\cdot\mathbf{B} + \nabla\cdot(\Phi\mathbf{B} + \mathbf{A}\times\mathbf{E})\\
\Rightarrow \int_{\mathcal{V}}\frac{\partial(\mathbf{A}\cdot\mathbf{B})}{\partial t}\mathrm{d}\mathcal{V} &= -2\int_{\mathcal{V}}\mathbf{E}\cdot\mathbf{B}\mathrm{d}\mathcal{V} + \int_{\mathcal{V}}\nabla\cdot(\Phi\mathbf{B}+\mathbf{A}\times\mathbf{E})\mathrm{d}\mathcal{V} \qquad (2.48)\\
\int_{\mathcal{V}}\frac{\partial(\mathbf{A}\cdot\mathbf{B})}{\partial t}\mathrm{d}\mathcal{V} &= -2\int_{\mathcal{V}}\mathbf{E}\cdot\mathbf{B}\mathrm{d}\mathcal{V} + \int_{\partial\mathcal{V}}(\Phi\mathbf{B}+\mathbf{A}\times\mathbf{E})\cdot\mathrm{d}\mathbf{S}\\
\int_{\mathcal{V}}\frac{\partial(\mathbf{A}\cdot\mathbf{B})}{\partial t}\mathrm{d}\mathcal{V} &= -2\int_{\mathcal{V}}\mu_0\eta\mathbf{J}\cdot\mathbf{B} - \mathbf{B}\cdot(\mathbf{v}\times\mathbf{B})\mathrm{d}\mathcal{V} + \int_{\partial\mathcal{V}}(\Phi\mathbf{B}+\mathbf{A}\times\mathbf{E})\cdot\mathrm{d}\mathbf{S}
\end{aligned}$$

where we have used Faraday's Law and its uncurled version to substitute for the temporal derivative terms, and Ohm's Law to substitute for $\mathbf{E}$ in the first volume integral; the second volume integral was transformed into a surface integral by invocation of the Divergence Theorem. If we assumed that the surface integral were to vanish for the case of a closed volume [10], then the magnetic helicity obeys the evolution equation given by:

$$\boxed{\frac{\mathrm{d}\mathcal{H}_M}{\mathrm{d}t} = -2\mu_0\eta \int_{\mathcal{V}} \mathbf{J}\cdot\mathbf{B}\mathrm{d}\mathcal{V}.} \tag{2.49}$$

From here, it is clear that the magnetic helicity's temporal evolution is dependent on the magnetic diffusivity. Together with this, it is also immediately seen that in the ideal case ($\eta = 0$), the quantity is conserved exactly. It can also be shown that in the limit as $\eta \to 0$, this quantity is conserved quite well, despite being dissipated at a finite rate [10] – a property that makes the magnetic helicity crucial in helping to understand the saturation of large-scale dynamos, as well as the non-linear evolution of dynamos in general [10].

2.3.4.2 Kinetic Helicity

Consider now the velocity field, $\mathbf{v}$. From here, we define the **vorticity** of the velocity field via $\boldsymbol{\omega} = \nabla \times \mathbf{v}$. As we did with the magnetic helicity, we may now also define the quantity:

$$\boxed{\mathcal{H}_K = \int_{\mathcal{V}} \mathbf{v}\cdot\boldsymbol{\omega}\mathrm{d}\mathcal{V},} \tag{2.50}$$

which is known as the **kinetic helicity**, where the integral is once more taken over some closed volume, $\mathcal{V}$. As before, we apply the temporal derivative to this quantity and find its governing equation. This is given by [10]:

$$\boxed{\frac{\mathrm{d}\mathcal{H}_K}{\mathrm{d}t} = 2\int_{\mathcal{V}} \boldsymbol{\omega}\cdot\mathbf{f}\mathrm{d}\mathcal{V} - 2\nu\int_{\mathcal{V}} \boldsymbol{\omega}\cdot\boldsymbol{\varpi}\mathrm{d}\mathcal{V},} \tag{2.51}$$

where we have defined the quantity $\boldsymbol{\varpi} = \nabla\times\boldsymbol{\omega}$, and all other symbols retain their original meanings. In the absence of any external forces, denoted by $\mathbf{f}$, *and* inviscid flow ($\nu = 0$), it is immediately obvious that the kinetic helicity is conserved exactly. Unlike its magnetic counterpart, however, this helicity is *not* conserved in the limit as $\nu \to 0$ – it blows up instead [10]. Despite this consequence, however, kinetic helicity is known to be important in the growth of large-scale magnetic fields in the presence of forced MHD turbulence [36], where it helps to drive the field generation, thus promoting dynamo action [10, 53].

★

Now that our considerations of the key results of MHD required for this work are complete, we

finally turn to some comments on the Theory of Turbulence. Here, we only introduce some of the key concepts that are used for the later work in this dissertation.

2.3.5 Comments on the Theory of Turbulence

The Theory of Turbulence is central to MHD, especially when studying small-scale dynamos, and is extensively covered in a number of good textbooks, for example, [42].

A velocity field (or **flow**), $\mathbf{v}$, is classified as turbulent when its **fluid Reynolds number**[4], Re, is very large [42]. The fluid Reynolds number is defined via:

$$\mathrm{Re} = \frac{vL}{\nu}, \tag{2.52}$$

where v and L are the characteristic velocity and length scale associated with the flow; ν is the usual kinematic viscosity. Central to the concept of a turbulent flow is the **eddy**. Though there is no strict definition of what an eddy is, it is generally accepted that many of these "turbulent motions" [42] are what make up a turbulent flow. To this end, it is possible to think of an eddy as a type of rotating vortex-like structure within a given flow. It should also not be surprising that a single large eddy can most likely contain many smaller eddies. Regardless of their size, all eddies have three important attributes:

- The region of length, l, which an eddy occupies is often called its **length scale** or size [42]. Some larger eddies may have length scales that are comparable to the length scale, L, of the flow itself [42].
- The velocity measured within the eddy's length scale is known as the eddy's **characteristic velocity**, $u(l)$ [42]. Again, some of the larger eddies have characteristic velocities that are comparable to the velocity, v, of the flow [42].
- The time that an eddy with length, l, and velocity, u, takes to complete one "rotation" is known as its **characteristic timescale**, $\tau(l)$. It is also usually called a **turnover time**. This timescale is typically defined through the eddy's characteristic velocity and length scale as $\tau(l) \equiv l/u(l)$.

It is widely accepted that large eddies do not persist for many turnover times and usually dissipate quite quickly as a result thereof [42]. When these larger eddies dissipate, they transfer all of their

[4]Later on, we shall also define a magnetic Reynolds number, whose significance will be explained in the context of dynamo action.

energy to the smaller eddies, which again undergo a similar dissipation after a number of turnover times – a process known as an **energy cascade**[5] [42]. This energy cascade runs from the largest eddies (on scales where the viscosity of the flow is small compared to the inertial forces within the flow) right down to the smallest eddies, where the flow could effectively be regarded as **laminar** [42]. On these scales, the eddy motion becomes stable because the viscosity and inertial forces now become comparable to each other and energy is dissipated via viscous processes [42].

The concept of energy-bearing eddies is central to the study of MHD turbulence, and its relevance shall be discussed further in Chapter 5 when the dynamo process is considered in detail.

2.4 Closing Points

The purpose of this chapter was to introduce, in brief, some of the key concepts of Fluid Dynamics and Electromagnetism, with the goal of building up to the equations governing MHD. Some points of Turbulence Theory were also discussed in brief.

Within Fluid Dynamics, the derivations of the Continuity Equation, Momentum Equations and Navier-Stokes Equations were done, and all important assumptions made during the derivation process were taken into account and discussed.

In Electromagnetism, the simple forms for the Lorentz Force Law and Ohm's Law were developed and the origin of the Maxwell Equations as solutions to the Euler-Lagrange Equations for a given Lagrangian Density was mentioned. The key equations of MHD that were of importance in this work were then put into place by combining the equations derived in the previous sections, discussing their combined relevance within a plasma environment. The Navier-Stokes Equations received a new Lorentz Force term, whilst Ohm's Law was married to Faraday's Law in order to obtain the Induction Equations. Some comments were also made on the origins of the evolution equation for the internal energy as well as the inclusion of an equation of state to help close the set of MHD equations. As an aside, and for later use, we also introduced the concepts of magnetic- and kinetic helicity and mentioned their importance in the study of dynamos.

Finally, from Turbulence Theory, we introduced the concept of an eddy and some of its attributes were discussed; it was noted that this concept is central to the understanding of MHD turbulence.

[5] This is the reverse process of the **inverse cascade**, where energy is transferred from smaller eddies to larger eddies instead.

Chapter 3

The PENCIL CODE: A Brief Discourse

On two occasions I have been asked, – "Pray, Mr. Babbage, if you put into the machine wrong figures, will the right answers come out?" In one case a member of the Upper, and in the other a member of the Lower, House put this question. I am not able rightly to apprehend the kind of confusion of ideas that could provoke such a question.

— Charles Babbage (1791 – 1871)

Now that the equations of MHD have been introduced, we are in a position to proceed further in answering our research question. It should be noted that the equations needing to be solved are themselves extremely complex and possess virtually no analytical solutions. This is especially true for the Navier-Stokes Equations. For this reason, it is essential to make use of a computer code to numerically solve the full set of MHD equations under various conditions. As shall be seen later on, the dynamo process is largely convective, and often involves turbulence, motivating the need to make use of an MHD code which is specially adapted for various types of turbulence and convection simulations. This code should also be capable of making use of a multi-core CPU (i.e. doing parallel computations), as the numerical solution of the MHD equations is almost always computationally intensive, with potentially long run-times.

A high-order Finite Difference code making use of the Message Passing Interface (MPI) communications protocol for parallelization and speed-up was sought after and used: the PENCIL CODE[1]. The PENCIL CODE solves the basic equations of compressible MHD, with provisions for modifications to be made, should the user choose to do so, to one or more of these equations. Due to its modular structure, a feature of the Fortran programming language, extra equations can also be incorporated into the standard set for solving different problems.

In this chapter, we briefly present and discuss the equations solved by the code, as well as some issues surrounding the use of physical units in simulation results. A short discussion of the numerical methods employed by the code, and their importance in obtaining numerical solutions that have good fidelity is also made. Modifications made to the code for the purposes of other simulations are also presented here. Finally, we present the results of two sets of simulations focussing on the correlation between exact and effective wavenumbers and decaying magnetic fields, respectively, which were conducted for validatory purposes.

3.1 The PENCIL CODE Equations

Adapted from the accompanying manual [8], a short description of the standard equations solved by the PENCIL CODE follows.

3.1.1 The Continuity Equation

$$\frac{\mathrm{D}\ln\varrho}{\mathrm{D}t} = -\nabla\cdot\mathbf{v}. \tag{3.1}$$

[1]The code may be obtained at the following URL: `http://www.nordita.org/software/pencil-code/`.

Equation (3.1) is the familiar **Continuity Equation**. It is numerically advantageous to solve for a logarithmic quantity in this type of application, due to the fact that there may be extremely large variations in the ranges of both temperature and density [8].

3.1.2 The Navier-Stokes (or Momentum) Equations

$$\frac{\mathrm{D}\mathbf{v}}{\mathrm{D}t} = -c_s^2\gamma\nabla\left(\frac{s}{c_p} + \ln\varrho\right) - \nabla\Phi_{\mathrm{grav}} + \frac{\mathbf{J}\times\mathbf{B}}{\varrho} + \nu\left(\nabla^2\mathbf{v} + \frac{1}{3}\nabla\nabla\cdot\mathbf{v} + 2\mathbb{S}\cdot\nabla\ln\varrho\right) + \zeta(\nabla\nabla\cdot\mathbf{v}) + \mathbf{f}. \tag{3.2}$$

Equations (3.2) are the **Navier-Stokes Equations** which describe the temporal evolution of the fluid velocity field, $\mathbf{v}$. As can be seen, our previous derivation in Section 2.1.3 of Chapter 2 accounted for extra forces which may act on the fluid under consideration. In this case, all other forces unaccounted for (such as any extra body- and surface forces) are contained in the final term, $\mathbf{F}$.

Here, $\mathbb{S}$ is the traceless rate-of-strain tensor, given as

$$\mathbb{S}_{ij} = \frac{1}{2}\left(\frac{\partial v_i}{\partial x_j} + \frac{\partial v_j}{\partial x_i} - \frac{2}{3}\delta_{ij}\nabla\cdot\mathbf{v}\right) \tag{3.3}$$

in Cartesian co-ordinates and c_s^2 is the squared sound-speed, given by

$$c_s^2 = \gamma\frac{p}{\varrho} = c_{s_0}^2\exp\left[\frac{s\gamma}{c_p} + (\gamma-1)\ln\frac{\varrho}{\varrho_0}\right]. \tag{3.4}$$

The constant $\gamma = c_p/c_v$ is the ratio of specific heats as from Thermodynamics, with c_p being the specific heat at constant pressure; s is the quantity denoting entropy. Additionally, ν describes the kinematic viscosity, ζ the so-called shock viscosity, Φ_{grav} an arbitrary gravitational potential and c_{s_0} some reference value of the speed of sound at some reference height[2] [8]. Note that the first term in the Navier-Stokes Equations, the pressure term, has been rewritten whilst assuming an Ideal Gas equation of state [8]. A brief explanation of this simplification follows.

The pressure term was written in Equations (2.20) as $\nabla p/\varrho$, disregarding the leading negative sign. If we assume an Ideal Gas equation of state (EoS) of the form

[2] As the code is mainly used for solving convection-related problems, the use of these reference values at some reference height is important.

$$p = c_s^2 \varrho, \tag{3.5}$$

then we may do the following:

$$\begin{aligned} p &= c_s^2 \varrho \\ \Rightarrow \nabla p &= \varrho \nabla c_s^2 + c_s^2 \nabla \varrho \\ \Leftrightarrow \frac{\nabla p}{\varrho} &= \nabla c_s^2 + c_s^2 \nabla \ln \varrho, \end{aligned}$$

where it has also been assumed that the speed of sound need not necessarily be constant in space for a given medium. Recalling Expression (3.4) for c_s^2, we may then substitute in and simplify:

$$\begin{aligned} \frac{\nabla p}{\varrho} &= \nabla \left\{ c_{s_0}^2 \exp\left[\frac{s\gamma}{c_p} + (\gamma - 1) \ln \frac{\varrho}{\varrho_0} \right] \right\} + c_s^2 \nabla \ln \varrho \\ \Leftrightarrow \frac{\nabla p}{\varrho} &= c_{s_0}^2 \exp\left[\frac{s\gamma}{c_p} + (\gamma - 1) \ln \frac{\varrho}{\varrho_0} \right] \left[\nabla s \frac{\gamma}{c_p} + (\gamma - 1) \nabla \ln \frac{\varrho}{\varrho_0} \right] + c_s^2 \nabla \ln \varrho \\ \Leftrightarrow \frac{\nabla p}{\varrho} &= c_s^2 \left[\nabla s \frac{\gamma}{c_p} + \gamma \nabla \ln \varrho - \nabla \ln \varrho \right] + c_s^2 \nabla \ln \varrho \\ \Leftrightarrow \frac{\nabla p}{\varrho} &= c_s^2 \gamma \nabla \left[\frac{s}{c_p} + \ln \varrho \right], \end{aligned}$$

leaving us with the required result. It is also through this term that the pressure enters into the standard evolution equations. We shall refer to this term again in Section 3.3.3 when we make modifications to the code to incorporate an exotic EoS, and again also when formally considering the incorporation of an exotic EoS into the MHD equations in Section 4.2 of Chapter 4 of this dissertation.

3.1.3 The Induction Equations

$$\frac{\partial \mathbf{A}}{\partial t} = \mathbf{v} \times \mathbf{B} - \eta \mu_0 \mathbf{J}. \tag{3.6}$$

Equations (3.6) are the **Induction Equations** solved by the code and describe the temporal evolution of the **magnetic vector potential** field, $\mathbf{A}$, and, subsequently, the magnetic flux density field, $\mathbf{B}$. For our work, solutions to these equations are of primary interest.

Due to the Gauss' Law for Magnetism in Maxwell's Equations providing us the constraint that $\mathbf{B}$ is to remain divergenceless, i.e.

$$\nabla \cdot \mathbf{B} = 0,$$

we may take advantage of this constraint and write $\mathbf{B} = \nabla \times \mathbf{A}$. Thus, $\mathbf{B}$ can always be easily recovered from $\mathbf{A}$ after a simulation is complete.

3.1.4 The Entropy Equation

$$\varrho T \frac{\mathrm{D}s}{\mathrm{D}t} = \mathcal{H} - \mathcal{C} + \nabla \cdot (K \nabla T) + \nu \mu_0 \mathbf{J}^2 + 2\varrho\nu \mathbb{S} \otimes \mathbb{S} + \zeta \varrho (\nabla \cdot \mathbf{v})^2. \tag{3.7}$$

Equation (3.7) is the **Entropy Equation** and describes the temporal evolution of the entropy, s. Here, $\mathbb{S} \otimes \mathbb{S} := \mathbb{S}_{ij}\mathbb{S}_{ij}$. The PENCIL CODE chooses to solve this instead of the **Thermal Energy Equation**, which would describe the temporal evolution of the thermal energy, e, instead. This implies that $\ln \varrho$ and s are seen as the two fundamental thermodynamical variables. It is reasoned that entropy is the natural choice of physical variable when considering various convection processes, along with their associated stability or instability [8]. Here, $\mathcal{H}$ and $\mathcal{C}$ represent explicit heating and cooling terms respectively, T the temperature and K the radiative thermal conductivity [8]. All other symbols seen here retain their original meanings as described previously.

3.2 Cautionary Notes on Physical Units

All results obtained from the code remain independent of the physical unit system used to interpret them. This is due to the "unit-agnostic" nature of many of the calculations performed [8]. The following example is taken from the manual to illustrate this:

> "*... if you simulate a simple hydrodynamical flow in a box of length* $L = 1.$ *and get a maximum velocity of* $u_{\max} = 0.5$ *after* $t = 3$ *time units, then you may interpret this as* $L = 1$m, $u_{\max} = 0.5$m/s, $t = 3$s, *or as* $L = 1$pc, $u_{\max} = 0.5$pc/Myr, $t = 3$Myr, *depending on the physical system you have in mind. The units you are using must of course be consistent, thus in the second example above, the units for diffusivities would be* pc^2/Myr, *etc.*"

— PENCIL CODE Manual [8], pg. 33

The code itself, of course, makes use of an internal "unit system" which we shall be referred to as **code units** or, more simply, as **units**.

In order to determine the units of the magnetic flux density, $[B]$, the code makes use of the internal value $\mu_0 = 1$. Units of temperature (only when making use of the module `noionization.f90`) are also determined internally in a similar way, only using the internal value $c_p = 1$.

Using the Alfvén velocity definition, the units of the magnetic flux density are determined by

$$[B] = \sqrt{\mu_0 [\varrho]}[v], \tag{3.8}$$

where we have assumed that our chosen units for density and velocity are $[\varrho]$ and $[v]$ respectively[3]. The units of temperature, although defined in a slightly more complicated manner, follow a similar definition [8].

The units of length, $[L]$, velocity, $[v]$, and density, $[\varrho]$, may chosen by the user and are typically appropriate to the problem that is to be considered. There are, however, a few nuances which have to be kept in mind when choosing relevant units for the latter two quantities. The PENCIL CODE makes use of the value c_{s_0}, as described in Section 3.1.2, in order to set the unit of velocity. In particular, when one sets $c_{s_0} = 1$, the unit of velocity is measured in units of the chosen sound speed relevant to the problem at hand. Similarly, if one were to choose $\varrho_0 = 1$, then units of density are also measured in units of density applicable to the problem at hand[4]. Once these are chosen, units of temperature and magnetic flux density are obtained via the means outlined above. Similarly, units of time, $[t]$, are obtained by noting that $[t] = [L]/[v]$.

In the context of computation, the subject with physical units, their choice and calculation can quickly become out-of-hand. We refer the interested reader to the PENCIL CODE manual [8], as well as relevant related threads[5] on the PENCIL CODE discussion group for further information regarding the interpretation of simulation results in terms of physical units. The user may specify the desired units in the relevant input file before runtime. In order to ease the rescaling of the numerical results obtained after a run, post-processing scripts written for the commercial data visualization programming language, Interpreted Data Language, or IDL, are provided. Should one not have access to

[3] Here, we use $[\cdot]$ to denote only the units of a particular quantity and not a dimensional analysis

[4] Here, ϱ_0 is a reference value of the density, taken at some reference height, $z_{\rm ref}$.

[5] Our questions relating to the issue with physical units in the code may be found at the following URL: `http://bit.ly/WyMd2o`.

an IDL package, the correct physical units obtained via the same calculations above may simply be multiplied into the output manually.

For the purposes of the simulation results which shall be presented in the following chapters of this dissertation, we shall always only quote results in code units, unless a physical comparison is made, in which case the correct physical unit(s), together with the corresponding code unit(s), shall be quoted.

3.3 Numerical Methods

We now look briefly at some of the numerical methods and techniques that are employed in the PENCIL CODE.

3.3.1 Finite Difference Digression

The Method of Finite Differences (FDM) plays an important role in the numerical solution of partial differential equations. They rely on the use of a set of discrete points, collectively called a **stencil**, which form a discrete approximation to the derivative of a function. An example of a typical one-dimensional FDM stencil may be seen in Figure 3.1. Once discretised, the derivative approximations are then substituted back into the partial differential equation, causing it to become a **partial difference equation**. A typical FDM scheme is formulated on a grid of discrete points called a **mesh**, which may be of arbitrary size, on which the resulting partial difference equation is solved. Each point on the mesh then represents a particular spatial point on the solution domain of the original partial differential equation. Due to the nature of their formulation, FDM schemes are also considered to be **embarrassingly parallel**, meaning that they are easily adapted when writing computer code that is intended for (massively) parallel computations.

Important in any particular FDM is the **truncation error**, which is described by the next-highest-order derivative term in the Taylor Series when it is truncated to form the approximation to the derivative. In other words, a second-order FDM scheme would usually possess a truncation error term that is proportional to h^2, where h is the distance between two nodes on the mesh. Here, the derivative term multiplying h^2 is $f'''(x)/3!$. In this way, an n-th order FDM scheme will always possess an h^n-order truncation error (which is where the scheme gets its name from), which is then also multiplied by the $f^{(n+1)}(x)$ derivative term in the series. Depending on whether the derivative multiplying the truncation error is an odd or even derivative, the truncation error itself may be referred to as a **dispersive error** (if the derivative is even) or a **diffusive error** (if the derivative is odd) [7]. Using a high-order

FDM scheme is important if one is to ensure the fidelity of the numerical solution obtained.

The PENCIL CODE makes use of a variety of FDM approximations to the spatial derivatives, including second-, sixth- and tenth-order approximations. By default, the sixth-order approximation is always used for the spatial derivative, but the user may change this before compile-time by specifying in the makefile that the code use a particular module to approximate the spatial derivatives.

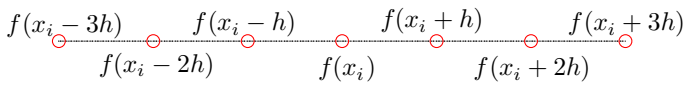

Figure 3.1: A typical one-dimensional stencil for the sixth-order, centered-difference approximation to the first- and second derivatives to a function, $f(x)$. Nodes here are equally-spaced with spacing h.

In the following, we present a brief derivation of the sixth-order, central-difference approximation to the first- and second derivatives of a function, $f(x)$. Note that for the case of a multivariable function, $h(x, y, z, \ldots)$, the same derivations still hold, only now that whilst the derivative is taken with respect to one particular spatial variable, the others are held constant, as is the normal procedure of partial differentiation.

Consider some sufficiently differentiable function, $f(x)$, that is defined on some domain $[-L, L]$ which has been discretised into equally-spaced nodes, $x_i = -L + ih$, where h is the spacing between the nodes and $i \in \mathbb{Z}$. We may then denote the value of $f(x)$ at a discrete point, x_i, on the domain as $f(x_i) \equiv f_i$. We wish to approximate the first derivative, $f'(x)$, via the use of the discrete points as shown in Figure 3.1. Dropping the notation for the discrete points for the moment, we assume that we may approximate $f'(x)$ at the point $f(x)$ using six equally-spaced "sample" points as [7]:

$$\begin{aligned} f'(x) \quad &\approx \quad Af(x+3h) + Bf(x+2h) + Cf(x+h) + Df(x-h) \\ &\quad\quad + Ef(x-2h) + Ff(x-3h), \end{aligned} \tag{3.9}$$

where the coefficients A to F are as yet undetermined. This situation corresponds to Figure 3.1, in which the first derivative at the middle point, $f(x_i)$, is now being approximated by the sample points surrounding it. The Taylor Series expansions around each of these sample points may then be written in a unified manner as:

$$
\begin{aligned}
f(x \pm nh) &= f(x) \pm nhf'(x) + \frac{n^2h^2}{2}f''(x) \pm \frac{n^3h^3}{3!}f'''(x) + \frac{n^4h^4}{4!}f^{(4)}(x) \\
&\quad \pm \frac{n^5h^5}{5!}f^{(5)}(x) + \mathcal{O}\left(h^6\right). \qquad (3.10)
\end{aligned}
$$

By substituting each of the Taylor expansions of the sample points back into Expression (3.9) and then regrouping all coefficients multiplying to a like derivative, one obtains the linear system of equations:

$$
\begin{pmatrix}
1 & 1 & 1 & 1 & 1 & 1 \\
3 & 2 & 1 & -1 & -2 & -3 \\
9 & 4 & 1 & 1 & 4 & 9 \\
27 & 8 & 1 & -1 & -8 & -27 \\
81 & 16 & 1 & 1 & 16 & 81 \\
243 & 32 & 1 & -1 & -32 & -243
\end{pmatrix}
\begin{pmatrix} A \\ B \\ C \\ D \\ E \\ F \end{pmatrix}
=
\begin{pmatrix} 0 \\ 1/h \\ 0 \\ 0 \\ 0 \\ 0 \end{pmatrix}, \qquad (3.11)
$$

where, since we wish to obtain an approximation to $f'(x)$, each of the other remaining coefficient groups multiplying the function and derivative terms have been set to zero. This system then has the unique solution given by:

$$
\begin{pmatrix} A \\ B \\ C \\ D \\ E \\ F \end{pmatrix}
= \frac{1}{h}
\begin{pmatrix} 1/60 \\ -3/20 \\ 3/4 \\ -3/4 \\ 3/20 \\ -1/60 \end{pmatrix}, \qquad (3.12)
$$

which then yields the coefficients needed to approximate $f'(x)$ in Expression (3.9). If we choose to revert to the discrete notation as described before, then the sixth-order, central finite difference approximation to the first derivative may be written as [7]:

$$
\boxed{f'(x) \approx \frac{\frac{1}{60}f_{i+3} - \frac{3}{20}f_{i+2} + \frac{3}{4}f_{i+1} - \frac{3}{4}f_{i-1} + \frac{3}{20}f_{i-2} - \frac{1}{60}f_{i-3}}{h}}. \qquad (3.13)
$$

Similarly, we may assume that the second derivative, $f''(x)$, may be approximated by the form:

$$\begin{aligned} f''(x) &\approx Af(x+3h)+Bf(x+2h)+Cf(x+h)+Df(x)+Ef(x-h) \\ &\quad +Ff(x-2h)+Gf(x-3h), \end{aligned} \tag{3.14}$$

where the coefficients A to G again need to be determined. This situation again corresponds to Figure 3.1, in which the second derivative at the middle point, $f(x_i)$, is now being approximated by it *and* the sample points surrounding it. Again, the Taylor Series expansions around each of these sample points (excluding $f(x_i)$) may then be written in a unified manner as:

$$\begin{aligned} f(x \pm nh) &= f(x) \pm nhf'(x) + \frac{n^2h^2}{2}f''(x) \pm \frac{n^3h^3}{3!}f'''(x) + \frac{n^4h^4}{4!}f^{(4)}(x) \\ &\quad \pm \frac{n^5h^5}{5!}f^{(5)}(x) + \frac{n^6h^6}{6!}f^{(6)}(x) \pm \mathcal{O}\left(h^7\right), \end{aligned} \tag{3.15}$$

where we have now expanded to an extra term in the Taylor Series due to the inclusion of the extra point, $f(x_i)$. Substitution back into Expression (3.14) and regrouping of coefficients multiplying a common derivative then leads to the linear system given by:

$$\begin{pmatrix} 1 & 1 & 1 & 1 & 1 & 1 & 1 \\ 3 & 2 & 1 & 0 & -1 & -2 & -3 \\ 9 & 4 & 1 & 0 & 1 & 4 & 9 \\ 27 & 8 & 1 & 0 & -1 & -8 & -27 \\ 81 & 16 & 1 & 0 & 1 & 16 & 81 \\ 243 & 32 & 1 & 0 & -1 & -32 & -243 \\ 729 & 64 & 1 & 0 & 1 & 64 & 729 \end{pmatrix} \begin{pmatrix} A \\ B \\ C \\ D \\ E \\ F \\ G \end{pmatrix} = \begin{pmatrix} 0 \\ 0 \\ 2/h^2 \\ 0 \\ 0 \\ 0 \\ 0 \end{pmatrix}, \tag{3.16}$$

which has the unique solution,

$$\begin{pmatrix} A \\ B \\ C \\ D \\ E \\ F \\ G \end{pmatrix} = \frac{1}{h^2} \begin{pmatrix} 1/90 \\ -3/20 \\ 3/2 \\ -49/18 \\ 3/2 \\ -3/20 \\ 1/90 \end{pmatrix}. \tag{3.17}$$

These are then the coefficients needed to approximate $f''(x)$ in Expression (3.14). Adopting the simple notation described before, the sixth-order, central finite difference approximation to the second derivative may be written as:

$$\boxed{f''(x) \approx \frac{\frac{1}{90}f_{i+3} - \frac{3}{20}f_{i+2} + \frac{3}{2}f_{i+1} - \frac{49}{18}f_i + \frac{3}{2}f_{i-1} - \frac{3}{20}f_{i-2} + \frac{1}{90}f_{i-3}}{h^2}.} \tag{3.18}$$

The finite difference approximations for the second-, fourth- and tenth-orders are all derived in a similar fashion, using less sample points than the sixth-order (in the case of the second- and fourth-order approximations) or more sample points (in the case of the tenth-order approximation). High-order FDM schemes are always deemed favourable due to their versatility and the fact that they can offer truncation error orders that can almost match those of the spectral methods [7]. Despite this, however, they do suffer a major drawback: the higher the order of the FDM scheme, the more sample points are required in the stencil in order to form the approximation.

In practical terms, this poses a problem near the boundaries of the mesh, as larger **ghost zones** are required for points on the stencil that lie outside of the mesh. Thus, more storage space is required to store the mesh and ghost zones. This can be partially overcome by the use of so-called **compact finite difference schemes**, such as those proposed by Lele (1992) [34], which also offer much better truncation errors [7], though these schemes are somewhat impractical to use in parallel computations due to their compact nature. Coefficients for the approximation of the derivative also become more difficult to calculate due to the fact that more and more terms are taken into account from the resulting Taylor Series. This is trivial, though, as the coefficients for the derivative approximation are only calculated once and then hardcoded into a module (in the case of the PENCIL CODE) or function that deals with the numerical differentiation. Thus, when choosing an FDM scheme, one has to take all of the above factors into account and make some sort of tradeoff. In the case of the PENCIL CODE, the sixth-order (explicit) finite difference approximation to the derivatives then is the most appealing in light of the above factors.

3.3.2 Timestepping and the Method of Lines

Another factor which plays a critical role in the proper functioning of any FDM code is that of **time integration**. In essence, time integration allows the numerical solution to the partial differential equation being solved "evolve" in time, making it important to pay careful attention to how this integration is implemented in a code.

The simplest method of time integration is accomplished by, once more, approximating the temporal

derivative term in the partial differential equation under consideration via a simple **forward finite difference** approximation. This first-order approximation is derived trivially from the Taylor Series expansion of the function $g(t)$ and involves approximating the function's first derivative, $g'(t)$, by making use of the sample point $f(t+\tau)$, where τ is the temporal step size. Expanding around the point $f(t+\tau)$ and discarding all terms like $\mathcal{O}(\tau^2)$, the approximation may then be written as

$$f'(t) \approx \frac{f(t+\tau) - f(t)}{\tau} + \frac{\tau}{2} f''(t), \tag{3.19}$$

where the trailing second-derivative term represents the truncation error. As this term is proportional to τ only, it has a **first-order truncation error**, from whence this approximation gets its name. Due to the low-order truncation error, this approximation is not very good and in the PENCIL CODE it is mainly used for testing purposes only. Other FDM approximation schemes for the time integration exist; examples of these are the central difference scheme as used for approximation of the spatial derivatives above, as well as the **backward finite difference approximation** which involves approximating the first derivative using the sample point $f(t-\tau)$ instead of the point $f(t+\tau)$ in a first-order Taylor Series expansion.

Whilst these FDM time integration methods are all easily implemented, they all require potentially massive amounts of storage space to compute the numerical solution at subsequent time steps (both the central and forward FDM time integration schemes need to access values of the numerical solution at previous time levels) and can also be potentially expensive to calculate at each time step (in the case of the backward FDM scheme, which usually requires solving a potentially large system of equations in order to obtain the value of the numerical solution at subsequent time steps). For this reason, more sophisticated time-integration techniques are employed. One such time-integration technique that is used by the PENCIL CODE is a specialised version of the famous **third-order Runge-Kutta method**, which is also employed by many other excellent numerical software packages (MATLAB and Octave being two such examples).

In order to apply the Runge-Kutta scheme to a set of partial differential equations, one has to convert these equations into a set of ordinary differential equations (ODEs) via the **Method of Lines** (MoL). The MoL involves only replacing the spatial derivatives in the partial differential equations by their finite-difference approximations, which then leaves the equations, though they are still coupled to each other through the spatial derivatives, essentially only dependent on the time variable. For example, applying this method to the partial differential equation $u_t = -\alpha u_x$ [7], for a function $u = u(x,t)$ and using a first-order FDM approximation for the spatial derivative, one will arrive at the set of ODEs given by:

$$\frac{\mathrm{d}u_i}{\mathrm{d}t} = -\alpha \frac{u_{i+1} - u_i}{h}, \tag{3.20}$$

where α is some arbitrary constant. A set of initial and boundary conditions are needed to complete the system. The original partial differential equation is now approximated by a system of ODEs instead. Time-integration of the system may now either be done via Euler's Method or any one of the high-order Runge-Kutta schemes. It is in this that the power of the MoL is now realised: instead of having to develop new time-integration schemes for sets of partial differential equations, they may simply be reduced to a set of ODEs and then time-integrated using an already well-established scheme.

In the context of the PENCIL CODE, even though the the resulting system of ODEs is vastly complex, the same time-integration idea applies. As mentioned before, time-integration is, by default, done through the use of a specialised third-order Runge-Kutta (RK3) scheme. The RK3 scheme in use is from a family of RK methods known as RK-2N schemes which were proposed in Williamson (1980) [59]. The N in the name refers to the amount of variables that need to be updated at every time step, meaning that only $2 \times N$ variables need to be stored in the computer's memory at any given time [7] – a real bargain! Unfortunately, not all RK schemes can be reformulated as RK-2N schemes [7, 59].

If we take as a prototype, the ODE system

$$\frac{\mathrm{d}u}{\mathrm{d}t} = F(u, t), \tag{3.21}$$

which is to be time-integrated via the RK-2N scheme in use by the PENCIL CODE, then we may express its iteration as [7]:

$$w_i = \alpha_i w_{i-1} + \tau F(u_{i-1}, t_{i-1}) \tag{3.22}$$

$$u_i = u_{i-1} + \beta_i w_i, \tag{3.23}$$

where $i = 1 \ldots 3$ (corresponding to a third-order RK-2N scheme [7]), w_i are weights that need to be determined at every step in the iteration and τ is the adaptive time step size that is determined according to the **Courant-Friedrich-Levy condition** at every iteration. In order to move from the current approximation to the numerical solution, $u^{(n)} \equiv u(t_n)$, to the next approximation, $u^{(n+1)} \equiv u(t_n + \tau)$ (i.e. to go from time t_n to time $t_n + \tau$), three time steps (two intermediate; the third step being counted as the time $t + \tau$) need to be taken according to the iteration described by Equations (3.22) and (3.23). This involves determining the values of the coefficients α_i and β_i, as well as the

values of the intermediate time steps, t_i. Fortunately, these are only calculated once via a detailed analysis of the iteration itself [7, 59] and then coded into the code's default time stepping routine.

3.3.3 In-context Modifications to the Pencil Code

All of the simulations conducted in Section 4.2 of Chapter 4 required the PENCIL CODE's functionality to be extended in some way. In this section, we present and make brief commentary on the changes that were made to the code in order to make these simulations possible.

3.3.3.1 Giving the Induction Equations a Battery Term

In order to study Magnetogenesis, it was determined that a battery term needed to be added into the Induction Equations to allow for the growth of magnetic fields from the initial condition $\mathbf{A} = \mathbf{0}$. We approached the code's developers via their discussion group and the `battery_term` simulation was added to the code's sample simulations by Brandenburg. Modifications were made only to the `magnetic.f90` module, which deals with all magnetic field-related aspects of the code.

In Listing 3.1, we display the relevant sections of the `magnetic.f90` module that reflect Brandenburg's modification. It is to be noted here that the original modification reflects an error (i.e. the use of the term `baroclinic`; see Equations (4.13)), as this was done in the context of having the Induction Equations being solved for $\mathbf{B}$ and not $\mathbf{A}$ (which would use the correct term, coincidentally now the pencil, `fpres`; see Equations (4.21)). We modified this term to the correct form, as noted by Brandenburg, and submitted notice of the error to the relevant channels for correction in future revisions.

```
!  Add Battery term.
!
      if (battery_term/=0.0) then
        if (headtt) print*,'daa_dt: battery_term=',battery_term
        !call cross_mn(p%fpres,p%glnrho,baroclinic) !unneeded now
        !df(l1:l2,m,n,iax:iaz)=df(l1:l2,m,n,iax:iaz)+battery_term*baroclinic
                          !incorrect, as noted by Brandenburg
        df(l1:l2,m,n,iax:iaz)=df(l1:l2,m,n,iax:iaz)-battery_term*p%fpres
                           !correct form now
        if (headtt.or.ldebug) print*,'daa_dt: max(battery_term) =',&
            battery_term*maxval(p%fpres) !not sure what to do here
```

```
      endif
```

Listing 3.1: Calculation of the battery term in the code, along with its incorporation into the Induction Equations

3.3.3.2 Adding the Chaplygin Gas Equation of State

Inspection of the code suggested to us that pressure entered into the equations via the pressure term in the Navier-Stokes Equations (Equations (3.2)). This was also noted in Section 3.1.2. From further inspection, we found that this pressure term is actually a key pencil that is used in the code, namely, the pencil called `fpres`, which originates in the module `entropy.f90`. As all of our simulations considered an Ideal Gas EoS, we "lazily" modified only the calculation of `fpres` in the corresponding section of the `entropy.f90` module. Thus, if we wished to make use of the Chaplygin Gas EoS in our simulations, the corresponding calculation of `fpres` was selected by simply uncommenting the relevant line and re-compiling the code. We note, though, that this is a rather inelegant "hotfix", as inclusion of this EoS into the PENCIL CODE would warrant the creation of a specialised module that deals with the EoS specifically.

In Listing 3.2, we present our modification to the pencil `fpres`, reflecting the forms for the two types of Chaplygin Gas EoSs that were studied.

```
! fpres
!...
if (leos_idealgas) then
  do j=1,3
  p%fpres(:,j)=-p%cs2*(p%glnrho(:,j) + p%glnTT(:,j))*gamma_inv !Ideal Gas
  !p%fpres(:,j)=-exp(-2*p%lnrho)*p%glnrho(:,j) !Chaplygin B=1
  !p%fpres(:,j)=-exp(-2*p%lnrho)*(exp(p%lnTT)*p%glnrho(:,j) - &
  !               exp(p%lnTT)*p%glnTT(:,j)) !Chaplygin B=T
enddo
```

Listing 3.2: Calculation of the pencil `fpres` assuming an Ideal Gas EoS, together with the modifications made assuming the Chaplygin EoS.

3.4 The Induction Sandbox...

In the following section we present the results of simulations of the Induction Equations, performed for testing and validation purposes. We "turn off" all of the other MHD evolution equations, allowing sole focus on the Induction Equations themselves.

3.4.1 Stationary Induction

In the absence of the other evolution equations (implying that all of the other quantities have been set to zero), the Induction Equations reduce to the simple form of:

$$\frac{\partial \mathbf{A}}{\partial t} = -\eta \mu_0 \mathbf{J}. \tag{3.24}$$

Note that if we specify an initial field, $\mathbf{A} = \mathbf{0}$, we would obtain the constant solution of $\mathbf{A} = \mathbf{0}$. However, should we specify an initial field of a given, arbitrary magnitude, it is be expected that $\mathbf{A}$ would decay within some finite time. We should also expect that in the limit $\eta \to 0$, the field would decay slower (characteristic of a medium with low magnetic diffusivity). Similarly, in the limit $\eta \to \infty$, the field would decay faster (characteristic of a medium with high magnetic diffusivity).

We return to a proper analysis of this limit of the Induction Equations in Section 5.2.2 of Chapter 5.

3.4.2 Stationary Results

3.4.2.1 Numerical Derivatives and Effective Wavenumbers

Before continuing numerical study of Equations (3.24), we consider the effects of the FDM derivative approximation scheme on the calculation of effective wavenumbers for a given initial field. The results of the simulations presented in this subsection are based on a periodic one-dimensional computational domain of length 2π. Numerical tests in this subsection have been based on the work done in [7].

Given a function, $f(x)$, its Fourier Series in terms of the complex exponential may be expressed as:

$$f(x) = \sum_{k=-\infty}^{k=\infty} c_k e^{ikx}, \tag{3.25}$$

where c_k's and k's are the complex Fourier coefficients and wavenumber respectively. Concentrating only on the exponential part of the series, it is of particular interest to see how well its higher-order derivatives, particularly at high wavenumbers, are evaluated analytically [7, 35].

By inspection, it is clear that the n-th derivative of the e^{ikx}-term is given by:

$$\frac{\mathrm{d}^n e^{ikx}}{\mathrm{d}x^n} = (ik)^n e^{ikx},$$

where $n = 1, 2, 3, \ldots$, and the wavenumber is assumed to be constant.

Considering a uniformly-spaced mesh of points $x_j = jh$, where h is the spatial distance between two mesh points and $j = 1, 2, 3 \ldots$, we can introduce the discretised function, $g(x_j) \equiv g_j = e^{ikx_j}$ to represent the e^{ikx}-term under consideration [35]. For illustrative purposes, applying a second-order-accurate finite difference approximation to the first derivative yields the following:

$$\begin{aligned}
\left(\frac{\mathrm{d}e^{ikx}}{\mathrm{d}x}\right)_j &\approx \frac{g_{j+1} - g_{j-1}}{2h} \\
&= \frac{e^{ikh(j+1)} - e^{ikh(j-1)}}{2h} \\
&= \frac{e^{ikhj}}{2h}\left(e^{ikh} - e^{-ikh}\right) \\
&= \frac{e^{ikhj}}{2h}\left(\cos kh + i\sin kh - \cos kh + i\sin kh\right) \\
&= \frac{e^{ikhj}}{2h}\left(2i\sin kh\right) \\
&= \frac{ie^{ikhj}}{h}\sin kh,
\end{aligned}$$

where we now define the **modified** or **effective wavenumber** as $k_{\mathrm{eff}} = \sin kh/h$ [7, 35], which appears in place of the normal wavenumber, k, had the derivative been taken analytically. The effective wavenumber describes how well a given wavenumber component of a numerical solution obtained is resolved over the entire range of wavenumbers on a mesh of range $[0, \pi]$ [35] and is bounded by the **Nyquist Frequency**, $k_{\mathrm{Ny}} \equiv \pi/h$ [7]. Note that the form of the effective wavenumber changes, depending on the order and type of finite difference scheme under consideration.

Following the work of Brandenburg [7], we consider the effective wavenumbers for the numerical first- and second derivatives of the function $f(x) = \cos kx$, calculated via

$$\frac{\mathrm{d}\cos kx}{\mathrm{d}x} = -k_{\mathrm{eff}}\sin kx \quad \text{and}$$
$$\frac{\mathrm{d}^2\cos kx}{\mathrm{d}x^2} = -k_{\mathrm{eff}}^2\cos kx.$$

Our purpose is to determine how well the calculated effective wavenumbers compare to their expected theoretical counterparts, where both wavenumbers are normalised by the Nyquist frequency.

The results presented in Figure 3.2 were obtained by using the initial field $\mathbf{A}_0 = (0, \sin kx, \cos kx)$, called the Beltrami field in the accompanying manual [8], and evolving it using *only* the Induction Equations in one dimension for one time step, using the default sixth-order-in-space FDM approximation to the spatial derivatives[6] and Euler's Method to perform the time-integration.

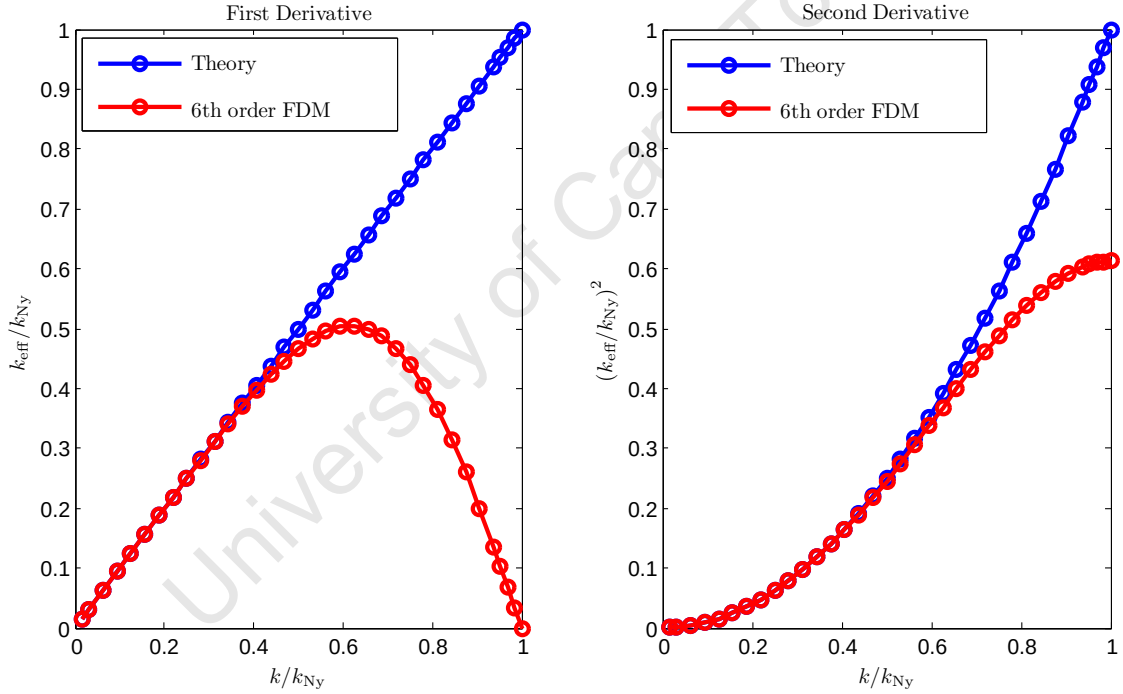

Figure 3.2: Comparison of effective wavenumbers to their expected theoretical counterparts for a sixth-order FDM spatial first- and second derivative approximation scheme. Effective wavenumber approximations to their theoretical counterparts worsen as the Nyquist Frequency is approached.

At lower wavenumbers, the correlation between the theoretical and effective wavenumbers is excellent and becomes gradually worse as the Nyquist frequency is approached, agreeing with the findings

[6]The specifics of this simulation are based on an exercise about effective wavenumbers, set by Brandenburg. The reader may access this at the following URL: `http://www.nordita.org/~brandenb/teach/PencilCode/keff.html`

of [7][7].

The bad correlation between the two wavenumbers as the Nyquist frequency is approached is an unfortunate consequence of the FDM approximation of the spatial derivatives and is usually only overcome by the use of spectral methods or higher-order (compact) FDM schemes [7]. Despite this drawback, the simulations conducted here serve to highlight the importance of using accurate high-order FDM schemes in approximating higher-order spatial derivatives, ensuring that quantities such as the current density, $\nabla \times \nabla \times \mathbf{A} = \mathbf{J}$, which is a second derivative quantity, are accurately calculated (here, of course, we have assumed units of $\mu_0 = 1$ for simplicity).

3.4.2.2 Decaying Uniform and Gaussian Fields

The results of the simulations presented in this subsection are based on a periodic two-dimensional computational domain of dimensions $2\pi \times 2\pi$. The reader is once more reminded that only the Induction Equations are being solved.

We have considered the evolution two types of initial fields: x-uniform (i.e. an initial field uniform in the x-direction and zero elsewhere) and (random) Gaussian Noise. Note that because the Induction Equations solved by the PENCIL CODE are given in terms of the magnetic vector potential, $\mathbf{A}$, the initial conditions used are also for this field.

For the purposes of these tests, we follow only the temporal evolution of the **root-mean-squared (rms) magnetic flux density**, B_{rms}, also denoted $\langle \mathbf{B}^2 \rangle^{1/2}$, where $\langle \cdot \rangle$ indicates a volume-averaged quantity. As B_{rms} is one of the many diagnostic variables that the user may choose to be output by the code at specified time steps, any further post-processing to the raw data output by the code is unnecessary. Along with the two initial conditions, we also experimented with various choices of the magnetic diffusivity, η, in order to determine how it affects the decaying field.

A summary of the simulation parameters may be seen in Table 3.1, whilst the results may be seen in Figures 3.3 and 3.4. As results are qualitatively identical, we shall consider them in a unified manner.

Examining Figure 3.3, it is evident that as we increase the value of η, the fields decay extremely quickly, whereas if we decrease the value of η, the opposite behaviour is observed (that is, the fields do not decay as quickly). It is interesting to note that the field decay appears to be exponential in nature.

[7]Note that Brandenburg considers several finite-difference schemes for comparison in this regard, as well as a spectral method scheme. We only reproduce the sixth-order-in-space result here; the rest may be found in the aforementioned paper.

Run	$\mathbf{A}_0$	η	Run	$\mathbf{A}_0$	η
1a	Uniform-x	10^{-1}	1b	Gaussian Noise	10^{-1}
2a	Uniform-x	10^{-2}	2b	Gaussian Noise	10^{-2}
3a	Uniform-x	10^{-3}	3b	Gaussian Noise	10^{-3}
4a	Uniform-x	10^{0}	4b	Gaussian Noise	10^{0}
5a	Uniform-x	10^{1}	5b	Gaussian Noise	10^{1}
6a	Uniform-x	10^{2}	6b	Gaussian Noise	10^{2}

Table 3.1: Simulation parameters for runs of the fiduciary model described in Section 3.4.1. Here, $\mathbf{A}_0$ and η represent the initial choices for the magnetic vector potential field, $\mathbf{A}$, and magnetic diffusivity respectively.

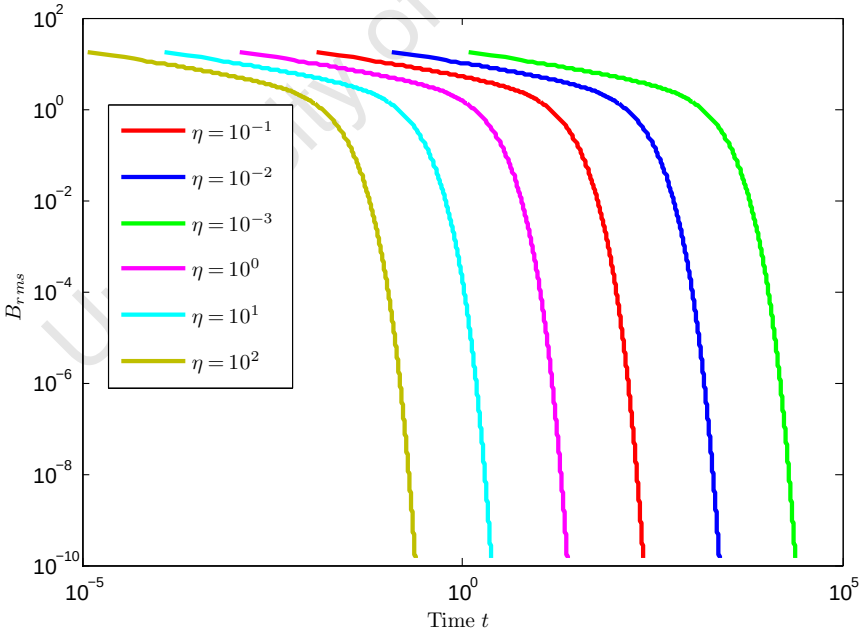

Figure 3.3: Decay of B_{rms} for the initial x-uniform $\mathbf{A}$-field for various values of the magnetic diffusivity, η.

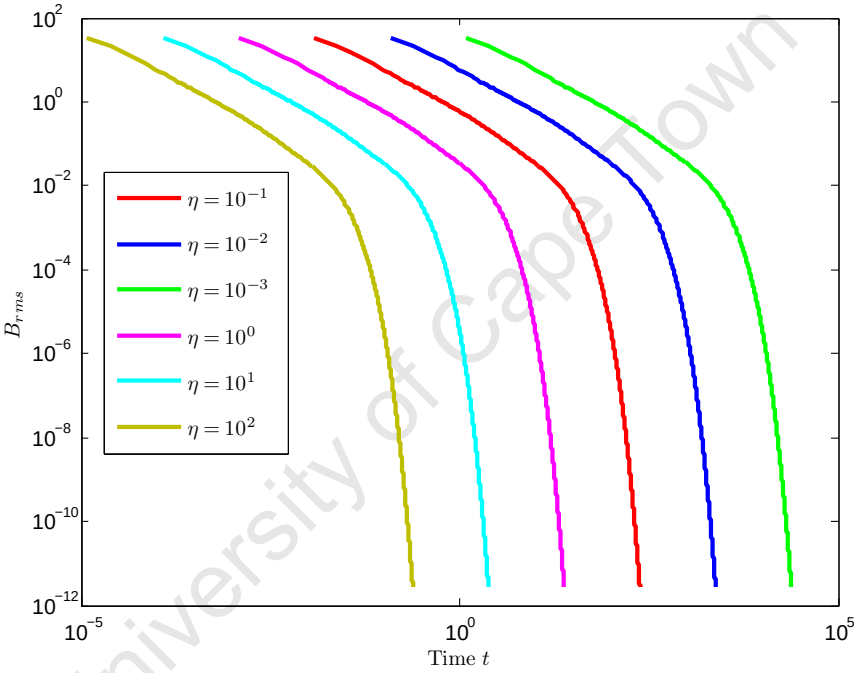

Figure 3.4: Decay of B_{rms} for the initial Gaussian Noise **A***-field for various values of the magnetic diffusivity, η.*

The magnetic diffusivity is a quantity that is intrinsic to a given (conducting) medium. If the medium has a high magnetic diffusivity, it would mean that the magnetic field would then diffuse through it fairly quickly, thus also appearing to quickly decay in strength. The opposite behaviour can then also be inferred for the case of a medium with a low magnetic diffusivity. As described in Section 3.4.1, this is then exactly the behaviour that we had expected to see.

Furthermore, one could argue that the results observed could be time-step-dependent, due to η being one of the parameters playing a role in the selection of the time step size for a particular iteration. This was ruled out by explicitly choosing a time step of an appropriate size, which was then kept constant for the duration of the run, validating the results obtained before. We conclude, then, that the results obtained initially are in fact time-step-independent and correct.

3.5 Closing Points

In this chapter, we introduced a high-order finite-difference code, the PENCIL CODE, which was used to conduct all of the simulation work presented in this dissertation.

We briefly considered each of the equations of compressible MHD, solved by the code, along with any particular assumptions which were made in their posing. In particular, we payed attention to the usage of the logarithmic density, $\ln \varrho$, in the Continuity Equation over the usual density, ϱ, the simplification of the pressure term, $\nabla p / \varrho$, in the Navier-Stokes Equations, which made use of the Ideal Gas equation of state, the usage of the magnetic vector potential field, $\mathbf{A}$, over the usual magnetic flux density, $\mathbf{B}$, in order to immediately impose the divergencelessness condition for the latter field and, finally, the usage of the entropy, s, in the Entropy Equation, rather than the usual Thermal Energy, e, in the Thermal Energy Equation.

Brief comments on the usage of physical units in the code were made. Here, we noted that the code makes use of its own internal unit system, leaving the user to impose units appropriate to the problem under consideration and rescale results as necessary, should physical comparisons need to be made. For our purposes in particular, we noted how the units of the magnetic field are calculated.

Consideration was also given to the importance of both the FDM approximation schemes used to approximate the spatial derivatives *and* the usage of the high-order RK3-2N time-integration scheme used to evolve the numerical solution obtained. It was noted that the high-order FDM approximation schemes are favourable as they offer good truncation errors and are easily adapted for parallel computation, the only drawback arising when more storage space to accommodate larger ghost zones is required if the FDM scheme's order is very high. It was also stated that RK-2N time-integration

schemes are most preferable to use, as they are an excellent saving on storage space in the computer's memory, with the scheme only needing to store a total of $2 \times N$ variables in memory at any given time if N is the number of variables that needed to be updated at every time step.

In addition to this, modifications made to the code for the simulations conducted in Chapter 4 were also shown and their need motivated.

Finally, two brief simulations with the code were done for validatory purposes. The first of these focussed on the correlation between effective wavenumbers, as appearing in the finite-difference approximations of the exponential term of the Fourier Series decomposition of a function, $f(x)$, and exact wavenumbers, as appearing in the exact differentiation of the same exponential component of the Fourier Series decomposition. We found that the correlation between the two types of wavenumbers was good at lower values of the exact wavenumber normalised by the Nyquist frequency, and became progressively worse as the Nyquist frequency was approached, which is an unfortunate drawback of the finite-difference derivative approximation. Comments on the importance of accurate high-order finite-difference schemes in calculating high-order derivatives were then also made.

The second set of simulations focussed on the decay of the magnetic field in the stationary Induction Equations. Two types of initial fields were considered, as well as different values of the magnetic diffusivity. We found that our numerical results agreed with the results we expected by inspection of the Induction Equations themselves: a decaying field was always produced and the timescale of decay varied with the choice of magnetic diffusivity, becoming longer as the diffusivity was decreased and shorter as the diffusivity was increased. The results were checked for time-step-independence and were found to be time-step-independent – the same qualitative decay behaviour was still observed, even when the time step size was fixed for all values of the diffusivity. Based on the outcomes of the two simulations conducted, it was asserted that the PENCIL CODE was producing the expected results, clearing the way for more complex simulations.

Chapter 4

The Biermann Battery

Questo è quel pezzo
Di calamita:
Pietra mesmerica,
Ch'ebbe l'origine
Nell'Alemagna,
Che poi sì celebre
Là in Francia fu.

— Despina, *Così fan tutte*, W. A. Mozart (1759 – 1791) & L. Da Ponte (1749 – 1838)

The primary objective of this chapter is to address the problem of generating magnetic fields from a set of zero initial conditions: the problem of **magnetogenesis**. Recall that the equations presented in Chapter 2 have been formulated in the context of a fluid consisting only of a single species of particle. This is known as the **single-fluid** approximation. In order to generate magnetic fields from zero, a violation to Ohm's Law is required. One possible way to create such a violation is via the use of a battery effect. It shall be seen that the simplest way of obtaining this battery, mathematically, arises if a fluid consisting of two or more species of particles is assumed.

In the following, we present the derivation of Ohm's Law from the point-of-view of a simple two-fluid approximation, where we assume a fluid consisting of only ions and electrons (i.e. a **plasma**). After re-deriving the Induction Equations using the new form of Ohm's Law, we also introduce the Chaplygin Gas EoS and discuss its relevance to the magnetogenesis problem. Results of the magnetogenesis simulations that were performed are then presented and comments are made on the various qualitative features observed during the field's temporal growth.

Finally, motivation is given for further study into the amplification mechanisms of magnetic fields, using the simulation results obtained in this chapter as motivation.

4.1 Multi-fluid Approximations and the Biermann Battery

We now concentrate on the two-fluid approximation and one of its resultant effects – the thermal battery.

4.1.1 The Two-fluid Approximation and the General Ohm's Law

The simplest approach to the two-fluid approximation of a plasma is to consider a charged fluid consisting only of ions and electrons. Following the work presented in [51], using all conventions and unit systems as in the reference, we immediately write down the equation of motion in a unified form for the two particle species comprising the fluid:

$$\begin{aligned} n_{\mathrm{k}} m_{\mathrm{k}} \left(\frac{\partial \mathbf{v}_{\mathrm{k}}}{\partial t} + \mathbf{v}_{\mathrm{k}} \cdot \nabla \mathbf{v}_{\mathrm{k}} \right) &= \frac{n_{\mathrm{k}} Z e}{c} \left(\mathbf{E} + \mathbf{v}_{\mathrm{k}} \times \mathbf{B} \right) - \nabla \cdot \tilde{\boldsymbol{\sigma}}_{\mathrm{k}} - n_{\mathrm{k}} m_{\mathrm{k}} \nabla \Phi_{\mathrm{grav}} + \mathbf{P}_{\mathrm{kk'}} \\ \Leftrightarrow \frac{\mathrm{D}\mathbf{v}_{\mathrm{k}}}{\mathrm{D}t} &= \frac{Ze}{m_{\mathrm{k}} c} \left(\mathbf{E} + \mathbf{v}_{\mathrm{k}} \times \mathbf{B} \right) - \frac{\nabla \cdot \tilde{\boldsymbol{\sigma}}_{\mathrm{k}}}{n_{\mathrm{k}} m_{\mathrm{k}}} - \nabla \Phi_{\mathrm{grav}} + \frac{\mathbf{P}_{\mathrm{kk'}}}{n_{\mathrm{k}} m_{\mathrm{k}}}. \end{aligned} \tag{4.1}$$

Here, the subscript k may be replaced with either of the subscripts e or i to denote ions or electrons

respectively, with the subscript k' taking on the opposing particle species present in the fluid. In this case, the particles are assumed to carry a charge Ze/c, where c is the speed of light, e the standard charge on a proton in Electron Standard Units (ESU) and Z the particle charge in units of the proton charge [51]. The quantity $\tilde{\boldsymbol{\sigma}}$ represents the stress tensor as seen in Section A.2 of Chapter 2 and the term $\mathbf{P}$ the total momentum that has been transferred to the particular species of particle, per unit volume and per unit time, by collision with the other species of particle present in the fluid [51].

It is suggested by Spitzer that Equations (4.1) are exact both when considering a non-relativistic, perfect gas and where the gas's random-velocity distribution is sufficiently well-behaved [51]. If we make the latter assumption, then the divergence of the stress tensor may be written in the very simple form given by [51]:

$$\nabla \cdot \tilde{\boldsymbol{\sigma}} = \nabla p. \tag{4.2}$$

This arises specifically when the gas's random-velocity distribution is isotropic, leaving a stress tensor that has only three on-diagonal components, σ_{xx}, σ_{yy} and σ_{zz}, which are equal to each other and to the scalar pressure, p [51]. Using this, Equations (4.1) may be written as [51]:

$$\frac{\mathrm{D}\mathbf{v}_\mathrm{k}}{\mathrm{D}t} = \frac{Ze}{m_\mathrm{k}c}\left(\mathbf{E} + \mathbf{v}_\mathrm{k} \times \mathbf{B}\right) - \frac{\nabla p_\mathrm{k}}{n_\mathrm{k} m_\mathrm{k}} - \nabla \Phi_\mathrm{grav} + \frac{\mathbf{P}_{\mathrm{kk}'}}{n_\mathrm{k} m_\mathrm{k}}. \tag{4.3}$$

Separating the equations into their ion- and electron components, and taking the difference between $n_\mathrm{e}\mathrm{D}\mathbf{v}_\mathrm{e}/\mathrm{D}t$ and $n_\mathrm{i}Z\mathrm{D}\mathbf{v}_\mathrm{i}/\mathrm{D}t$ [51], yields:

$$\frac{m_\mathrm{e}c^2}{n_\mathrm{e}e^2}\frac{\partial \mathbf{J}}{\partial t} = \mathbf{E} + \mathbf{v} \times \mathbf{B} + \frac{c}{en_\mathrm{e}}\nabla p_\mathrm{e} - \frac{c}{en_\mathrm{e}}\mathbf{J} \times \mathbf{B} - \eta \mathbf{J}. \tag{4.4}$$

If we choose units of $c = 1$, this then reads as

$$\frac{m_\mathrm{e}}{n_\mathrm{e}e^2}\frac{\partial \mathbf{J}}{\partial t} = \mathbf{E} + \mathbf{v} \times \mathbf{B} + \frac{\nabla p_\mathrm{e}}{en_\mathrm{e}} - \frac{\mathbf{J} \times \mathbf{B}}{en_\mathrm{e}} - \eta \mathbf{J}, \tag{4.5}$$

where $\eta = P_\mathrm{ei}/en_\mathrm{e}J$ is a constant of proportionality [51]. Note that in the special case where $\partial\mathbf{J}/\partial t$, $\mathbf{B}$ and ∇p_e all vanish, we are left with the familiar Ohm's Law, where η is recognised as the **electrical resistivity** (*ergo*, the **magnetic diffusivity**) [51].

In the following, however, we shall use the electrical conductivity of the material, given by [10, 51]:

$$\sigma = \frac{1}{\eta} = \frac{n_\mathrm{e}e^2\tau_\mathrm{ei}}{m_\mathrm{e}} \equiv \frac{en_\mathrm{e}J}{P_\mathrm{ei}}, \tag{4.6}$$

along with the form of Equations (4.4), as given by [10]:

$$\mathbf{E} + \mathbf{v}_{\mathrm{i}} \times \mathbf{B} = -\frac{\nabla p_{\mathrm{e}}}{e n_{\mathrm{e}}} + \frac{\mathbf{J}}{\sigma} + \frac{\mathbf{J} \times \mathbf{B}}{e n_{\mathrm{e}}} + \frac{m_{\mathrm{e}}}{e^2 n_{\mathrm{e}}} \frac{\partial \mathbf{J}}{\partial t}. \tag{4.7}$$

The forms given by Equations (4.4) and (4.7) are sometimes both called the **Generalised Ohm's Law** and provide some illuminating properties essential to generating magnetic fields from a set of zero initial conditions.

The first term on the RHS of Equations (4.7) is recognised as the so-called **thermal battery** term. This term represents the effects of the gradient of the electron pressure [10] in the thermal generation of electric fields. Mathematically, if we wished to generate magnetic fields from this vector term, it would be required that it has a form which consists of both a pure vector part, as well as a "scalar" part: $\mathbf{V} = \mathbf{W} + \nabla S$, where S is a scalar. If this assumption is not made, and the term is the gradient of some scalar potential, Φ, then it would lead to the case of $\nabla \times \nabla \Phi$, which is identically zero.

In the following section, we make use of Equations (4.7) in order to re-derive the Induction Equations. For this derivation, the effects of the remaining two terms on the RHS of Equations (4.7) are regarded as negligible, as we only wish to study the effects and consequences of both the resistive- and battery terms on the evolution of the magnetic field in the Induction Equations.

4.1.2 Into Being from Zero: The Induction Equations $\times$ Biermann Battery

The inherent problem with generating magnetic fields from a set of zero initial conditions, particularly on cosmic scales, is that even though the Induction Equations admit $\mathbf{B} = \mathbf{0}$ as a perfectly valid solution, no fields will grow – thus, some initial "seed field" is required!

The battery term in Equations (4.7) was proposed by L. Biermann in 1950 [5], as one of the first examples of a cosmic battery; for this reason, this battery term is also known as the **Biermann battery term**. Considering Equations (4.7) together with the battery and resistive terms, we can re-derive the Induction Equations with this "violated" version of Ohm's Law, in the hopes of possibly being able to generate magnetic fields from absolute zero. A brief re-derivation of the Induction Equations follows.

As before, the Induction Equations come from the marriage of Faraday's and Ampère's Laws:

$$\begin{aligned} \nabla \times \mathbf{E} &= -\frac{\partial \mathbf{B}}{\partial t} \\ \nabla \times \mathbf{B} &= \mu_0 \mathbf{J} + \mu_0 \varepsilon_0 \frac{\partial \mathbf{E}}{\partial t}. \end{aligned} \tag{4.8}$$

Using the General Ohm's Law, given by Equation (4.7), we may substitute for $\mathbf{E}$ in Faraday's Law, giving:

$$\begin{aligned} -\frac{\partial \mathbf{B}}{\partial t} &= \nabla \times \mathbf{E} \\ \Rightarrow \frac{\partial \mathbf{B}}{\partial t} &= \nabla \times \left[\mathbf{v}_\mathrm{i} \times \mathbf{B} + \frac{\nabla p_\mathrm{e}}{e n_\mathrm{e}} - \frac{\mathbf{J}}{\sigma} \right]. \end{aligned} \tag{4.9}$$

From here, was may substitute for $\mathbf{J}$ from Ampère's Law, giving

$$\frac{\partial \mathbf{B}}{\partial t} = \nabla \times \left[\mathbf{v}_\mathrm{i} \times \mathbf{B} + \frac{\nabla p_\mathrm{e}}{e n_\mathrm{e}} - \frac{\nabla \times \mathbf{B}}{\sigma \mu_0} - \frac{1}{\sigma \mu_0} \frac{\partial \mathbf{E}}{\partial t} \right] \tag{4.10}$$

The temporal derivative term involving the electric field is called the **Faraday displacement current**, but can be neglected (due to the time-scales of the simulations being longer than $\sim 10^{-20}$s [10]). Thus, the Induction Equations finally read as

$$\boxed{\frac{\partial \mathbf{B}}{\partial t} = \nabla \times \left[\mathbf{v}_\mathrm{i} \times \mathbf{B} - \frac{\mathbf{J}}{\sigma} \right] + \nabla \times \left[\frac{\nabla p_\mathrm{e}}{e n_\mathrm{e}} \right],} \tag{4.11}$$

where we have made the identification once more that $\nabla \times \mathbf{B} = \mathbf{J}$, again assuming units of $\mu_0 = 1$.

Note that should we now impose the zero initial conditions mentioned previously, the Induction Equations would now allow a (weak) seed field to grow due to the presence of the battery term. Consider now the battery term on its own. If we assume that $p_\mathrm{e} = n_\mathrm{e} k_\mathrm{B} T$, via the Ideal Gas Law, then we may rewrite the last term in Equations (4.11) as:

$$\begin{aligned} \nabla \times \left[\frac{\nabla p_\mathrm{e}}{e n_\mathrm{e}} \right] &= \frac{k_\mathrm{B}}{e} \nabla \times \left[\frac{\nabla (n_\mathrm{e} T)}{n_\mathrm{e}} \right] \\ &= \frac{k_\mathrm{B}}{e} \nabla \times \left[\frac{T \nabla n_\mathrm{e} + n_\mathrm{e} \nabla T}{n_\mathrm{e}} \right] \\ &= \frac{k_\mathrm{B}}{e} \left[\nabla \times \left(\frac{T \nabla n_\mathrm{e}}{n_\mathrm{e}} \right) + \nabla \times \nabla T \right] \\ &= \frac{k_\mathrm{B}}{e} \left[\nabla \times (T \nabla \ln n_\mathrm{e}) \right], \end{aligned}$$

where the temperature-gradient term vanishes due to it being the curl of a gradient. The remaining curl term may then be expanded as

$$\begin{aligned}\nabla \times (T\nabla \ln n_{\rm e}) &= T\nabla \times \nabla \ln n_{\rm e} - \nabla \ln n_{\rm e} \times \nabla T \\ &= -\nabla \ln n_{\rm e} \times \nabla T,\end{aligned}$$

where we again are left with a vanishing curl-of-the-gradient term. The Induction Equations with the thermal battery term now then read as

$$\frac{\partial \mathbf{B}}{\partial t} = \nabla \times \left[\mathbf{v} \times \mathbf{B} - \frac{\mathbf{J}}{\sigma}\right] - \frac{k_{\rm B}}{e}\left[\nabla \ln n_{\rm e} \times \nabla T\right]. \tag{4.12}$$

These modifications to the battery term now cast it in a slightly more revealing light: if we wish to generate magnetic fields from zero, we require that the gradients of the electron number density and temperature *not* be parallel to each other initially – should this happen, the net contribution from this term will be identically zero. If we assume that we are dealing with a plasma consisting solely of purely ionized Hydrogen, and that its ionization factor, χ, is constant in space *and* that the temperature is the same for protons and electrons [10], then we may express the electron pressure, $p_{\rm e}$, electron number density, $n_{\rm e}$, and temperature, T, as the following [10]:

$$\begin{aligned}p_{\rm e} &= \frac{\chi p}{1+\chi} \\ n_{\rm e} &= \frac{\chi \varrho}{m_{\rm p}} \\ T &= \frac{p_{\rm e}}{n_{\rm e} k_{\rm B}}.\end{aligned}$$

The battery term may now be further simplified by incorporating these above expressions:

$$
\begin{aligned}
-\frac{k_{\mathrm{B}}}{e}\left[\nabla \ln n_{\mathrm{e}} \times \nabla T\right] &= -\frac{k_{\mathrm{B}}}{e}\left[\frac{\nabla\left(\chi\varrho/m_{\mathrm{p}}\right)}{m_{\mathrm{p}}/\chi\varrho} \times \nabla\left(\frac{p_{\mathrm{e}}}{n_{\mathrm{e}}k_{\mathrm{B}}}\right)\right] \\
&= -\frac{1}{e}\left[\frac{\nabla\varrho}{\varrho} \times \nabla\left(\frac{p}{1+\chi}\frac{m_{\mathrm{p}}}{\varrho}\right)\right] \\
&= -\frac{m_{\mathrm{p}}}{e(1+\chi)}\left[\frac{\nabla\varrho}{\varrho} \times \nabla\left(\frac{p}{\varrho}\right)\right] \\
&= -\frac{m_{\mathrm{p}}}{e(1+\chi)}\left[\frac{\nabla\varrho}{\varrho} \times \left(\frac{\nabla p}{\varrho} + p\nabla\left(\frac{1}{\varrho}\right)\right)\right] \\
&= -\frac{m_{\mathrm{p}}}{e(1+\chi)}\left[\frac{\nabla\varrho \times \nabla p}{\varrho^2}\right],
\end{aligned}
$$

yielding the final form of

$$
\boxed{\frac{\partial \mathbf{B}}{\partial t} = \nabla \times \left[\mathbf{v} \times \mathbf{B} - \frac{\mathbf{J}}{\sigma}\right] + \frac{m_{\mathrm{p}}}{e(1+\chi)}\left[\frac{\nabla p \times \nabla\varrho}{\varrho^2}\right].} \tag{4.13}
$$

Disregarding the two fundamental constants in front of the battery term, note that the ionization factor plays the role of "scaling" the magnitude of the fields that the battery term produces. Physically, a fully-ionized plasma (i.e. where $\chi = 1$) would produce the weakest magnetic fields, whilst a fully un-ionized plasma (i.e. where $\chi = 0$) would produce the strongest. The latter assumption of the value of χ may come as a contradiction, as we had initially considered it to by non-zero. However, any real plasma would never be fully un-ionized, meaning that the case where $\chi = 0$ may be regarded as a type of ideal limit. The early universe, however, is assumed to have had a high degree of ionization, making the latter case a possibly invalid assumption when wishing to simulate magnetogenesis in the very early epochs. Since we have effectively done away with the electron number density and temperature and are left instead with the scalar pressure and density, it is now required that the gradients of these latter scalar functions not be parallel to each other in order to produce magnetic fields from zero.

★

4.1.3 An Observation: The Induction Equations in Co-moving Form

When studying the temporal evolution of magnetic fields on cosmological scales, the Induction Equations must be modified in order to take into account the effects of the ever-expanding space. In their **non-resistive** co-moving form, the Induction Equations are given by [31]:

$$
\boxed{\frac{\partial \mathbf{B}}{\partial t} = \frac{1}{a}\nabla \times (\mathbf{v} \times \mathbf{B}) - 2\frac{\dot{a}}{a}\mathbf{B} + C\frac{1}{1+\chi}\frac{1}{a^2}\frac{\nabla p \times \nabla\varrho}{\varrho^2}.} \tag{4.14}
$$

Here, the constant C depends on, among others, $m_{\rm p}$ and e [31]. Note that the Induction Equations now also depend on the temporal evolution of the scale factor, a, which is described by the Friedmann Equation:

$$\boxed{\frac{\mathrm{d}a}{\mathrm{d}t} = H_0\sqrt{\frac{\Omega_{\rm rad}}{a^2} + \frac{\Omega_{\rm mat}}{a} + 1 - \Omega + \Omega_{\rm vac}a^2},} \tag{4.15}$$

where H_0 is the **Hubble Constant**, $\Omega_{\rm mat}$ is the **total matter density**, $\Omega_{\rm rad}$ the **total radiation density**, $\Omega_{\rm vac}$ the **vacuum energy density** or **cosmological constant** and Ω the **total energy density** or **curvature** of the universe. Approximate values for these quantities can be obtained from observation of anisotropies in the Cosmic Microwave Background (CMB).

Should the evolution of a cosmological magnetic field be studied, the Friedmann Equation would also have to be solved together with the standard set of MHD equations. Note that the other MHD equations may also carry a dependence on the scale factor, though we have only shown this as a brief example, using the Induction Equations.

★

4.1.4 Physical Significance of the Biermann Battery

The Biermann Battery is itself thought to be an astrophysical battery [55], though may also be thought of as a cosmological battery if the distance scale is correct, and addresses the problem of producing finite currents from absolute zero. As was seen in the derivation of the General Ohm's Law, this problem is addressed by assuming that positively- and negatively-charged particles do not share identical properties [55]. Using the assumed environment of a plasma consisting of fully-ionized Hydrogen, it is then obvious that the electrons generally tend to be more accelerated than the protons, due to their smaller mass, given some pressure gradient of the plasma. From here, a re-coupling electric field arises [55], inducing the time-varying magnetic field, via Faraday's Law.

Revisiting the argument of non-parallel gradients between electron number density and temperature made in deriving Equations 4.12, Section 4.1.2, it is suggested that the physics are entirely possible if one were to consider cosmic ionization fronts sweeping across arbitrarily-laid density fluctuations in the Intergalactic Medium (IGM) [55]. In these fronts, the temperature gradient is usually normal to the ionization front itself, but could also arise in a different direction if the density fluctuations are arbitrarily-laid. As before, the thermally-generated electric field will be produced, resulting in a time-varying magnetic field [55]. This is exactly the phenomenon originally proposed by Biermann [5],

thus the battery effect is known as the thermal battery [10]. In the scenario of IGM reionization with the Biermann Battery, numerical simulations such as those done by Gnedin *et al.* [17] and Kulsrud *et al.* [31], field strengths of approximately 3×10^{-20}G (in the case of the former work) have been observed in the simulation box [17, 55], as can be confirmed via a simple dimensional analysis of the battery term [55].

4.1.5 The Chaplygin Gas

The **Chaplygin Gas**, a hypothetical substance proposed by Chaplygin in 1992 [11], is primarily used in Cosmology as an alternative when modelling Dark Energy (e.g. [19]). It obeys an exotic EoS of the form

$$p = -\frac{\mathcal{B}}{\varrho}, \tag{4.16}$$

where $\mathcal{B}$ is assumed to be a positive constant. In some other related applications, the so-called **Generalised Chaplygin Gas** is also considered,

$$p = -\frac{\mathcal{B}}{\varrho^{\alpha}}, \tag{4.17}$$

where α is some positive constant obeying the constraint $0 < \alpha \leq 1$ [4, 19].

Observation and theoretical results both suggest that the universe has, over time, undergone different regimes. These past regimes are thought to primarily include Dark Matter dominance at higher redshifts and Dark Energy dominance at lower redshifts. If we use Equation (4.16) in the energy conservation equation in a homogeneous cosmological model [4, 6, 27], we are led to

$$\varrho(a) = \sqrt{\mathcal{B} + \frac{\mathcal{C}}{a^6}}, \tag{4.18}$$

where $\mathcal{C}$ is an integration constant [4, 6]. This shows that the Chaplygin Gas can naturally interpolate between Dark Energy and Dark Matter simply by sending $a \to \infty$ and $a \to 0$, respectively.

In line with our simulations, we consider magnetogenesis with the Chaplygin Gas EoS in order to assess the temporal evolution and resulting strength of the induced magnetic fields. For these purposes, we consider the magnetic fields induced by employing the EoS defined by Equation (4.16), where we choose $\mathcal{B} = 1$ to represent the pure Chaplygin Gas. We also introduce a modification of

the Chaplygin Gas by making the choice $\mathcal{B} = \mathcal{B}_0 T$, thus letting $\mathcal{B}$ be proportional to the temperature, where the constant $\mathcal{B}_0$ is dependent on the initial conditions. For our purposes, we make the choice $\mathcal{B}_0 = 1$. Our motivation for the choice of $\mathcal{B} = \mathcal{B}_0 T$ stems from the fact that it is known that the universe was initially very hot and cooled down over time. In addition to this, it is also known that the scalar pressure may also carry a dependence on the temperature, as is the case for the Ideal Gas law. The former statement then implies that we assume that magnetic fields were indeed present during the high-temperature epochs, although they would have been very weak. Note that the modified form of the Chaplygin Gas EoS does not necessarily hold for the early and late universe, as can be expected by inspection of Equation (4.18), but could possibly hold for a short period of time in-between these two scenarios.

4.2 Ideal Magnetogenesis and the Chaplygin Competition

In this section we present the results of simulations run with the PENCIL CODE involving the Induction Equations given by Equations (4.13). All results obtained here have assumed a **laboratory-type environment**, making no particular preference to any one of the universe's previous epochs, save the zero initial conditions, and a periodic computational box of dimensions $2\pi \times 2\pi \times 2\pi$, using 64^3 mesh points. Code units, rather than physical units, are primarily favoured. Three separate groups of simulations are done: the first dealing with magnetogenesis using varying values of the ionization fraction, χ (viz. $\chi = 0,\ 0.9$ and 0.99[1]) at constant η, the second dealing with the strength and evolution of the magnetic field produced using varying values of η and the third, dealing once more with the strength and evolution of the magnetic field produced using varying values of η, when making use of the Chaplygin Gas EoS. In all cases, the temporal growth of the rms time-averaged magnetic field flux density, B_{rms}, is assessed. A summary of key simulation parameters may be found in Table 4.1.

As mentioned in Section 3.3.3 of Chapter 3, the simulations performed here required modification of two of the code's evolution equations. In the following, we comment on these modifications to the relevant equations.

[1]Note that the case of $\chi = 1$ can also be considered.

4.2.1 Comments on the Navier-Stokes and Induction Equations

4.2.1.1 Numerical Forcing and the Navier-Stokes Equations

Due to the zero initial conditions imposed at the start of the simulations, some numerical forcing term is needed in order to generate the magnetic fields. Physically, this may correspond to a plasma developing instabilities whilst cooling down. When this happens, a coupling electric field then develops which then induces a time-varying magnetic field as per Faraday's Law (provided, of course, that this electric field actually has a curl, as explained in Section 4.1.2) [55].

In the PENCIL CODE, such numerical forcing enters through the Navier-Stokes Equations, via the term accounting for external forces. If this numerical forcing is not included in the simulation, then no magnetic fields are generated. As we do not wish for the fields to grow too quickly, we set the amplitude of the numerical forcing term to the arbitrary value of 10^{-5}, using a cosine-type forcing form.

4.2.1.2 Modifying the Navier-Stokes Pressure Term, $\nabla p/\varrho$

In Section 3.1.2 of Chapter 3, we mentioned that the pressure, p, entered into the system of evolution equations via the Navier-Stokes pressure term, $\nabla p/\varrho$. Here, we present a modification of this pressure term when the Chaplygin Gas EoS is assumed. Recall that this EoS is given by

$$p = -\frac{\mathcal{B}}{\varrho}, \tag{4.19}$$

where $\mathcal{B}$ is either constant or proportional to T. Applying the ∇-operator to the EoS then yields the following:

$$\begin{aligned} \nabla p &= -\nabla\left(\mathcal{B}\varrho^{-1}\right) \\ &= -\left(\varrho^{-1}\nabla\mathcal{B} + \mathcal{B}\nabla\varrho^{-1}\right) \\ &= -\frac{1}{\varrho}\left(\nabla\mathcal{B} - \mathcal{B}\nabla\ln\varrho\right), \end{aligned}$$

which implies:

$$\boxed{\frac{\nabla p}{\varrho} = \frac{1}{\varrho^2}\left(\mathcal{B}\nabla \ln \varrho - \nabla \mathcal{B}\right).} \tag{4.20}$$

4.2.1.3 The Induction Equations with a Battery Term, in terms of A

We finally make a brief commentary on the Induction Equations. Recalling that the PENCIL CODE solves the Induction Equations in terms of the magnetic vector potential, rather than the magnetic flux density, reduction to the former form is trivial. Note that both sides of the Induction Equations may be written as the curl a single vectorial quantity, and so we must set the result to zero. In a similar way, the battery term may also trivially be written in this form. This is done by expanding the following curl term:

$$\begin{aligned} \nabla \times \frac{\nabla p}{\varrho} &= \frac{1}{\varrho}\nabla \times p + \nabla\left(\frac{1}{\varrho}\right) \times \nabla p \\ &= -\frac{\nabla \varrho \times \nabla p}{\varrho^2} \\ &= \frac{\nabla p \times \nabla \varrho}{\varrho^2}. \end{aligned}$$

This is identically the battery term as seen in Equations (4.13)! Thus, we may write the Induction Equations with the Biermann battery term, finally, as

$$\boxed{\frac{\partial \mathbf{A}}{\partial t} = \mathbf{v} \times \mathbf{B} - \eta \mathbf{J} + \frac{1}{1+\chi}\frac{\nabla p}{\varrho},} \tag{4.21}$$

where we have once more reverted to the usage of the magnetic diffusivity, η. Note that the battery term is now identical to the pressure term found in the Navier-Stokes equations.

4.2.2 Results and Discussion

4.2.2.1 The Ideal Gas

Figure 4.1 presents the full-time evolution of B_{rms} for varying values of χ. As can be seen from Equations (4.21), the term involving χ acts as a coefficient to the battery term that is able to "amplify" the resultant fields that are produced. In this case, χ obeys the restriction $0 \leq \chi \leq 1$, with the case of

Run	$[\ln \varrho]_0$	$\mathbf{A}_0$	η	χ	$\mathbf{v}_0$	s_0	Forcing	Amplitude
1X	`zero`	`zero`	10^{-1}	0	`zero`	`nothing`	`cosx*cosy*cosz`	10^{-5}
2X	`zero`	`zero`	10^{-1}	0.9	`zero`	`nothing`	`cosx*cosy*cosz`	10^{-5}
3X	`zero`	`zero`	10^{-1}	0.99	`zero`	`nothing`	`cosx*cosy*cosz`	10^{-5}
1I	`zero`	`zero`	10	0	`zero`	`nothing`	`cosx*cosy*cosz`	10^{-5}
2I	`zero`	`zero`	10^{-1}	0	`zero`	`nothing`	`cosx*cosy*cosz`	10^{-5}
3I	`zero`	`zero`	10^{-2}	0	`zero`	`nothing`	`cosx*cosy*cosz`	10^{-5}
1C1	`zero`	`zero`	10^{-1}	0	`zero`	`nothing`	`cosx*cosy*cosz`	10^{-5}
2C1	`zero`	`zero`	10^{-2}	0	`zero`	`nothing`	`cosx*cosy*cosz`	10^{-5}
2CT	`zero`	`zero`	10^{-1}	0	`zero`	`nothing`	`cosx*cosy*cosz`	10^{-5}
3CT	`zero`	`zero`	10^{-2}	0	`zero`	`nothing`	`cosx*cosy*cosz`	10^{-5}

Table 4.1: Simulation parameters for magnetogenesis runs, assuming the various EoSs. Runs in the X-group concentrated on varying χ, those in the I-group concentrated on varying η, whilst those in the C1- and CT-groups concentrated on varying η, assuming either a normal ($\mathcal{B} = 1$) or temperature-proportional (modified; $\mathcal{B} = \mathcal{B}_0 T$) Chaplygin Gas EoS respectively. Here, all symbols retain their original meanings as outlined in Chapter 3, with subscript zeros indicating initial values for time-evolving parameters. Input given in `typewriter face` are valid PENCIL CODE *input parameter choices.*

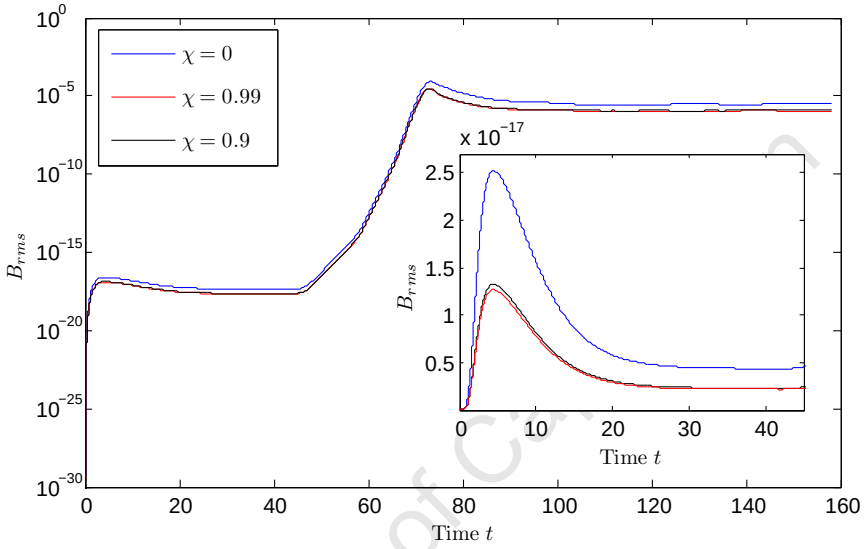

Figure 4.1: Full time-evolution of $B_{\rm rms}$ for the X-group of magnetogenesis runs. This group assumes an Ideal Gas EoS. Two growth maxima, followed by subsequent decay and an apparent steady state respectively are observed for the length of the run. It is evident that varying the value of the degree of ionization, χ, causes a very slight change in the strength of the magnetic field produced. The inset depicts the intermediate behaviour of time-evolution of $B_{\rm rms}$, using a linear scale on the y-axis in order to more clearly show the field strength's temporal behaviour. It is apparent that the field grows to a certain strength and then approaches a smaller, but finite value.

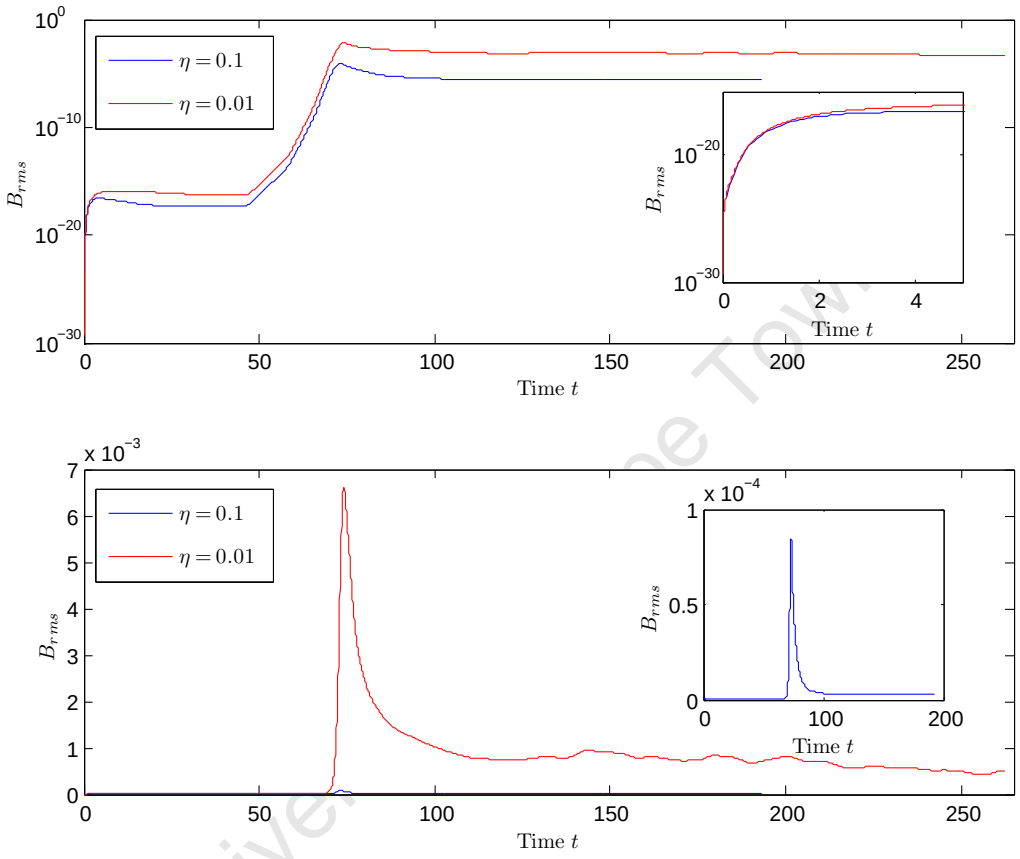

Figure 4.2: Full time-evolution of $B_{\rm rms}$ for two of the I-group of magnetogenesis runs. This group assumes an Ideal Gas EoS. On the top plot, the same two growth maxima as in Figure 4.1, followed by the respective decay and steady states are observed. The inset panel on this plot serves to show the growth of the field at early times. The plot on the bottom panel is the plot presented on the top panel, using a linear scale on the y-axis. The inset on this plot serves to show that a sharp, exponential-like growth in the field strength is observed for both choices of η. It is evident that the choice of η strongly affects the strength of the resulting field.

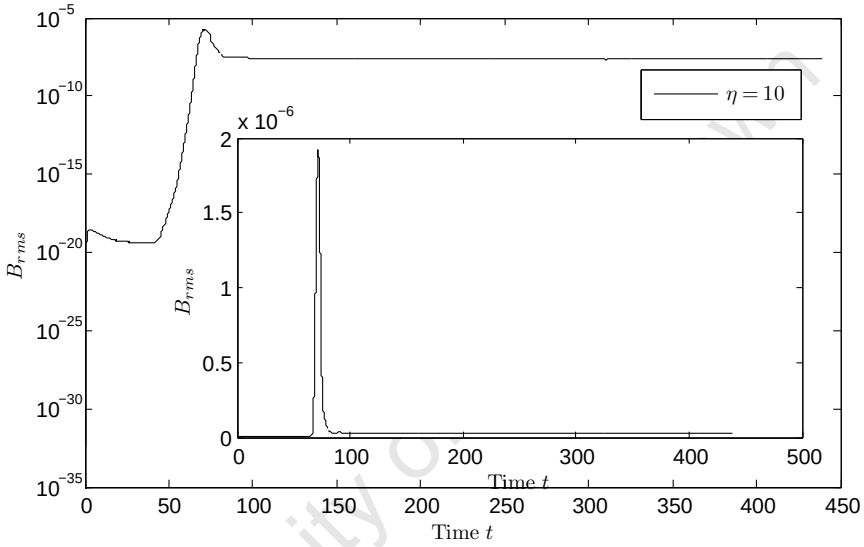

Figure 4.3: Full time-evolution of $B_{\rm rms}$ for two of the I-group of magnetogenesis runs. Here, $\eta = 10$. Two growth maxima, followed by subsequent decay, are again observed for the length of the run. The inset plot once more presents the main plot by making use of a linear scale on the y-axis. It is once again evident that the choice of η strongly affects the strength of the resulting field, with this field being noticeably weaker than its predecessors.

$\chi = 0$ considered as ideal. From examining Figure 4.1, it is immediately apparent that a fully non-ionized plasma produces the strongest magnetic fields over a period of time, whilst a fully-ionized plasma (not shown here) produces the weakest fields. Physically, the latter realisation makes sense, as the coefficient $1/(1+\chi)$ would evaluate to 0.5 for $\chi = 1$. As can be seen from Figure 4.1, the cases of $\chi = 0.9$ and 0.99 produce magnetic fields which appear to be very similar in terms of strength.

The inset in Figure 4.1 illustrates the intermediate-time evolution of the magnetic fields for the varying values of χ. It can be seen from here that the fields immediately begin growing from time $t = 0$ and reach a maximum that occurs around time $t \sim 4.5$, before beginning to decay monotonically to some minimum around time $t \sim 41.9$. After reaching this minimum value, the field enters an exponential growth phase around time $t \sim 45$ and reaches a global maximum around time $t \sim 73.2$. After this maximum is attained, the field immediately begins to decay to another local minimum occurring around time $t \sim 114.2$, after which an apparently persistent "steady-state" is reached around time $t \sim 127.3$.

We turn our attention now to Figure 4.2. Here, we have varied the value of η and once more observed the temporal evolution of B_{rms}. It is immediately apparent that smaller values of η tend to produce stronger magnetic fields. This is to be expected, as there is less magnetic diffusion in the system, allowing stronger fields to grow with time. Again, the same qualitative features of growth, decay, exponential growth, decay and then settling down to a persistent "steady-state" are observed, the only difference now being that the field strength of the "steady-state" settled into by B_{rms} is larger for $\eta = 0.01$, corresponding to the case where magnetic diffusion is much less. For the purposes of illustrating the importance of the value of η on the strengths of the resulting magnetic field strength, a run with the value of $\eta = 10$ was done. This result is presented in Figure 4.3. Once more, the same qualitative features noted before are observed, only now with the resulting field being much weaker than those produced with $\eta = 0.1$ and 0.01 respectively.

Can the temporal evolution behaviour of B_{rms} observed so far be explained in terms of the Induction Equations? Inspection of Equations (4.21) suggests that, initially, the growth of the field is supported by the battery and velocity terms (i.e. $\nabla p/\varrho$ and $\mathbf{v} \times \mathbf{B}$). During this regime, the diffusive term, $\eta\mathbf{J}$, would be small compared to its counterparts. Beyond times greater than $t \sim 4.5$, the resistive term possibly becomes large compared to its counterparts, causing the field to decay monotonically. This behaviour is not permanent, however, as the positive terms eventually become large compared to the resistive term, and the field enters an exponential growth phase (around $t \sim 45$). When the exponential growth phase completes, the diffusive term again possibly becomes large compared to its counterparts and the field once more begins to decay, appearing to level out to a "steady-state" at later times.

Ignoring the diffusive- and battery terms in Equations (4.21), it can be seen that a significant portion

of the magnetic field's growth could be attributed to the contribution made by the velocity-term, $\mathbf{v} \times \mathbf{B}$. This gives cause to also inspect the temporal evolution of the rms velocity field strength, v_{rms}, shown in Figure 4.4. Recall that for the Ideal Gas runs, the following qualitative features were observed in the temporal evolution of B_{rms} so far:

- Immediate growth from time $t = 0$ until around time $t \sim 4.5$, where a local maximum is reached.
- Monotonic decay beyond time $t \sim 4.5$ to a local minimum, occurring around time $t \sim 41$.
- A phase of exponential growth beginning around time $t \sim 45$, ending in a global maximum around time $t \sim 73.2$.
- Evident decay beyond the global maximum, until an apparently persistent "steady-state" is reached.

Let us now consider the temporal evolution behaviour of the velocity field.

The inset axes in Figure 4.4 illustrate the temporal evolution of v_{rms} for the various EoSs for early times. Examining the corresponding lines for the Ideal Gas EoS, it is evident that the velocity field itself also begins to grow immediately after time $t = 0$ and reaches an early local maximum around time $t \sim 0.6$, after which a phase of monotonic decay begins. This phase continues until a local minimum is reached around time $t \sim 43.3$. Beyond this time, a phase of exponential growth takes over (around $t \sim 48$) and results in a global maximum around time $t \sim 72.8$, after which there is once more a monotonic decay to another local minimum around time $t \sim 83.1$. Growth beyond this local minimum is very slight, reaching a maximum at time $t \sim 93.8$, after which an apparent steady-state sets in.

Evidently the velocity field exhibits the same qualitative features during its temporal evolution as the magnetic field does, though they tend to occur at different times. A summary of these is presented in Table 4.2. From the simulation results presented thus far, it is reasonable to assume that the magnetic- and velocity fields are in constant interaction with each other. Aside from inspection of the Induction Equations, this fact is found to be true and is elaborated on in Chapter 5. We now investigate the temporal evolution of the velocity field in an attempt to explain the temporal evolution observed for the magnetic field.

During the initial growth phase of the magnetic field, the velocity field is also seen to be undergoing growth, though it attains its first local maximum and monotonic decay phases much earlier than the magnetic field. The velocity field's initial decay does not seem to hamper the growth of the magnetic field, however, as it continues to grow until it attains its first local maximum. This continued growth,

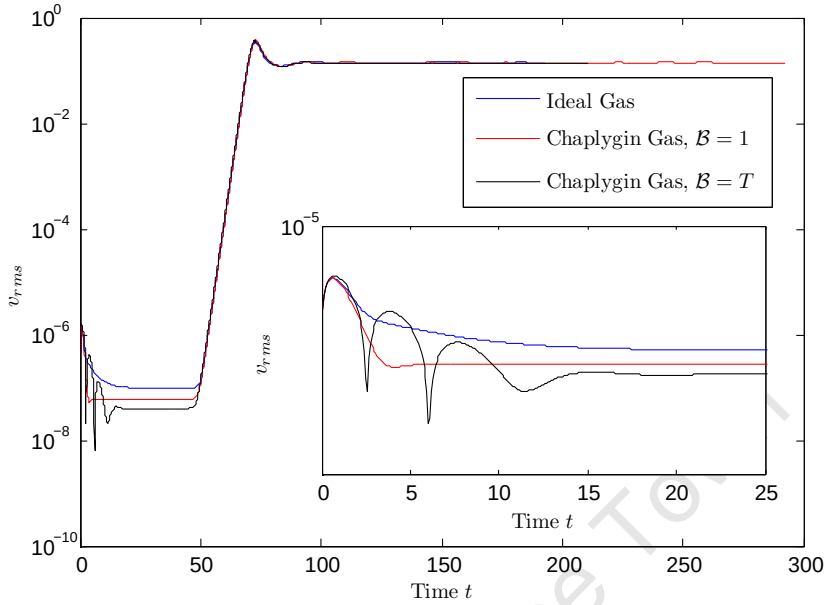

Figure 4.4: Full time-evolution of v_{rms} for the Ideal and Chaplygin Gas (1 and T) EoS groups. All plots were obtained from the solutions where $\eta = 0.1$. As can be seen, the evolution of the velocity fields only differ in the initial stages. After exponential growth, they display the same qualitative features, as well as similar strengths. This also holds true for the remaining velocity fields taken with $\eta = 0.01$.

Feature	v_{rms}	B_{rms}
Local Max. 1	0.6s	4.5s
Local Min. 1	43.3s	41.9s
Exponential Growth	48s	45s
Global Max.	72.8s	73.2s
Local Min. 2	83.1s	114.2s
Local Max. 2 (steady-state)	93.8s	127.3s

Table 4.2: Times indicating when the investigated variables v_{rms} and B_{rms} reach various features in their temporal evolution, as described in Section 4.2.2. All time units quoted are in PENCIL CODE *units.*

despite decay from the velocity field, could possibly be attributed to the presence of the battery term. True to form, however, the eventual monotonic decay phase begins and was originally attributed to the contribution made by the diffusive term in the Induction Equations. As the velocity field is still decaying by this point, it could be possible that its decay also aids in the decay of the magnetic field.

The exponential growth phase is then started first by the magnetic field, and followed by the velocity field; the early start possibly being due to the added presence of the battery term. It should be noted, however, that the exponential growth phase of the velocity field is much shorter than that of the magnetic field, also ending first. The magnetic field on the other hand, increases its strength by $\sim$13 orders of magnitude, compared to its velocity counterpart which increases its strength by only $\sim$6 orders of magnitude. It is suggested that this massive "growth spike" in the strength of the magnetic field could largely be supported by the velocity field's exponential growth and, to some extent, the battery term.

The post-maximum decay follows again for both fields. The magnetic field's decay is once more attributed to the action of the diffusive term, but could also be aided by the decay of the velocity field itself. Beyond these times, both fields appear to enter a persistent "steady-state" phase which lasts for the remainder of the simulation. In terms of the interaction between the magnetic- and velocity fields, it could be suggested that the magnetic field's strength has stopped growing because the velocity field has entered a steady-state. The effects of the battery term may now also be negligible and largely negated by the effects of the diffusion term.

4.2.2.2 The Chaplygin Gases

We now turn to a discussion of the qualitative features of the temporal evolution behaviour of the magnetic fields that are generated via the Chaplygin Gas EoS. These are presented in Figure 4.5 and are plotted together with the Ideal Gas magnetic field evolution for purposes of easy comparison. As can be seen from Figure 4.5, although much of the general qualitative temporal evolution behaviour seen in the Ideal Gas case is also seen here, there are some marked differences. These are discussed below.

For the choice $\mathcal{B} = 1$, the magnetic field immediately begins to grow from time $t = 0$ as before, but this time does *not* attain a local maximum and then decay, as was observed in the Idea Gas case. Instead, the field now does one of two things: for the choice $\eta = 0.1$, a temporary "steady-state" is reached which is then followed by exponential growth beginning around time $t \sim 32.9$; for the choice $\eta = 0.01$, the field simply continues growing at a rate slightly slower than that seen during its initial upshoot and then also enters an exponential growth phase, also around time $t \sim 32.9$. The exponential

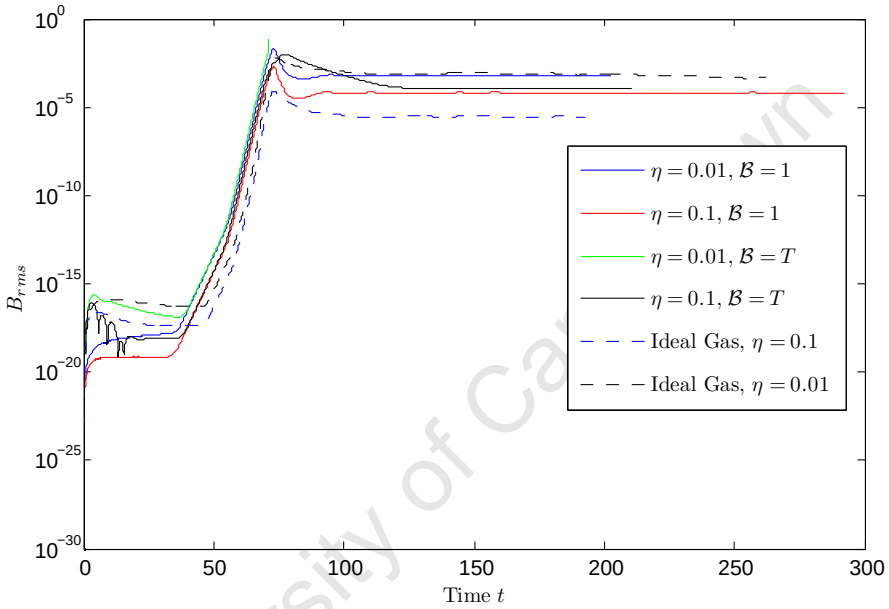

Figure 4.5: Full time-evolution of $B_{\rm rms}$ for two of the C1- and CT-groups of magnetogenesis runs. These groups assume a Chaplygin Gas EoS for two different choices of $\mathcal{B}$. Two growth maxima, followed by subsequent decay, are observed for the length of the run. Time evolutions for B_{rms} assuming the Ideal Gas EoS with the corresponding values of η are also plotted for comparison. It is evident that the cases of $\eta = 0.01$ produce the stronger magnetic fields.

growth phase then terminates for both fields at a global maximum occurring around time $t \sim 73$. Both fields then immediately begin a short exponential decay phase terminating in a local minimum (the first and last one for both of these fields) around times $t \sim 82.8$ and $t \sim 85$ for the choices of $\eta = 0.1$ and 0.01 respectively, finally followed by a slight growth phase which immediately runs into the familiar, persistent, "steady-state" phase also observed in the Ideal Gas case.

Unlike its counterparts, the case of $\mathcal{B} = T$ exhibits some peculiar behaviour. It must be noted that for the choice $\eta = 0.01$, the simulation terminated itself due to the time-step naturally becoming too short[2]. It is possible that the temporal evolution behaviour of this case could be better-investigated with a finer spatial resolution. Its short-lived rise to the global maximum aside, the magnetic field appears to mimic the Ideal Gas case in the sense that it also grows to a local maximum, occurring around time $t \sim 4.1$. After this, a short phase of exponential decay is entered, terminating in a local minimum around time $t \sim 36.7$, after which the exponential growth phase immediately begins. Termination then occurs around time $t \sim 72$, seemingly before the field attains its global maximum. For the choice of $\eta = 0.1$, the magnetic field also initially begins growing from time $t = 0$, reaching a local maximum around time $t \sim 3.2$. Beyond this, a series of spurious "hops" are noted, each ending in a separate local maximum and beginning again from a local minimum. This odd behaviour is also seen in the corresponding velocity field evolution (see Figure 4.4). Four "hops" later, the magnetic field then appears to enter a very brief "steady-state", after which the exponential growth phase begins, around time $t \sim 36.3$. This phase terminates in a global maximum around time $t \sim 77.1$, after which another phase of exponential decay begins, ending around time $t \sim 134.5$ and immediately leading into the familiar persistent "steady-state", also observed in the Ideal Gas case.

The magnetic- and velocity field's tendencies to "hop" during their early temporal evolution phases can potentially be cause for concern: it may be that these spurious "hops" are, in fact, a numerical artifact, and could thus possibly be dealt with using finer spatial resolution, or they could be due to some other unknown mechanism. The numerical explanation does appear to be slightly dubious, though, as one should expect to observe similar behaviour in the case of $\eta = 0.01$ – and none is observed. Further simulation can then only confirm this behaviour.

4.2.2.3 Ideal Gas or Chaplygin Gas?

The last issue to consider now is how all of the generated magnetic fields compare in terms of strength. This is presented once more in the rather busy Figure 4.5.

[2]This is a rather useful feature of the adaptive time-integration employed by the PENCIL CODE.

Considering the case of $\eta = 0.1$, and before the exponential growth phase, it can clearly be seen from Figure 4.5 that the temperature-dependent Chaplygin Gas magnetic field dominates in terms of strength, followed closely by the Ideal Gas; the regular Chaplygin Gas magnetic field turning out to be the weakest. The temperature-dependent gas field once more dominates during the exponential growth phase, closely followed by the regular Chaplygin Gas field; the Ideal Gas magnetic field now ending up as being the weakest. After the global maximum (taken once more by the temperature-dependent Chaplygin Gas field), the temperature-dependent Chaplygin Gas field is noted to have the highest strength when the "steady-state" phase is entered, followed closely by the regular Chaplygin Gas field; the Ideal Gas field is once more the weakest.

The case of $\eta = 0.01$ presents similar behaviour: the times before the exponential growth phase are now initially dominated by the temperature-dependent Chaplygin Gas and Ideal Gas magnetic fields respectively; the regular Chaplygin Gas still turning out to be the weakest. The exponential growth phase is again dominated by the two Chaplygin Gas fields, with the temperature-dependent gas field once more turning out to be the strongest. During the "steady-state" phase, the Ideal Gas and regular Chaplygin Gas fields now dominate, with the Ideal Gas field appearing to be the stronger of the two – different to what was observed in the $\eta = 0.1$ case. It is interesting to note here, that although the magnetic diffusivities are different, the strengths of the two Chaplygin Gas fields from the $\eta = 0.1$ case are not very far off from those of the Ideal- and Chaplygin Gas fields for the case of $\eta = 0.01$, the former fields possibly being only two or three orders of magnitude smaller.

Overall, the simulation results would suggest that magnetogenesis using the Chaplygin Gas EoS could actually produce magnetic fields that are decent contenders to those produced by the Ideal Gas EoS. In particular, the temperature-dependent Chapylgin EoS could potentially produce strong magnetic fields, though further numerical investigation into its anomalous behaviour at early times and towards the end of the exponential growth phase (for the case of a small η) warrants further investigation.

★

With the discussion of magnetogenesis with the Ideal and Chaplygin Gas EoSs now complete, we turn our attention to the odd behaviour of the magnetic fields' evolution for large times. Recalling that *all* of the magnetic fields (as well as their corresponding velocity fields) appeared to enter an apparently persistent "steady-state" phase after the decay following their exponential growth phases, the following two questions now arise:

- Have the systems, in fact, reached a persistent "steady-state"?
- Would it be possible to predict what would happen to the magnetic field strengths *without*

necessarily running the simulations for a much longer period of time[3]?

In order to formulate a proper answer to these questions, we have to consider *how* magnetic fields actually grow. This specifically gives cause to examine mechanisms that perform, and are involved in, the amplification of the strength of a magnetic field over a given period of time. This is considered in the following chapter, where we also attempt to answer both of the above questions.

4.3 Closing Points

In this chapter, we addressed the problem of generating magnetic fields from absolute zero initial conditions. This was done by first introducing the two-fluid approximation of an ideal plasma and then by considering one of its consequences: the thermal battery. Magnetogenesis via the battery term was then discussed in detail. The Induction Equations were also re-derived, now incorporating the battery term. By assuming to relate the electron pressure to number density via the Ideal Gas Law, the thermal nature of the battery term was revealed and confirmed. In accordance with the PENCIL CODE requirements, the Induction Equations were also expressed in terms of the magnetic vector potential field, $\mathbf{A}$.

The Chapylgin Gas, along with its exotic EoS, was then introduced. Consideration to its relevance and significance in Cosmology was mentioned, and intentions for its use in the magnetogenesis simulations conducted were stated. For the purposes of simulations conducted, merely the temporal evolution behaviour and strengths of the resulting magnetic fields were deemed to be of interest.

Additional comments on the inclusion of a numerical forcing term in the Navier-Stokes Equations were made. It was found that this term was necessary for the numerical generation of magnetic fields. We assumed that this would correspond to an ideal plasma developing instabilities (cf. the recoupling electric field with curl, as mentioned earlier), allowing the magnetic fields to come into existence.

Results on the main simulations for this chapter were then presented and discussed at length. It was found that changing the values of the ionization fraction and magnetic diffusivity affected the resulting strengths of the magnetic fields that were produced. All magnetic fields simulated appeared to share similar qualitative behaviour that included an initial upshoot in strength, slight decay, exponential growth to a global maximum and then decay into an apparent "steady state". It was also found that the temperature-dependent Chaplygin Gas appeared to generate the strongest magnetic fields when

[3]Of course this assumes that one would know how long to run the simulation for. In other words, knowing how long *long enough* would be.

the “steady state” phase commenced.

Finally, two questions regarding the apparent “steady-state” phases observed in all of the magnetic field evolutions were posed. These specifically asked whether the fields *did*, in fact, enter a truly persistent “steady-state” and whether it would be possible to determine what would happen to the magnetic field strengths without having to run the simulations for an extended period of time. In an attempt to provide an answer to these two questions, motivation for further study into the amplification mechanisms acting on magnetic fields was made.

★

With the study of magnetogenesis complete, we now move on to the study of the mechanisms involved in the amplification of magnetic fields.

Chapter 5

Dynamos, TurBulence and Amplification

I have harnessed the cosmic rays and caused them to operate a motive device.

— Nikola Tesla (1856 – 1943)

From the simulations conducted in Chapter 3, we observed that the initial magnetic field's strength appeared to decay over time and would eventually reach zero in the limit $t \to \infty$. In Chapter 4, simulation results showed that the magnetic field generated from the zero initial conditions underwent a period of exponential growth in strength after a finite time and then eventually decayed slightly and reached an apparently persistent "steady state". We are now in a position to ask the following questions:

- *Why* does a magnetic field of a given strength decay over a period of time?
- *How* is a magnetic field amplified in strength?

Any mechanism that amplifies the strength of a given magnetic field is known as a **dynamo**. The latter question, then motivates the need to perform a study of the **dynamo process** – the process by which a magnetic field's strength is amplified. In order to avoid decaying in strength, the magnetic field must be subjected to this dynamo process.

From the previous chapter, we know that one way of generating the original "seed fields" in nature is via the thermal effects of cosmic ionization fronts spreading through the IGM [55] (i.e. the thermal battery) during the early epochs. These seed fields would have been subjected to some sort of dynamo process by the still-forming galaxies [10, 55], thereby growing in strength.

The study of the dynamo process firstly requires us to understand the energetics that are at play; that is, we must understand how various types of energy (turbulent, thermal, kinetic or potential) are converted into magnetic energy and how this conversion affects the rest of the energy reservoirs in the system. It can be shown that the dynamo process primarily favours the conversion of kinetic energy to magnetic energy [10], whilst the remaining energy reservoirs remain largely in the background. As both Astrophysical and Cosmological dynamo action is known to occur on both large *and* small length scales[1], the study of the flow of energy within the system also leads to an understanding of how the energy flows between these scales; this is commonly referred to as the **energy cascade**.

Equally important to the understanding of the dynamo process, is the reverse process: what can cause a dynamo stop working, or, what can cause a dynamo *not* to work at all. It shall be seen that the reverse process is very subtle in its operation, largely relying on too much magnetic diffusion within the system, or a velocity field that is not suited to perform the required amplification of the magnetic field.

[1]Here, we mean length scales that are considered large or small in relevance to either Astrophysics or Cosmology, whichever context is under consideration.

This chapter first focusses on a brief study of the two main participants in dynamo energetics, and how their generation affects their respective reservoirs. Following this, the Perfect Conductor and Free Decay limits of the Induction Equations are considered and their relationship to the dynamo process is stated. We then consider some elements of the reverse-dynamo process by way of the Cowling and Zel'dovich Antidynamo theorems. A brief qualitative discussion on the Zel'dovich Stretch-Twist-Fold dynamo is then made, and its relevance to the general dynamo problem is stated. Two simple examples of dynamos are then considered: the kinematic dynamo and the small-scale, turbulent dynamo. The results of several simulations that serve to illustrate and quantify the theory of the dynamos discussed then follows, finally ending in a brief discussion of the simulations done in Chapter 4 within the context of dynamo theory.

5.1 ...And All That Energetics

Dynamos amplify magnetic field strengths by converting kinetic energy into magnetic energy. This exact process occurs by different means, specific to the environment under consideration, and is very briefly discussed later on. In the following, we derive the equations governing the energetics of a dynamo and comment on how they demonstrate the amplification of magnetic field strengths via energy exchange.

5.1.1 The Magnetic Energy Equation

In order to derive the Magnetic Energy Equation, we need to know the work done by the Lorentz Force, $\mathbf{J} \times \mathbf{B}$, within some volume, $\mathcal{V}$, that is bounded by a surface, S. In symbols the work done by the Lorentz Force is given by:

$$\text{Rate of Work} = \mathbf{v} \cdot (\mathbf{J} \times \mathbf{B}) .$$

Using the vector dot-product identities, we rewrite this as:

$$\mathbf{v} \cdot (\mathbf{J} \times \mathbf{B}) = -\mathbf{J} \cdot (\mathbf{v} \times \mathbf{B}) . \tag{5.1}$$

Recalling the single-fluid approximation version of Ohm's Law:

$$\mathbf{J} = \sigma\left(\mathbf{E} + \mathbf{v} \times \mathbf{B}\right),$$

we may substitute for the term $\mathbf{v} \times \mathbf{B}$, leaving:

$$\begin{aligned} \mathbf{v} \cdot (\mathbf{J} \times \mathbf{B}) &= -\mathbf{J} \cdot \left(\frac{\mathbf{J}}{\sigma} - \mathbf{E}\right) \\ \mathbf{v} \cdot (\mathbf{J} \times \mathbf{B}) &= -\frac{\mathbf{J}^2}{\sigma} - \mathbf{J} \cdot \mathbf{E}. \end{aligned} \tag{5.2}$$

Recalling that $\mu_0 \mathbf{J} = \nabla \times \mathbf{B}$, the last term may then be expressed as

$$\begin{aligned} \mathbf{J} \cdot \mathbf{E} &= \frac{1}{\mu_0} \left[(\nabla \times \mathbf{B}) \cdot \mathbf{E}\right] \\ &= \frac{1}{\mu_0} \left[\nabla \cdot (\mathbf{B} \times \mathbf{E}) + \mathbf{B} \cdot (\nabla \times \mathbf{E})\right] \\ &= \frac{1}{\mu_0} \left[\nabla \cdot (-\mathbf{E} \times \mathbf{B}) + \mathbf{B} \cdot \left(-\frac{\partial \mathbf{B}}{\partial t}\right)\right], \end{aligned} \tag{5.3}$$

by application of the vector cross-product and Vector Calculus identities, as well as Faraday's Law. Substituting this into Expression (5.1) and rearranging terms, we are left with

$$\frac{1}{\mu_0} \mathbf{B} \cdot \frac{\partial \mathbf{B}}{\partial t} = -\mathbf{v} \cdot (\mathbf{J} \times \mathbf{B}) - \frac{\mathbf{J}^2}{\sigma} - \frac{1}{\mu_0} \nabla \cdot (\mathbf{E} \times \mathbf{B}) \tag{5.4}$$

Consider now taking the temporal derivative of the quantity $\mathbf{B}^2 = \mathbf{B} \cdot \mathbf{B}$:

$$\frac{1}{2} \frac{\partial \mathbf{B}^2}{\partial t} = \mathbf{B} \cdot \frac{\partial \mathbf{B}}{\partial t}. \tag{5.5}$$

Substituting this result into Equation (5.4) and integrating over the volume, $\mathcal{V}$, leaves us with:

$$\int_{\mathcal{V}} \frac{1}{2\mu_0} \frac{\partial \mathbf{B}^2}{\partial t} \mathrm{d}\mathcal{V} = -\int_{\mathcal{V}} \mathbf{v} \cdot (\mathbf{J} \times \mathbf{B}) \, \mathrm{d}\mathcal{V} - \frac{1}{\sigma} \int_{\mathcal{V}} \mathbf{J}^2 \mathrm{d}\mathcal{V} - \frac{1}{\mu_0} \int_{\mathcal{V}} \nabla \cdot (\mathbf{E} \times \mathbf{B}) \, \mathrm{d}\mathcal{V}. \tag{5.6}$$

Invoking the Divergence Theorem on the last term yields the full statement of the **Magnetic Energy Equation**:

$$\boxed{\frac{1}{2\mu_0}\frac{\mathrm{d}}{\mathrm{d}t}\int_{\mathcal{V}}\mathbf{B}^2\mathrm{d}\mathcal{V} = -\int_{\mathcal{V}}\mathbf{v}\cdot(\mathbf{J}\times\mathbf{B})\,\mathrm{d}\mathcal{V} - \frac{1}{\sigma}\int_{\mathcal{V}}\mathbf{J}^2\mathrm{d}\mathcal{V} - \frac{1}{\mu_0}\int_{\partial\mathcal{V}}(\mathbf{E}\times\mathbf{B})\cdot\mathrm{d}\mathbf{S},} \tag{5.7}$$

where the partial temporal derivative on $\mathbf{B}^2$ has been made a total derivative and pulled out of the volume integral, due to the fact that $\mathbf{B}^2$ represents the magnitude of the magnetic flux density field, whose integral can only now vary with time. The three terms on the RHS of Equation (5.7) represent the Lorentz Force, Ohmic losses and losses via Poynting Flux, respectively [10]. The term on the LHS represents the magnetic energy within a confined volume, $\mathcal{V}$. Examining the equation, we then see that the only way to increase the magnetic energy is to do work *against* the Lorentz Force, whilst also ensuring that the work done exceeds the Ohmic and Poynting Flux losses.

5.1.2 The Kinetic Energy Equation

Consider the Navier-Stokes Equations of the form:

$$\varrho\frac{\partial\mathbf{v}}{\partial t} + \varrho\mathbf{v}\cdot\nabla\mathbf{v} = -\nabla p + \frac{1}{\mu_0}\mathbf{J}\times\mathbf{B} + \mathbf{g} + \mathbf{F}_{\text{visc}}, \tag{5.8}$$

where the Lagrangian derivative has been expanded into its Eulerian counterpart, the term $\mathbf{F}_{\text{visc}}$ subsumes all viscous body forces acting on the fluid, and all other symbols retain their usual meanings. Taking the dot product of each term with $\varrho\mathbf{v}$ [10], and simplifying, yields:

$$\frac{1}{2}\varrho\frac{\partial\mathbf{v}^2}{\partial t} + \varrho\mathbf{v}\cdot(\mathbf{v}\cdot\nabla\mathbf{v}) = -\left[\nabla\cdot(p\mathbf{v}) - p\nabla\cdot\mathbf{v}\right] + \frac{1}{\mu_0}\mathbf{v}\cdot(\mathbf{J}\times\mathbf{B}) + \mathbf{v}\cdot\mathbf{g} + \mathbf{v}\cdot\mathbf{F}_{\text{visc}}. \tag{5.9}$$

If we assume a closed volume, $\mathcal{V}$, as we did with the Magnetic Energy Equation, we may integrate each term and further simplify the result. Additionally, we shall also assume stress-free boundary conditions [10], so that any resulting surface terms immediately vanish. This yields:

$$\frac{1}{2}\frac{\mathrm{d}}{\mathrm{d}t}\int_{\mathcal{V}}\varrho\mathbf{v}^2\mathrm{d}\mathcal{V} = \int_{\mathcal{V}}p\nabla\cdot\mathbf{v}\mathrm{d}\mathcal{V} + \frac{1}{\mu_0}\int_{\mathcal{V}}\mathbf{v}\cdot(\mathbf{J}\times\mathbf{B})\,\mathrm{d}\mathcal{V} + \int_{\mathcal{V}}\mathbf{v}\cdot\mathbf{g}\mathrm{d}\mathcal{V} + \int_{\mathcal{V}}\mathbf{v}\cdot\mathbf{F}_{\text{visc}}\mathrm{d}\mathcal{V}, \tag{5.10}$$

where the first term in parentheses on the RHS of Equation (5.9) was re-expressed as a vanishing surface integral by invocation of the Divergence Theorem after integration, and the temporal derivative was once more made total by way of the same reasoning as before. Depending on the assumed form of $\mathbf{F}_{\text{visc}}$, more vanishing surface terms may or may not appear; if we choose the form

$$\mathbf{F}_{\text{visc}} = \nu\left(\nabla^2\mathbf{v} + \frac{1}{3}\nabla\nabla\cdot\mathbf{v} + 2\mathbb{S}\cdot\nabla\ln\varrho\right),$$

then it may be shown [10] that the **Kinetic Energy Equation** may finally be expressed as:

$$\boxed{\frac{1}{2}\frac{\mathrm{d}}{\mathrm{d}t}\int_{\mathcal{V}}\varrho\mathbf{v}^2\mathrm{d}\mathcal{V} = \int_{\mathcal{V}}p\nabla\cdot\mathbf{v}\mathrm{d}\mathcal{V} + \frac{1}{\mu_0}\int_{\mathcal{V}}\mathbf{v}\cdot(\mathbf{J}\times\mathbf{B})\,\mathrm{d}\mathcal{V} + \int_{\mathcal{V}}\mathbf{v}\cdot\mathbf{g}\mathrm{d}\mathcal{V} - 2\int_{\mathcal{V}}\nu\varrho\mathbb{S}^2\mathrm{d}\mathcal{V}.} \tag{5.11}$$

5.1.3 Magnetic Energy $\rightleftharpoons$ Kinetic Energy

Examining the Kinetic and Magnetic Energy Equations, we note that the generation of both magnetic and kinetic energy are related through the Lorentz Force. We may equate Equations (5.7) and (5.11), arriving at the following important result:

$$\boxed{\frac{1}{2\mu_0}\frac{\mathrm{d}}{\mathrm{d}t}\int_{\mathcal{V}}\mathbf{B}^2\mathrm{d}\mathcal{V} + \ldots = -\frac{1}{2}\frac{\mathrm{d}}{\mathrm{d}t}\int_{\mathcal{V}}\varrho\mathbf{v}^2\mathrm{d}\mathcal{V} - \ldots.} \tag{5.12}$$

Equation (5.12) shows that the generation of magnetic energy goes at the expense of kinetic energy, and vice versa. When considering an astrophysical setting, four distinct energy reservoirs involved in the dynamo process can be identified: thermal energy, kinetic energy, potential energy and magnetic energy [10]. A simple example of the energetics at play is seen in Figure 5.1, which was adapted from [9]. In this simulation, the dynamo under consideration is driven convectively via luminosity entering the system from below and providing thermal energy. This thermal energy is then converted into kinetic energy via the work done by adiabatic compression [10], which in turn, is converted into magnetic energy via work done against the Lorentz Force. Both of these energies are converted into thermal energy again via Viscous and Joule heating respectively [10], whilst work done by buoyancy mediates the energy transfer between the kinetic and potential energy reservoirs [9].

5.2 Induction's Perfect, Free Decay Limits

Next, we consider two important limits of the Inductions Equations: the **Perfect Conductor Limit** and the **Free Decay Limit**, investigating their consequences for the dynamo problem.

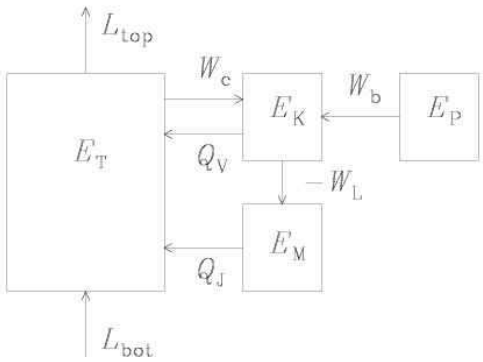

Figure 5.1: The flow of energy in a typical convection dynamo simulation. The dynamo operates convectively via the luminosity that enters from below. Work done through adiabatic compression converts thermal energy into kinetic energy, which is then converted into magnetic energy by doing work against the Lorentz Force. Adapted from [9].

5.2.1 Perfect Conduction

If we send the magnetic diffusivity, η, to zero in the Induction Equations, so that the magnetic field does not decay, we are left with the case of a perfect conductor. The Induction Equations then become:

$$\frac{\partial \mathbf{B}}{\partial t} = \nabla \times (\mathbf{v} \times \mathbf{B}) \,. \tag{5.13}$$

The term, $\mathbf{v} \times \mathbf{B}$, is also known as the **induction term** and in its curl form, may be expanded via the use of Vector Calculus identities to yield:

$$\nabla \times (\mathbf{v} \times \mathbf{B}) = \mathbf{v} (\nabla \cdot \mathbf{B}) - \mathbf{B} (\nabla \cdot \mathbf{v}) + (\mathbf{B} \cdot \nabla) \mathbf{v} - (\mathbf{v} \cdot \nabla) \mathbf{B}.$$

The first of these terms immediately vanishes due to the divergenceless condition on $\mathbf{B}$, leaving us with three more terms which in turn represent advection, stretching and compression respectively. The Induction Equations may now be written as:

$$\frac{\partial \mathbf{B}}{\partial t} = -\mathbf{B} (\nabla \cdot \mathbf{v}) + (\mathbf{B} \cdot \nabla) \mathbf{v} - (\mathbf{v} \cdot \nabla) \mathbf{B}. \tag{5.14}$$

Moving the advection term to the LHS allows for the Induction Equations to be expressed as:

$$\frac{\mathrm{D}\mathbf{B}}{\mathrm{D}t} = (\mathbf{B}\cdot\nabla)\,\mathbf{v} - (\mathbf{v}\cdot\nabla)\,\mathbf{B}, \tag{5.15}$$

where we have immediately recognised the definition of the Lagrangian Derivative after the rearrangement of terms. We may now make use of the Continuity Equation, Equation (3.1), to get rid of the velocity field divergence term, leaving:

$$\frac{\mathrm{D}\mathbf{B}}{\mathrm{D}t} = (\mathbf{B}\cdot\nabla)\,\mathbf{v} + \left(\frac{\mathrm{D}\ln\varrho}{\mathrm{D}t}\right)\mathbf{B}, \tag{5.16}$$

from whence we may once more rearrange terms to give:

$$\frac{\mathrm{D}\mathbf{B}}{\mathrm{D}t} - \frac{\mathbf{B}}{\varrho}\frac{\mathrm{D}\varrho}{\mathrm{D}t} = (\mathbf{B}\cdot\nabla)\,\mathbf{v}. \tag{5.17}$$

Multiplying both sides of the equations by a factor of $1/\varrho$ gives:

$$\frac{1}{\varrho}\frac{\mathrm{D}\mathbf{B}}{\mathrm{D}t} - \frac{\mathbf{B}}{\varrho^2}\frac{\mathrm{D}\varrho}{\mathrm{D}t} = \frac{1}{\varrho}(\mathbf{B}\cdot\nabla)\,\mathbf{v} \tag{5.18}$$

and we thus deduce that:

$$\boxed{\frac{\mathrm{D}}{\mathrm{D}t}\left(\frac{\mathbf{B}}{\varrho}\right) = \frac{1}{\varrho}(\mathbf{B}\cdot\nabla)\,\mathbf{v}.} \tag{5.19}$$

This is identical to the evolution equation for an infinitesimal separation vector, $\delta\mathbf{x}$, effectively allowing us to draw the following analogy: in the case of the separation vector evolution, we know that if two particles start off on the same line of force (or field line, in the case of a magnetic field), then they will remain on that line for all time. This property is known as the **frozen flux effect** of the induction term [10], or, **Alfvén's Frozen Flux Theorem** [25]. In other words, the magnetic field lines are simply frozen into the fluid and are carried in the same fashion for all time. We shall return to this idea when considering the Zel'dovich Dynamo.

5.2.2 Free Decay

Assuming the stationary case, letting $\mathbf{v} = \mathbf{0}$, the Induction Equations reduce to:

$$\frac{\partial \mathbf{B}}{\partial t} = \eta \nabla^2 \mathbf{B}. \tag{5.20}$$

This case was simulated numerically in Section 3.4.1 of Chapter 3 and shall now be shown to be true from the point of view of analysis of the Induction Equations. If we were to assume solutions of the form $\mathbf{B}(\mathbf{x}, t) = \mathbf{B}_\alpha(\mathbf{x}) e^{p_\alpha t}$, where the $\mathbf{B}_\alpha$ are all eigenfunctions corresponding to complex eigenvalues, p_α, then we may substitute these into the Induction Equations, regressing them to:

$$\begin{aligned} \frac{\partial}{\partial t}\left(\mathbf{B}_\alpha e^{p_\alpha t}\right) &= \eta \nabla^2 \mathbf{B}_\alpha e^{p_\alpha t} \\ \Rightarrow \left[\nabla^2 - \frac{p_\alpha}{\eta}\right] \mathbf{B}_\alpha &= \mathbf{0}, \end{aligned} \tag{5.21}$$

which is a version of the **Helmholtz Equation**. Consider some stationary conducting region, $\mathcal{R}$, bounded by a surface, S. On the outside of this region, we have the condition $\nabla \times \mathbf{B} = \mathbf{0}$ from Electrostatics, as well as $\mathbf{B}$ being a dipole field in the limit as $r \to \infty$ (i.e. $B \sim 1/r^3$ [38]).

It is clear from Equations (5.21) that each of the components of the magnetic field $\mathbf{B}$ follow the exact same Diffusion Equation, allowing us only to consider one particular component of the field, whilst being assured that the result will hold for the remaining components. We consider the x-component of the field and denote it, $B_{\alpha,x}$. The equations now take the simpler form:

$$\frac{p_\alpha}{\eta} B_{\alpha,x} = \nabla^2 B_{\alpha,x}. \tag{5.22}$$

Proceeding to multiply both sides of Equation (5.22) by $B_{\alpha,x}$ and integrating over the region, $\mathcal{R}$, gives:

$$\frac{p_\alpha}{\eta} \int_{\mathcal{R}} B_{\alpha,x}^2 \mathrm{d}\mathcal{R} = \int_{\mathcal{R}} B_{\alpha,x} \nabla^2 B_{\alpha,x} \mathrm{d}\mathcal{R}. \tag{5.23}$$

Here, we have pulled out the eigenvalues and magnetic diffusivity, due to neither of them being spatially-dependent by nature of the problem under consideration. The integral on the RHS of Equation (5.23) may be expanded by use of Green's First Identity, yielding

$$\frac{p_\alpha}{\eta} \int_{\mathcal{R}} B_{\alpha,x}^2 \mathrm{d}\mathcal{R} = \oint_{\partial\mathcal{R}} B_{\alpha,x} \left(\nabla B_{\alpha,x} \cdot \mathbf{n}\right) \mathrm{d}S - \int_{\mathcal{R}} \left(\nabla B_{\alpha,x}\right)^2 \mathrm{d}\mathcal{R}. \tag{5.24}$$

The surface term conveniently vanishes by the assumption that the field vanishes on the boundary of the region, leaving the remaining volume integral which is clearly positive-definite. Rearranging for the eigenvalues, p_α, finally leaves us with

$$\boxed{p_\alpha = -\frac{\eta \int_{\mathcal{R}} (\nabla B_{\alpha,x})^2 \, \mathrm{d}\mathcal{R}}{\int_{\mathcal{R}} B_{\alpha,x}^2 \mathrm{d}\mathcal{R}}.} \tag{5.25}$$

We have now shown for the x-component of the magnetic field, that all of the eigenvalues, p_α, are negative, leading to an inevitable decay to zero of the initial condition at large times for this component of the field. The same procedure may be repeated for the other field components, showing that the eigenvalues for those components also lead to a field component that decays to zero at large times. Effectively, the *entire* field decays at all times for this limit of the Induction Equations, which is exactly what was shown numerically in Section 3.4.1 of Chapter 3. As before, this result is also very important and we return to it when considering the Zel'dovich Antidynamo Theorem in Section 5.3.2.

5.2.3 Halfway to Turbulence: The Magnetic Reynolds Number, R_m

One final consideration is now made of the Induction Equations. In all cases, it is important to know the relative contributions from all of the terms in the Induction Equations (stated below once more for convenience), especially when dynamo action (or the onset of it) is being considered.

$$\frac{\partial \mathbf{B}}{\partial t} = \nabla \times (\mathbf{v} \times \mathbf{B}) - \eta \nabla \times \nabla \times \mathbf{B}. \tag{5.26}$$

As mentioned before, the first term on the RHS of Equations (5.26) is known as the induction term, whist the second is known as the diffusion term. Performing a dimensional analysis on the Induction Equations [12] by replacing the temporal derivative by a factor of $1/\tau$ and the spatial derivatives by a factor of $1/l$, where τ and l are time- and length scales which, respectively, characterise the temporal and spatial evolution of the magnetic- and velocity fields, we are left with

$$\frac{B_*}{\tau} = \frac{v_* B_*}{l} - \frac{\eta B_*}{l^2}, \tag{5.27}$$

where B_* and v_* are 'typical' values of the magnetic- and velocity fields, appropriate to the problem under consideration [12]. Taking the ratio of the first term to the second, we define the **magnetic Reynolds number**, R_m, of the problem as:

$$\boxed{R_m = \frac{v_* B_*}{l} \times \frac{l^2}{\eta B_*} = \frac{v_* l}{\eta},} \tag{5.28}$$

which is a dimensionless quantity that characterises the importance of induction to diffusion in the problem under consideration[2]. When it is very large, induction tends to dominate over diffusion, and the effects of the diffusion term may be regarded as negligible. This behaviour echoes the perfect conductor limit of the Induction Equations. The converse states that when this quantity is small, diffusion is dominant, resembling the free decay limit of the Induction Equations.

The importance of R_m is more readily seen when the Induction Equations are recast in a non-dimensional form [25], whence may define the following scaled variables and derivative operators:

$$\begin{aligned} t &= \frac{l_*}{v_*}\tilde{t} \\ \mathbf{x} &= l_* \tilde{\mathbf{x}} \\ \mathbf{v} &= v_* \tilde{\mathbf{v}} \\ \nabla &= \frac{1}{l_*}\tilde{\nabla} \\ \frac{\partial}{\partial t} &= \frac{v_*}{l_*}\frac{\partial}{\partial \tilde{t}}, \end{aligned}$$

where the bold-faced quantities with overhead tildes are *not* tensors, as per our usual notation, but rather are dimensionless fields. As before, all quantities with a subscript asterisk represent 'typical' length- and velocity scale values, respectively, applicable to the problem under consideration. The Induction Equations are now recast as:

$$\frac{\partial \mathbf{B}}{\partial \tilde{t}} = \tilde{\nabla} \times (\tilde{\mathbf{v}} \times \mathbf{B}) + \frac{\tilde{\nabla}^2 \mathbf{B}}{R_m}, \tag{5.29}$$

where R_m is defined exactly as before [25]. Due to the sheer size of astrophysical objects, however, R_m should always expected to be large.

When operating in the regime $R_m \ll 1$, the diffusion term dominates the evolution; we may replace the temporal derivative once more with the factor $1/\tau$ as before and, thus, define the quantity, τ_η, as

[2] Actually, like the fluid Reynolds number, the magnetic Reynolds number is also seen as a property of the flow in the problem under consideration and not strictly an inherent property of the problem itself.

$$\boxed{\tau_\eta = \frac{l_*^2}{\eta},} \tag{5.30}$$

which is called the **magnetic diffusion timescale** [12]. This timescale tells us how long it would take for a magnetic field to diffuse out of a particular volume. For astrophysical objects, this timescale is often horrendously large, at times even some orders of magnitude larger than the current age of the universe, reaffirming the fact that magnetic fields should indeed be visible in astrophysical objects today. In the opposite limit, $R_m \gg 1$, the induction term dominates the evolution; as before we may then define the quantity, τ_t, as

$$\boxed{\tau_t = \frac{l_*}{v_*},} \tag{5.31}$$

called the **turnover timescale associated with the flow**, $\mathbf{v}$ [12]. This timescale is used to characterise the progression of dynamo action in various flows, many of which are usually turbulent. We shall return to and expand upon this idea in Section 5.6 when we discuss small-scale, turbulent dynamos.

★

The magnetic Reynolds number plays an important role in the dynamo problem, being one of the key factors in determining whether dynamo action will or will not take place for a given flow and/or field-pair. This happens in the regime $R_m \gg 1$, so that induction dominates over diffusion. Two bounding theorems by Childress and Backus respectively [25], are in place to classify when one may expect dynamo action to occur based on the value of R_m. Both of these theorems assure only that dynamo action will *not* occur if R_m is below a certain threshold value – above this threshold, dynamo action may or may not occur.

★

A key question regarding the value of R_m is whether the solutions to the Induction Equations obtained will remain finite in the limit $R_m \to \infty$ and is known as the **Fast Dynamo Problem** [10]. Expanding the induction term in Equations (5.26), the Induction Equations may be written as

$$\frac{\mathrm{D}\mathbf{B}}{\mathrm{D}t} = \mathbf{B}\cdot\nabla\mathbf{v} + \frac{\nabla^2\mathbf{B}}{R_m}.$$

We may now argue as follows [25]:

Let time be scaled on the flow turnover timescale as we defined in Expression (5.31). When the

flow is in a steady state, then we may expect the magnetic field to grow exponentially like $\mathbf{B} \sim e^{pt}$, where p is the complex eigenvalue alluded to in Section 5.2.2 and shall be expanded on in Section 5.5. Considering the limit $R_m \to \infty$, we are left with two distinct possibilities. The first says that if:

$$\boxed{\lim_{R_m \to \infty} \Re\{p\}(R_m) = p_0 > 0,} \tag{5.32}$$

then the dynamo is called a **fast dynamo**. If, on the other hand:

$$\boxed{\lim_{R_m \to \infty} \Re\{p\}(R_m) = p_0 < 0,} \tag{5.33}$$

then the dynamo is called a **slow dynamo**.

Fast dynamos all grow on the flow turnover timescale (hence them being called *fast*), unlike their slow counterparts which rely on the effects magnetic diffusion and thus its timescale as well [25]. A classic qualitative example of what is considered to be a fast dynamo is the **Zel'dovich Stretch-Twist-Fold Dynamo**. It is to be noted that fast dynamos, though they offer high growth rates, are only meaningful in the linear approximation and break down once non-linear effects begin to modify the flow [10].

5.3 Ant(i/e)dynamos

We now consider two important results regarding dynamo action and the maintenance of a magnetic field via dynamo action. From now on, we shall refer to a given velocity field as being a **flow**, a given magnetic field as being a **field**.

As can be deduced from the previous discussion, not every flow is capable of acting as a dynamo. Much consideration was given to this when astronomers tried to explain the 11-year solar cycle, as well as the maintenance of global solar and terrestrial magnetic fields. We use the idea of the dynamo-shortfalls of certain flows and consider now two important theorems which serve to outline when a given flow will *not* produce a dynamo effect. These results are collectively known as the **Antidynamo Theorems**.

5.3.1 Cowling's Antidynamo Theorem

This result was formulated by Cowling in the short paper, *The Magnetic Field of Sunspots* (1933) [14], responding to Larmor's theory on the formation of sunspots. We do not cover these results in any great detail – it is beyond the scope of this dissertation – opting instead for a brief, qualitative discussion of the result itself.

Theorem (Cowling's Antidynamo). *"... it is impossible that an axially symmetric field shall be self-maintained"* — Cowling (1933) [14].

Proof: Cowling's Argument, as adapted from [14]. The proof of this theorem is itself very detailed and uses a proof by contradiction to show that in a steady state, for a given fluid density, ϱ, electrostatic potential, U, and conductivity, σ, one cannot find solutions to the equations:

$$\begin{aligned} \nabla \cdot (\varrho \mathbf{v}) &= 0 \\ \mathbf{J} &= \sigma(\mathbf{v} \times \mathbf{H} - \nabla U) \\ \nabla \cdot \mathbf{H} &= 0 \\ \nabla \times \mathbf{H} &= 4\pi \mathbf{J}, \end{aligned}$$

such that the velocity field, $\mathbf{v}$ and magnetic intensity field, $\mathbf{H}$ are both finite everywhere [14]. The statement of the result in the theorem then immediately follows from the contradiction obtained.

□

Another slightly less complicated way of proving the statement is by employing the method used by Charbonneau [12]. Assuming that no magnetic field sources exist outside some volume in space, we consider an axially-symmetric flow and magnetic field and study their dynamo capabilities.

Proof: As adapted from [12]. Working in spherical polar co-ordinates, we may decompose the magnetic- and velocity fields into their poloidal and toroidal components [12] as:

$$\begin{aligned}\mathbf{v}(r,\theta) &= \frac{1}{\varrho}\nabla\times(\Phi(r,\theta)\mathbf{e}_\phi)+\varpi\Omega(r,\theta)\mathbf{e}_\phi \\ \mathbf{B}(r,\theta,t) &= \nabla\times(A(r,\theta,t)\mathbf{e}_\phi)+B(r,\theta,t)\mathbf{e}_\phi.\end{aligned}$$

From this decomposition, Φ represents a stream function, $\varpi = r\sin\theta$ represents the co-ordinate system's Jacobian and the $\mathbf{e}_\phi$'s represents one of the co-ordinate system's fundamental basis vectors. Together, Φ and A define the poloidal components of their respective fields. The toroidal components of the fields are defined by B (which automatically respects the divergenceless condition of $\mathbf{B}$ by construction) and the angular fluid velocity, Ω, respectively.

By substituting this decomposition into the Induction Equations, it may be shown that two separate evolution equations for the magnetic vector potential- and magnetic flux density components (i.e. A and B) can be found. These are given by [12]:

$$\frac{\mathrm{D}\varpi A}{\mathrm{D}t} = \varpi\eta\left[\nabla^2 A-\frac{A}{\varpi^2}\right] \tag{5.34}$$

$$\frac{\mathrm{D}}{\mathrm{D}t}\left(\frac{B}{\varpi}\right) = \frac{\eta}{\varpi}\left[\nabla^2 B-\frac{B}{\varpi^2}\right]-\left(\frac{B}{\varpi}\right)\nabla\cdot\mathbf{v}_p+\mathbf{B}_p\cdot\nabla\Omega. \tag{5.35}$$

Here, $\mathbf{v}_p$ and $\mathbf{B}_p$ denote the poloidal components of the flow and field respectively, as they have been defined above. In addition, it was also assumed that the magnetic diffusivity, η, remains constant in space.

The evolution equation for A is once more a diffusion equation, and was shown to decay to zero in Section 5.2.2.

As the evolution equation for B takes the evolution equation for A into account via the term $\mathbf{B}_p\cdot\nabla\Omega$, and we have already shown that A decays to zero, the aforementioned equation will eventually lose its "source". The divergence term involving $\mathbf{v}_p$ is automatically zero if an incompressible flow is assumed and is also negligible as long as the flow remains subsonic [12]. Eventually, B itself then also meets its timely demise, showing that an axially symmetric flow indeed cannot maintain an axially symmetric field.

□

5.3.2 Zel'dovich's Antidynamo Theorem

The antidynamo theorem proposed by Zel'dovich in his work, *The magnetic field in the two-dimensional motion of a conducting turbulent fluid* (1957) [60], focusses on ruling out dynamo action for planar, compressible flows within the Cartesian co-ordinate system. Again, we do not delve into too much detail, opting once more for a brief qualitative discussion of the result and its proof. Though the original paper by Zel'dovich was not able to be found in any library, online or otherwise, the reader may find a more generalised result of the original antidynamo theorem in Zel'dovich and Ruzmaĭkin [61].

Theorem (Zel'dovich's Antidynamo). *An incompressible, steady, planar flow in the Cartesian geometry in a bounded volume, where the magnetic field vanishes at the boundaries, cannot support dynamo action.*

Proof: As adapted from [12]. Consider the flow defined by:

$$\mathbf{v}(x,y,z) = v_x(x,y,z)\mathbf{e}_x + v_y(x,y,z)\mathbf{e}_y,$$

which exists in some volume, $\mathcal{V}$, bounded by a surface, S, with the stipulations on the magnetic field as given above.

Following the method given in [12] once more, one may show that, for the field's z-component, the standard diffusion equation given by:

$$\frac{\mathrm{D}B_z}{\mathrm{D}t} = \eta\nabla^2 B_z \tag{5.36}$$

is obtained. From Section 5.2.2, we already know that this leads to a field which will eventually decay to zero on the diffusive timescale. We shall show this once more, but now not consider the eigenvalues of the equation as we have before.

Multiplying the diffusion equation through by B_z, and integrating over the volume under consideration, we obtain:

$$\frac{1}{2}\int_{\mathcal{V}} \frac{\mathrm{D}B_z^2}{\mathrm{D}t}\mathrm{d}\mathcal{V} = \int_{\mathcal{V}} \eta B_z \nabla^2 B_z \mathrm{d}\mathcal{V} \tag{5.37}$$

$$\frac{1}{2}\int_{\mathcal{V}} \frac{\mathrm{D}B_z^2}{\mathrm{D}t}\mathrm{d}\mathcal{V} = -\eta \int_{\mathcal{V}} (\nabla B_z)^2 \mathrm{d}\mathcal{V} + \oint_{\partial\mathcal{V}} B_z (\nabla B_z \cdot \mathbf{n}) \mathrm{d}S. \tag{5.38}$$

Here, Green's First Identity was once again used to expand the RHS integrand of Equation (5.37). Due to the initial assumption that the field vanishes on the boundary of the volume, the surface term on the RHS of Equation (5.38) vanishes. As the remaining gradient integrand always remains positive, we are left with:

$$\boxed{\frac{1}{2}\int_{\mathcal{V}} \frac{\mathrm{D}B_z^2}{\mathrm{D}t}\mathrm{d}\mathcal{V} = -\eta \int_{\mathcal{V}} (\nabla B_z)^2 \mathrm{d}\mathcal{V},} \tag{5.39}$$

implying once more that B_z will decay on the diffusive timescale. Thus, the field's z-component vanishes.

By decomposing the remaining two-dimensional field into its solenoidal and potential components (this may be seen in [12]), it is possible to show that they, too, obey a diffusion-like equation, implying that they, too, decay on the resistive timescale. Thus, the planar velocity flow described originally cannot sustain dynamo action. The full details of the proof of this theorem are argued in detail by Charbonneau [12] and involve considering the timescales (both resistive and diffusive) on which the various diffusion equations described above decay.

□

5.4 Where it all Began: The Zel'dovich Stretch-Twist-Fold Dynamo

The **Zel'dovich Stretch-Twist-Fold (STF) dynamo**, also known as the **Vainshtein and Zel'dovich Flux Rope Dynamo** [12], is a theoretical dynamo model that was proposed by Vainshtein and Zel'dovich in their 1972 work, *Origin of Magnetic Fields in Astrophysics (Turbulent "Dynamo" Mechanisms)* [57]. We outline its significance in Dynamo Theory, as well as its operation, in the following.

Although it is simple in its description, the model is ubiquitous in the field of Dynamo Theory, and is also thought to be a qualitative example of what a fast dynamo is [10].

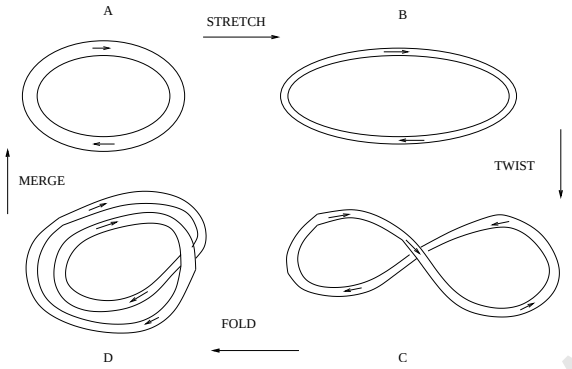

Figure 5.2: Illustration of the Zel'dovich STF dynamo algorithm. This algorithm forms the basis on which all dynamos are thought to operate. Adapted from [10].

The operation of the dynamo algorithm depends solely on the continual stretching, twisting and folding of a closed magnetic flux tube (or rope), that is embedded within a conducting medium, in order to amplify the resulting magnetic field [10, 12]. The algorithm proceeds as follows (the reader may refer to Figure 5.2 for a visual reference):

1. The flux tube is first stretched to twice its length, whilst also being compressed in such a way that its original volume is preserved [10] (A→B). As can be recalled from the Frozen Flux Theorem (Equations (5.19)), this stretching and corresponding compression of the flux tube both doubles the field strength *and* conserves the magnetic flux [10, 12].

2. The flux tube is then twisted once, so that it now looks like a figure of eight [10] (B→C). This is done so that in the final step of the algorithm, the magnetic field lines may be pointing in the same direction and thus add coherently, instead of cancelling out due to pointing in opposing directions [10, 12]. In the context of dynamo operation, the former type of folding is commonly referred to as **constructive folding**, whilst the latter is referred to as **destructive folding** [12].

3. The figure of eight is then folded over so that there are now *two* flux loops, instead of the original *one* [10, 12] (C→D). Note that because the magnetic field in both loops always points in the same direction (this is due to the twist step, as described above), the flux through any plane that intersects these two loops is now *double* than what would have originally been found had there been only one flux loop [10, 12].

4. The two flux loops are now merged into a single flux loop whose magnetic field strength is now double that of the original configuration [10] (D→A). It is important to note that it is not strictly necessary to perform this step immediately after completing Step 3; indeed, Steps 1 – 3 may be performed many times before the final merging step is taken [10, 12].

The Stretch-Twist-Fold (STF) algorithm may be repeated up to n times, with the field itself growing by a factor of two after every iteration completes. After n times, the field strength would turn out to have grown by a factor of 2^n [10]. If each of the STF-steps require a time, τ_{STF}, to complete, then the magnetic field growth rate of the STF algorithm may given by $\tau_{\mathrm{STF}}^{-1} \ln 2$ [10]. As this growth rate is apparently independent of the magnetic diffusivity, η, the STF model may be classified as a fast dynamo [10].

The STF model highlights some important features of dynamo action: firstly, the initial stretching step requires shearing motions within the fluid in order to stretch the flux tube, whilst the twist-step shows that the flux tube needs to enter the third spatial dimension in order for the step to complete successfully [10]. Thus, dynamo action requires three dimensions, as well as shear, to operate successfully. One final point deserves mention as well: if the merge step is not taken after a sufficient number of STF-iterations, the dynamo's growth rate may be retarded due to strong Lorentz forces that develop within the kinks and twists of the flux tube due to the preceding twisting and folding motions [10]; this typically occurs when the kinematic phase of the dynamo's operation is complete [10].

5.5 A (Slow) Means to an End: The Kinematic Dynamo

5.5.1 A Formal Definition of Sorts

The Kinematic Dynamo Problem assumes some given velocity field, $\mathbf{v}$, which is independent of time. This approximation removes the need to solve the Navier-Stokes Equations as was done in the previous chapter. This approximation, however, does not necessarily leave a simpler problem. We specifically look at the so-called **slow dynamos**, where magnetic diffusion is crucial to the operation of the dynamo [10].

Assuming a given velocity field, we may look for solutions to the Induction Equations of the form:

$$\mathbf{B} = \mathbf{B}_0(\mathbf{x}, t)e^{pt};\ \mathbf{B}_0 \to 0 \text{ as } \mathbf{x} \to \infty,$$

where the quantity $p \in \mathbb{C}$ and may be written as $p = \varsigma + j\omega$, and it itself is a complex eigenvalue corresponding to the eigenfunction $\mathbf{B}_0$; additionally, $\Re\{p\} = \varsigma$ is the growth rate, $\Im\{p\} = \omega$ is the frequency and j is the imaginary unit [25].

Substituting the *ansatz* into the Induction Equations, leaves an eigenvalue problem. Each of the eigenmodes, *ergo*, eigenfunctions, $\mathbf{B}_0$, have a corresponding eigenvalue, p. In most cases, oscillatory solutions are obtained for most choices of the growth rate, ς, but, there exist a small subset of eigenvalues that have $\varsigma > 0$ leading to dynamo action [25]. It should be noted that for eigenvalues with $\varsigma < 0$, only decaying solutions are obtained – these may possibly be thought of as "antidynamo solutions" – which will inevitably decay to zero at large times. Any initial condition that contains modes with $\varsigma > 0$ will have these modes dominating the solution at large times, leading to the desired growth, characteristic of a dynamo solution [25].

5.5.2 The Roberts Flow Dynamo

The Roberts Flow Dynamo, conceived by Roberts in his works *Spatially Periodic Dynamos* (1970) [43] and *Dynamo Action of Fluid Motions with Two-Dimensional Periodicity* (1972) [44], serves as an interesting compliment to both the Cowling and Zel'dovich antidynamo theorems.

This dynamo relies on a rather peculiar velocity field to amplify weak seed magnetic fields and, as it is heavily reliant on the amount of magnetic diffusion present, is a slow dynamo. The velocity field for this dynamo is usually described in terms of a stream function, $\psi = \psi(x, y)$, and is a **periodic flow** [10, 12]. Following the example given in [12], the stream function and velocity field are given by:

$$\psi(x, y) = \cos x + \sin y \tag{5.40}$$

$$\mathbf{v}(x, y) = \frac{\partial \psi}{\partial y}\mathbf{e}_x - \frac{\partial \psi}{\partial x}\mathbf{e}_y + \psi \mathbf{e}_z, \tag{5.41}$$

where the $\mathbf{e}_i$'s, as usual, represent the Cartesian basis vectors. Note that this flow is independent of the z-co-ordinate, though its z-component is itself *not* zero. Thus, even though the flow may be planar in the sense that it has no z-dependence, it does have three non-zero components. Because of this feature, the flow "escapes" the condition laid down by the Zel'dovich Antidynamo Theorem which stipulates that a planar flow shall not generate dynamo action [12].

Cowling's Antidynamo Theorem now also poses a potential problem, as it assures that no axially-symmetric magnetic field can be maintained by an axially-symmetric flow. However, the flow under consideration is *not* axially-symmetric, solving one part of the Cowling problem. In order to get

around the problem of an axially-symmetric field, we shall simply have to stipulate that the magnetic field depend on all three spatial co-ordinates [12]. As both of the antidynamo theorems are now, in a sense, "satisfied", we should expect a dynamo from the proposed flow.

Another important feature of the flow may be noted by computing the curl of the flow, $\nabla \times \mathbf{v}$. It is trivial to show that $\mathbf{v} \times \nabla \times \mathbf{v} = \mathbf{0}$ for this specific flow, where one may identify the **vorticity** of the flow as $\boldsymbol{\omega} \equiv \nabla \times \mathbf{v}$. Thus, the vorticity of the flow is everywhere parallel to the flow itself. Any flow exhibiting this property is said to be **maximally helical** (in the sense of kinetic helicity) and is also known as a **Beltrami Flow** [10, 12, 44]. In general, Beltrami Flows satisfy the condition:

$$\nabla \times \mathbf{v} = \alpha \mathbf{v}, \tag{5.42}$$

where α is some numerical constant [12]. A plot of the flow defined by Expressions (5.40) and (5.41) is shown in Figure 5.3. Note that the flow is divided into separate "cells" by lines called **separatrices**, which meet each other at **stagnation points** [12]. Because of this segregation of the flow into smaller cells, it is also known as the **Roberts Cell Flow** [12]. These seemingly odd features of the flow play an important role in the dynamo's amplification mechanism, which is briefly discussed later.

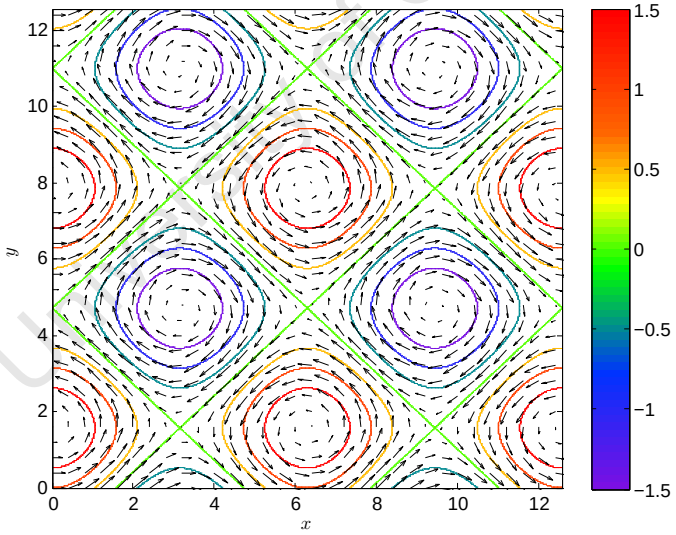

Figure 5.3: The velocity field streamlines for the z-component of the velocity field for the Roberts Flow Dynamo, as defined by Expressions (5.40) and (5.41). In the xy-plane, it is apparent that the flow is periodic. The diagonal lines (separatrices) separate this flow into separate "cells", hence this flow also being called the Roberts Cell Flow. Arrows indicate the direction of the flow in each cell.

We again seek separable solutions to the Induction Equations which are now of the form:

$$\mathbf{B}(x, y, z, t) = \mathbf{B}_0 e^{jk_z z}, \tag{5.43}$$

where k_z is some initially-specified wave vector that points in the z-direction and $\mathbf{B}_0$ is some complex eigenfunction [12]. When substituting this into the Induction Equations, we find that $\mathbf{B}_0$ obeys the evolution equations defined by [12]:

$$\frac{\mathrm{D}\mathbf{B}_0}{\mathrm{D}t} = (\mathbf{B}_0 \cdot \nabla)\mathbf{v} - jk_z v_z \mathbf{B}_0 + \frac{(\nabla^2 - k_z^2)\mathbf{B}_0}{R_m}, \tag{5.44}$$

supplemented with periodic boundary conditions for $\mathbf{B}_0$. These may be solved numerically to study the temporal growth of $\mathbf{B}_0$.

By performing an analysis on the field and flow given by Expressions (5.40) and (5.41), it is possible to determine how the given flow works to amplify the seed magnetic field [12]. Here, we give a brief qualitative explanation [12]:

Consider an initial magnetic field line that is directed in the x'-direction, crossing a separatrix in the flow, as shown in part (a) of Figure (5.4). As time progresses, the field line experiences exponential stretching in the y'-direction, effectively inducing a field component in this direction. There is danger here, as the induced component of the field changes polarity as it crosses the separatrix – this may lead to destructive folding [12]. However, we had originally specified the flow to also have a z-component and it is this flow component which negates the effects of destructive folding [12]. Note from Figure (5.3) that the z-component of the flow changes its sign across the separatrices. Consider now the initial position of several x'-directed field lines, as shown in part (b) of Figure (5.4). As time progresses, the z-component of the flow causes these x'-directed field lines to shear in the z-direction, essentially bringing the points of opposing polarity to come close to each other (see part (c) of Figure (5.4), eventually producing a new field that points in the y'-direction [12]. This new y'-directed field then serves as a seed field which will be stretched and sheared, eventually producing a new field that is once more x'-directed [12].

In this manner, the dynamo algorithm proceeds in a closed cycle, with the rate at which new fields in a particular area are being produced being directly proportional to the field strength in that area; as per the form of the solution to the Induction Equations, these fields also grow exponentially [12]. In terms of the action of the given flow, this exponential growth of the new fields would occur in the region of the stagnation points in the flow itself, showing that they are indeed of paramount importance to the amplification process [12].

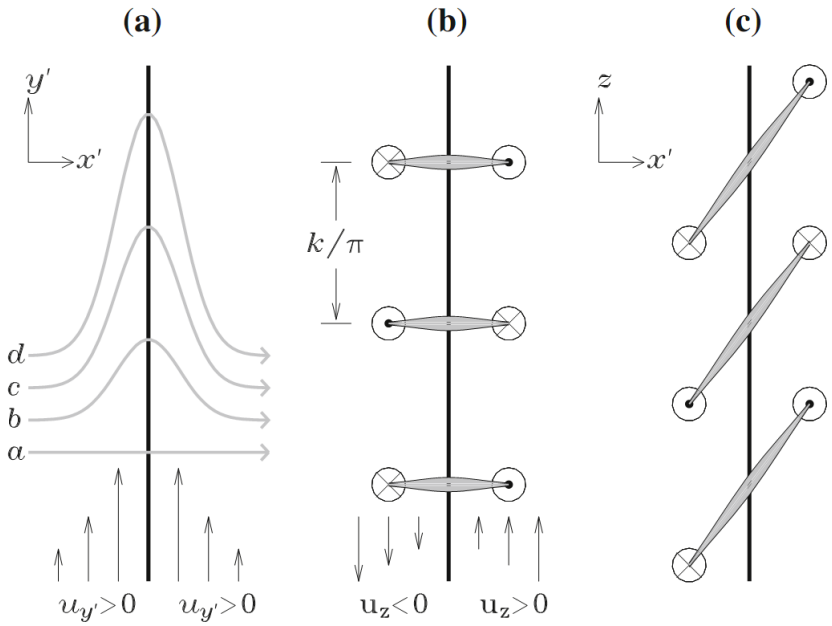

Figure 5.4: The magnetic field amplification mechanism employed by the Roberts Cell Flow. Here, a magnetic field line directed in the x'-direction experiences exponential stretching in the y'-direction, whilst also being sheared so that field components of like polarity are brought into close proximity of each other, producing a magnetic field that is now directed in the y'-direction, which is then subjected to a similar stretching and shearing process, meaning that the dynamo action occurs in a closed loop. Adapted from [12].

5.6 Small-scale, Non-helical, TurBulent Dynamos

We leave behind the droll realms of the kinematic dynamo and turn our attention now to the turbulent, small-scale dynamo (sometimes referred to as SSD). Dynamos are generally divided into two classes: small-scale and large-scale. Large-scale dynamos are responsible for, example, the Sun's 11-year cycle and produce magnetic fields which are coherent on large scales (for example, the mean, large-scale component of the Sun's magnetic field that is coherent on length-scales which are comparable to the solar radius) [10, 12]. These dynamos also tend to operate on timescales which are much longer than those timescales that are associated with the turbulent motions of the flow. Small-scale dynamos are responsible for producing small-scale magnetic fields which are typically on the order of, or smaller than, the energy carrying length-scales of the associated turbulent motions of the flow [10] – usually, this equates to around $R_m^{-1/2}$ times the aforementioned length scale[3] [12]. These dynamos tend to have much larger growth rates and are thus considered to belong to the families of fast dynamos [10, 12].

★

Recalling the result from Alfvén's Frozen Flux Theorem:

$$\frac{\mathrm{D}}{\mathrm{D}t}\left(\frac{\mathbf{B}}{\varrho}\right) = \frac{1}{\varrho}\left(\mathbf{B}\cdot\nabla\right)\mathbf{v},$$

we see that in a turbulent flow, as the fluid particles randomly move away from each other (effectively a "random walk" problem), a magnetic field line that is frozen into the fluid will, in the same way, also lengthen via stretching that is caused by the fluid particles moving away from each other – this is called **random stretching** [10]. This random stretching of the magnetic field lines will, by the Frozen Flux Theorem, lead to an increase in the magnitude of the term, $\mathbf{B}/\varrho$, if we also have that $\varrho \sim \mathrm{const.}$. Random stretching will continue to cause the field strength to grow until it is approximately balanced out by the losses due to Ohmic dissipation [10]. Much debate has been entered into on what happens beyond this critical point. In the work, *On the spontaneous magnetic field in a conducting liquid in turbulent motion* (1950) [3], Batchelor argued that should the flow have a magnetic Prandtl number that is greater than unity, then the magnetic field strength shall undergo exponential growth strength [3] – an argument now determined to be incorrect [10]. Kazantsev, on the other hand, managed to elucidate dynamo action in special flows that lack any sort of helicity via the use of specialised diagrammatical techniques, making a significantly stronger argument [28]. We expand slightly on the results Kazantsev's arguments in the remainder of this section and, in particular, study his proposed dynamo model – the **Kazantsev Dynamo** – and connect it to the effects and nature of turbulence in

[3] In the case of the Sun, once more, this only equates to a few hundred metres – tiny indeed!

the small-scale dynamo problem.

5.6.1 Kazantsev Theory, in Passing

In this section, we discuss the main result of problem considered by Kazantsev in his 1968 work, *Enhancement of a Magnetic Field by a Conducting Fluid* [28], which concerned the existence of dynamo action in a turbulent fluid flow which lacked any sort of helicity. Much of the theory, *ergo*, **Kazantsev Theory**, is based heavily on statistical analysis and the statistical properties of the magnetic- and velocity fields. As the scope of the dissertation is mainly in the interest of the simulation of turbulent flows and their connection to the small-scale, turbulent dynamo, we do not cover any of these theories in any great detail, concerning ourselves only with a discussion of the salient points [10, 52].

★

Before going further, the following decompositions are given. Due to the fact that both small-scale and large-scale dynamos are thought to interact with each other [10], we decompose both the velocity- and magnetic fields into two distinct components: one component representing the mean-field and the other representing the smaller-scale, fluctuating component of the respective fields. In symbols, the decomposition reads as [10]:

$$\mathbf{v} = \overline{\mathbf{v}} + \mathbf{u} \tag{5.45}$$

$$\mathbf{B} = \overline{\mathbf{B}} + \mathbf{b}. \tag{5.46}$$

Here, $\mathbf{v}$ and $\mathbf{B}$ now represent the *total* velocity- and magnetic fields, $\overline{\mathbf{v}}$ and $\overline{\mathbf{B}}$ the mean-field components and $\mathbf{u}$ and $\mathbf{b}$ the fluctuating, small-scale components of the respective fields. In this way, separate evolution equations may be obtained for both the mean-field and small-scale components [10], allowing further insight into how the dynamos operate.

Kazantsev originally considered a stochastic, statistically isotropic, homogeneous velocity field, $\mathbf{u}$,[4] which is also Gaussian-random with a zero-mean and delta-correlated in time (i.e. the velocity field is only auto-correlated at a single instant in time). This field may be likened to the small-scale component of the total velocity field, as described in Equations (5.45). The correlation function, which takes into account two spatial points (the homogeneity assumption on $\mathbf{u}$ implies this), $\mathbf{x}$ and $\mathbf{y}$, may be written as [52]:

[4]Here, we use $\mathbf{u}$ to emphasise the fact that this stochastic field is *not* a solution to the Navier-Stokes Equations. We shall elaborate more on this when we discuss large-scale dynamos.

$$\boxed{\langle u_i(\mathbf{x},t)u_j(\mathbf{y},s)\rangle = T_{ij}(r)\delta(t-s),} \tag{5.47}$$

where $\delta(t-s)$ is the Dirac delta distribution centered at the point, s, and T_{ij} is the **velocity correlation tensor** [52], defined by

$$\boxed{T_{ij} = \left(\delta_{ij} - \frac{r_i r_j}{r^2}\right) T_N(r) + \frac{r_i r_j}{r^2} T_L(r).} \tag{5.48}$$

Here, we may make the identifications $r = |\mathbf{x}-\mathbf{y}|$, $r_i = x_i - y_i$ and also note that the tensor, δ_{ij}, is the regular Krönecker Delta symbol. Like the velocity field, this velocity correlation tensor is also assumed to be statistically isotropic and homogeneous, thus producing the relatively simple form consisting only of terms that are proportional to δ_{ij} and $r_i r_j$ [10]. Additionally, these assumptions allow us to decompose this tensor into longitudinal and transverse parts, represented by the respective correlation functions T_L and T_N, which also only depend on r (again because of homogeneity) [10]. Next, we also assume that this stochastic flow is incompressible (i.e. $\nabla \cdot \mathbf{u} = 0$), which allows us to relate the transverse correlation function of the flow to the longitudinal correlation function of the flow in a simple manner [52]:

$$T_N = \frac{1}{2r}\frac{\partial}{\partial r}\left(r^2 T_L(r)\right), \tag{5.49}$$

where $T_L(0)$ has the form:

$$T_L(0) = \frac{1}{3}\int_0^t \langle \mathbf{u}(t)\cdot\mathbf{u}(t')\rangle \mathrm{d}t'. \tag{5.50}$$

If this statistical velocity field is used in the Induction Equations, then they become a set of stochastic partial differential equations from whence one can determine various statistical moments of the magnetic field [10].

Assuming that the total magnetic field's small-scale component correlation is also statistically homogeneous and isotropic, a two-point correlation function for this component may also be formed and expressed as:

$$\boxed{\langle b_i(\mathbf{x},t)b_j(\mathbf{y},t)\rangle = M_{ij}(r,t),} \tag{5.51}$$

where the quantity M_{ij} is the **magnetic correlation tensor**. Invoking the assumptions of homogeneity and isotropy as before, we may write the magnetic correlation tensor as: [52]

$$\boxed{M_{ij} = \left(\delta_{ij} - \frac{r_i r_j}{r^2}\right) M_N(r,t) + \frac{r_i r_j}{r^2} M_L(r,t).} \tag{5.52}$$

Here, M_L and M_N denote correlation functions for the transverse and longitudinal parts of the field respectively. The automatic divergenceless condition on $\mathbf{B}$ allows us to relate M_N to M_L in a simple manner, as with incompressible flow, via [52]:

$$T_N = \frac{1}{2r}\frac{\partial}{\partial r}\left(r^2 M_L(r,t)\right) \tag{5.53}$$

– a pleasing symmetry. From here, an equation describing the temporal evolution of M_L may now be derived. This involves noting that the action of the temporal derivative operator on M_{ij} may be written as [52]:

$$\frac{\partial M_{ij}}{\partial t} = \frac{\partial}{\partial t}\left(\langle b_i(\mathbf{x},t) b_j(\mathbf{y},t)\rangle\right) \tag{5.54}$$

$$= \frac{\partial}{\partial t}\left(\langle B_i B_j\rangle\right) - \frac{\partial}{\partial t}\left(\overline{B}_i \overline{B}_j\right). \tag{5.55}$$

It is evident now that the temporal evolution of the magnetic correlation tensor takes into account both the temporal evolution of total magnetic field *and* the mean-field component. Using the evolution equation for the mean-field term, the second term in Equations (5.55) may be evaluated [52], whereas the first term may be evaluated by partly noting that [52]:

$$\frac{\partial}{\partial t}\left(B_i(\mathbf{x},t) B_j(\mathbf{y},t)\right) = \frac{\partial B_i(\mathbf{x},t)}{\partial t} B_j(\mathbf{y},t) + B_i(\mathbf{x},t)\frac{\partial B_j(\mathbf{y},t)}{\partial t} \tag{5.56}$$

and rewriting the Induction Equations in their indicial form as [10]:

$$\frac{\partial B_i}{\partial t} = R^x_{ipq} v_p B_q + \eta \nabla^2 B_i, \tag{5.57}$$

where the convenience operator, R^x_{ipq}, is defined as

$$R^x_{ipq} = \varepsilon_{ilm}\varepsilon_{mpq}\left(\frac{\partial}{\partial x^l}\right);$$

ε_{abc} is recognised as the Levi-Civita Symbol. After some lengthly algebra, the full evolution equations for M_{ij}, which also involve terms that describe the mean-field components of both the velocity- and magnetic fields, are obtained [10, 52]. For the purposes of the small-scale dynamo treatment, these terms are dropped.

In references [10] and [52], this evolution equation is derived in the context of a flow which contains a form of helical turbulence. For the simple case of a non-helical, random flow, the derivation proceeds in the exact same manner as what is outlined in the aforementioned works [10, 52], only with one term that is ignored; the evolution equation for M_L is not derived in this work. The equation describing the temporal evolution of M_L for the case of a non-helical, random flow is given as [10]:

$$\boxed{\frac{\partial M_L}{\partial t} = \frac{2}{r^4}\frac{\partial}{\partial r}\left(r^4 \eta_T(r)\frac{\partial M_L}{\partial r}\right) - 2M_L\left(\frac{\mathrm{d}^2 T_L}{\mathrm{d}r^2} + \frac{4}{r}\frac{\mathrm{d}T_L}{\mathrm{d}r}\right).} \tag{5.58}$$

Here, the quantity η_T is defined as the sum of the microscopic magnetic diffusivity, η, and a turbulent, scale-dependent magnetic diffusivity, η_t, that is itself defined in terms of the turbulent diffusion coefficient of the mean field, $T_L(0)$, given by Equation (5.50), and the longitudinal component of the flow, $T_L(r)$. In symbols, this reads

$$\eta_T(r) = \eta + \eta_t(r), \tag{5.59}$$

$$\eta_t(r) = T_L(0) - T_L(r). \tag{5.60}$$

From Equation (5.58), we can see that the temporal evolution of M_{ij} involves the effects of the total magnetic diffusion, given by η_T[5], as well as the effects of the magnetic fluctuations generated by the second term. In fact, since this latter term generates these rapidly magnetic fluctuations via the stochastic velocity field correlation, it is also responsible for showing that a small-scale dynamo may exist independently of any large-scale field [52].

5.6.2 The Kazantsev Dynamo

Equation (5.58) was derived by Kazantsev in his aforementioned work [28] via the use of diagrammatical techniques is known as the **Kazantsev Equation**. Of immediate interest is how a small-scale dynamo would arise from the stochastic flow-field-pair and is discussed briefly in the following.

[5] In order to emphasise its difference from the normal magnetic diffusivity, we shall later call η_T the **turbulent diffusivity**.

5.6.2.1 Down the Potential Well

Defining the function $\Psi = r^2\sqrt{\eta_T}M_L$ [52] and making the relevant substitution into Equation (5.58) yields [52]:

$$\frac{1}{2}\frac{\partial\Psi}{\partial t} = \eta_T\frac{\partial^2\Psi}{\partial r^2} - U(r,t)\Psi \tag{5.61}$$

$$U(r,t) = \frac{\mathrm{d}^2T_L}{\mathrm{d}r^2} + \frac{2}{r}\frac{\mathrm{d}T_L}{\mathrm{d}r} + \frac{1}{2}\frac{\mathrm{d}^2\eta_T}{\mathrm{d}r^2} - \frac{1}{4\eta_T}\left(\frac{\mathrm{d}\eta_T}{\mathrm{d}r}\right)^2 + \frac{2\eta_T}{r^2}. \tag{5.62}$$

Note that Equation (5.61) resembles a version of the famous non-linear Schrödinger Equation with the corresponding 'potential', $U(r,t)$, given by Equation (5.62). In this form, $M_L(r,t)$ also comes with two boundary conditions attached to it: first, it should be regular at the origin and secondly, it should vanish completely in the limit $r \to \infty$ [52].

Recalling the original assumptions that were made on the stochastic flow, $\mathbf{u}$, we may, to this end, regard it as given. This effectively leaves us again with the familiar problem of the Kinematic Dynamo. How droll! This is an unexpected providence, however, as the essence of the kinematic dynamo is in the non-participation of the Navier-Stokes Equations in the velocity field evolution, meaning that the velocity field may be regarded as time-independent.

For the problem at hand, the Kinematic Dynamo limit means that the 'potential' described in Equation (5.62) is time-independent due to the velocity correlation function and magnetic diffusion both being time-independent. In Section 5.5, we discussed finding solutions to the Induction Equations that contained growing modes, which allowed the magnetic field to grow exponentially over time. Carrying on in this spirit, we now seek eigenmode solutions to Equation (5.61) that are of the form $\Psi(r,t) = \exp(2\Gamma t)\Phi(r)$ [10, 52]. Substituting this *ansatz* into Equation (5.61) yields:

$$\eta_T\frac{\mathrm{d}^2\Phi}{\mathrm{d}r^2} = \Phi(\Gamma + U), \tag{5.63}$$

which now resembles a version of the time-*independent* non-linear Schrödinger Equation.

The remainder of the argument is extremely elegant and proceeds as follows [10, 52]: if one can have the potential, $U(r)$, be sufficiently negative over some range of r-values, then one would effectively be left with a potential well that contains **bound states**; these bound states would have energy $E = -\Gamma < 0$. This implies that there are indeed existing growing eigenmode solutions with $\Gamma > 0$. The possibility of dynamo action may now finally be illicited from the Kazantsev Equation: should we

wish to obtain these growing eigenmode solutions, we would simply require that the potential, $U(r)$, exhibits these bound states and is also sufficiently negative over some range of r-values.

5.6.2.2 The Dynamo in the Well

We have now determined the conditions on the potential, $U(r)$, for dynamo action to take place. However, recalling Equation (5.62), we see that the form of U is entirely dependent on the form of T_L. Thus, even though the small-scale dynamo problem is itself dependent on U, we must pay special attention to the form of T_L in order to classify the dynamo action properly; this problem has been studied in great detail [10, 52].

Here, we treat the small-scale dynamo with turbulence; hence, T_L *should* be able to simulate some type of turbulence. A popular choice of T_L which simulates Kolmogorov turbulence is given by [52]:

$$T_L(r) = \frac{V}{3L}\left[1 - \left(\frac{r}{L}\right)^{4/3}\right] \quad l_c < r < L, \tag{5.64}$$

where l_c is defined as some turbulence cut-off length scale and L is some length scale that is defined on the outermost scale of the turbulence [52]. For this choice of T_L, the potential, U, takes on the following form [52]:

$$U(r) = \frac{V}{3L}\left[-\frac{8}{9}\left(\frac{r}{L}\right)^{-\frac{2}{3}} - \frac{4(r/L)^{2/3}}{9\left(3/R_m + (r/L)^{4/3}\right)} + \frac{6}{R_m}\left(\frac{L}{r}\right)^2\right], \tag{5.65}$$

where V is a velocity scale that is defined on the outermost scale of the turbulence [52]. The magnetic Reynolds number of the flow, $R_m = VL/\eta$, is defined on the outermost scale of the turbulence [52]. Depending on the value of R_m, this potential may or may not exhibit bound states (i.e. become negative over some range of r-values). For the potential defined by Expression (5.65), it may be shown that no bound states are exhibited when $R_m < 9/2$ [52]. A plot of this potential for various values of R_m may be seen in Figure 5.6. Also plotted for the purposes of visualisation only, another potential defined by the choice $T_L(r) = (V/3L)(1 - r^2/L^2)$ [10] and may be seen in Figure 5.5.

Of further interest in the potentials is the critical magnetic Reynolds number, $R_{m,\mathrm{crit}}$, that is associated with the potential itself. As discussed in Section 5.2.3, it is a *necessary* condition that $R_m \gg 1$ for any dynamo action to take place. The critical magnetic Reynolds number associated with the potential is defined to be that value of R_m beyond which a small-scale field shall grow exponentially in strength. For the potential defined by Expression (5.65), one would typically obtain the value $R_{m,\mathrm{crit}} \sim 60$ via

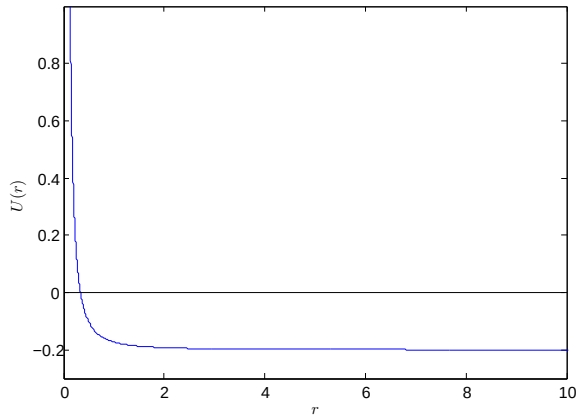

Figure 5.5: The resulting potential, $U(r)$, for $T_L(r) = (VL/3)(1 - r^2/L^2), r < L$ [10]. Here, $L = 100$ was picked arbitrarily, simply to visualise the structure of the potential. Note that this potential exhibits a bound state, as was alluded to in Section 5.6.2.

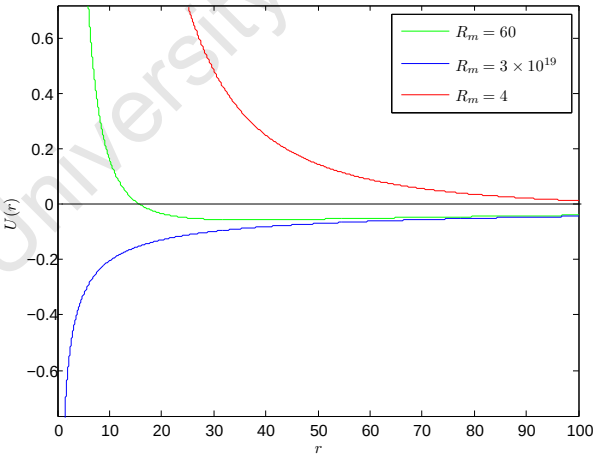

Figure 5.6: The resulting potential, $U(r)$, as given by Expression (5.65) [52]. Following the numerical values provided in reference [52], $L = 100$ and $V = 10$ were used, whilst R_m was varied to illustrate the manner in which the potential itself changes to allow for the possibility of dynamo action. Note that this potential also exhibits bound states, above a certain threshold value of R_m, as was alluded to in Section 5.6.2.

a **Wentzel-Kramers-Brillouin-Jeffreys (WKBJ) analysis** of the Kazantsev Equation [52]. It should be noted that the value of $R_{m,\mathrm{crit}}$ will vary with the choice of T_L, as well as the type of analysis method that is used [10].

5.6.2.3 Into Fourier Space, Pursued by Turbulence

As was seen, the Kazantsev Problem is, in fact, *not* easy to solve. On equal footing with this is the solution of Equation (5.58):

$$\frac{\partial M_L}{\partial t} = \frac{2}{r^4}\frac{\partial}{\partial r}\left(r^4\eta_T(r)\frac{\partial M_L}{\partial r}\right) - 2M_L\left(\frac{\mathrm{d}^2T_L}{\mathrm{d}r^2} + \frac{4}{r}\frac{\mathrm{d}T_L}{\mathrm{d}r}\right).$$

One way of lightening this cumbersome load, analytically at least, is to employ the use of the Fourier Transform. Equation (5.58) is traditionally Fourier-transformed and then studied in wavenumber-space, as opposed to real space. In this way, we no longer are interested in the magnetic field, nor its correlation tensor, but now rather devote ourselves to studying the features and behaviour of a **magnetic energy spectrum**. We briefly discuss the Fourier-transformed Equation (5.58) and some features of the magnetic energy spectrum in the following.

It may be shown, following the method in the work by Kulsrud *et al* [30], that Equation (5.58) may be Fourier-transformed to yield the integro-differential equation:

$$\frac{\partial M}{\partial t} = \int K_m(k,k')M(k')\mathrm{d}k' - \frac{2k^2\eta_T}{4\pi}M(k) - \frac{2k^2\eta_S}{4\pi}M(k), \tag{5.66}$$

$$K_m(k,k') = \int \sin^3\theta\left(k^2 + k'^2 - kk'\cos\theta\right)\frac{J(k'',0)}{k''^2}\mathrm{d}\theta, \tag{5.67}$$

$$\frac{\eta_T}{4\pi} = \frac{2\pi}{3}\left(\frac{L}{2\pi}\right)^3\int J(k'',0)\mathrm{d}\mathbf{k}'', \tag{5.68}$$

where $k'' = \sqrt{k^2 + k'^2 - 2kk'\cos\theta}$. Here, $M(k)$ is now the **magnetic energy spectrum** over the wavenumbers, k, η_T is the familiar turbulent diffusivity from before, η_S is the **Spitzer resistivity** and $J(k'',0)$ is the zero-frequency part of the hydrodynamical spectrum. Primed k's denote different components of the wavenumber k, which is defined as a vector quantity, $\mathbf{k} = \mathbf{k}' + \mathbf{k}''$.

If the term containing the Spitzer resistivity is neglected and an integration over all k is performed, then the temporal rate of change of the total magnetic energy present may be written as:

$$\frac{\mathrm{d}E_M}{\mathrm{d}t} = \frac{1}{2}\frac{\mathrm{d}}{\mathrm{d}t}\int M\mathrm{d}k = 2\gamma E_M, \tag{5.69}$$

$$\gamma = \frac{2\pi}{3}\left(\frac{L}{2\pi}\right)^3 \int k^2 J(k,0)\mathrm{d}\mathbf{k}. \tag{5.70}$$

Here, γ is the reciprocal of the turnover time of the smallest energy-carrying eddy [30]. In terms of wavenumbers, this particular eddy would have the wavenumber $k = k_{\max}$. Note that Equation (5.69) only holds true when the Spitzer resistivity, η_S, is identically zero. It is then prudent to meditate on its importance in the evolution of the magnetic energy spectrum, M. Reasoning from the point-of-view of the wavenumbers once more, consideration must be given to those wavenumbers, k, which are all much greater than the wavenumber $k_{\max}$, as it was defined before [10, 30]. Equivalent to this is the assumption that the spectrum, M, is peaked on scales that are much smaller than the scales applicable to the flow under consideration [10]. This allows one to examine the energy spectrum, M, on scales where the resistivity in fact *does* play an important role in the amplification of the magnetic field [30]. In the $k \gg k_{\max}$ approximation [30], Equation (5.66) then reduces to:

$$\boxed{\frac{\partial M}{\partial t} = \frac{\gamma}{5}\left(k^2\frac{\partial^2 M}{\partial k^2} - 2k\frac{\partial M}{\partial k} + 6M\right) - \frac{2k^2\eta_S}{4\pi}M.} \tag{5.71}$$

When solving this new equation for M, one should be aware that the following assumption is implied: M itself is initially peaked at some wavenumber, k_{ref}, that is much smaller than the resistive wavenumber, k_R [10]. Taking this *ansatz* into account, it is possible to form a solution to Equation (5.71) in terms of a **Green's Function**. This solution [30] is given as:

$$M(k,t) = \int_0^{\tau} M(k_{\mathrm{ref}}, t-\tau)\mathcal{G}\left(\frac{k}{k_{\mathrm{ref}}}, \tau\right)\mathrm{d}\tau \tag{5.72}$$

$$\mathcal{G}(k,t) = \sqrt{\frac{5}{4\pi}}\frac{k^{3/2}\ln k}{\tau^{3/2}\gamma^{1/2}}\exp\left(-\frac{5\ln^2 k}{4\gamma\tau} + \frac{3\gamma\tau}{4}\right). \tag{5.73}$$

Here, $\mathcal{G}$ is the Green's Function referred to above. It may be seen from the Green's Function that M has a temporal growth rate of $e^{3\gamma\tau/4}$ [30]. As mentioned before, M is peaked around some wavenumber and decreases for all values of k beyond it. As M evolves in time, this peak appears to "migrate" to increasingly higher wavenumbers at a rate of $e^{2\gamma\tau}$ [30].

Assume now that one may assert the following "initial" condition at the wavenumber k_{ref}: $M(k_{\mathrm{ref}}, t) = M_1 e^{3\gamma t/4}$, where M_1 is some spectrum, then we may evaluate the Green's Function solution via exact analytical integration, yielding [30]:

$$M(k,t) = M_1 e^{3\gamma t/4} \left(\frac{k^{3/2}}{k_{\rm ref}}\right) \left\{1 - \mathrm{erf}\left[\sqrt{\frac{5}{4\gamma t}} \ln\left(\frac{k}{k_{\rm ref}}\right)\right]\right\}. \tag{5.74}$$

When M's peak wavenumber, k_p, eventually reaches the resistive wavenumber, k_R, the effects of the Spitzer resistivity must then be taken into account and the solution given by Expression (5.74) may then be written approximately as [30]:

$$M \approx k^{3/2} K_0 \left(\sqrt{\frac{5\eta_S}{2\pi\gamma}} k\right) e^{3\gamma t/4}, \tag{5.75}$$

where K_0 is a Bessel Function of the second kind. Examining the solutions given by Expressions (5.74) and (5.75), it is clear that as M evolves and increases in amplitude, it leaves behind a tail that is proportional to $k^{3/2}$ [30]. At any given time, t, M increases until it reaches the peak wavenumber, k_p, as mentioned before (Kulsrud *et al* gives this value as $k_p \sim e^{\gamma t}$), beyond which it decreases exponentially [30]. It is also obvious that the magnetic energy will also continue to grow as the spectrum evolves in time. Physically, the growing amplitude of the spectrum, as well as its characteristic features mentioned, can be attributed to the amplification of the magnetic field strength via the random stretching of the magnetic field lines [10].

★

Note that the analysis presented above possibly only holds much meaning in the kinematic limit; as the non-linear effects of the flow begin to dominate, the analysis becomes slightly fuzzier. In the following section, we briefly look at some of the non-linear effects of the flow that come into play as the field and flow evolve in time, and also discuss the consequences these have for the dynamo process.

5.6.3 The Inevitable Saturation: Non-linear Effects and the Small-scale Dynamo

At early times, before any non-linear effects enter the system, the dynamo is said to be in a kinematic phase. In this form, most analyses on the problem are markedly easier to perform, as the equations themselves are effectively linear. The dynamo's temporal evolution, however, eventually causes the kinematic phase to pass away, allowing any non-linear effects to become increasingly important. Most of these non-linear effects are themselves treated as model problems, usually uncompelling, as the study of the non-linear saturation of the small-scale dynamo not yet well understood.

Why, then, are these effects so important to the problem under consideration? Both from direct simulation, and confirmed by theory [10], these non-linear effects eventually impede the growth of

the magnetic field, eventually causing it to stop. When this occurs, it is said that **the dynamo has become saturated**. From the point-of-view of the energetics, the total kinetic and magnetic energies eventually end up in equal quantities, effectively causing the dynamo to stop operating. As before, we shall not cover any these effects in great detail, reserving ourselves only to the salient points of the models.

The pertinent question to be asked now is exactly *how* these non-linearities happen to come about. Consider the velocity field, $\mathbf{v}$, which is a solution to the Navier-Stokes Equations. In the previous section, we stated that this field may be broken up into two main parts: one describing the mean-field-component and the other describing some assumed stochastic component. Leaving the mean-field part of the flow aside once more, let us consider the decomposition given by [10]:

$$\mathbf{v} = \mathbf{u} + \mathbf{w}. \tag{5.76}$$

Here, $\mathbf{u}$ is the stochastic component of the flow as from before and $\mathbf{w}$ is now some component describing a non-linear effect in the flow. Specifically, we consider the non-linear effect known as **ambipolar drift**, which is particularly important in the consideration of galactic dynamos [10]. In this context, $\mathbf{w}$ is then known as the **ambipolar drift velocity** of the flow. This new term may be able to take on different forms, along with the standard assumptions of compressibility or incompressibility, each bringing in a slightly different non-linearity into the evolution equation for M_L [10]. In the following, we describe two examples of assumptions of the ambipolar drift term, discussing in brief how the dynamo may saturate because of it.

5.6.3.1 A Simple (Compressible) Ambipolar Modification: Considering the Lorentz Force

The simplest form that may be assumed for the ambipolar drift term is one that is proportional to the Lorentz force:

$$\mathbf{w} = a\mathbf{J} \times \mathbf{B}, \tag{5.77}$$

where the quantity a may be related to the properties of a partially-ionized plasma in the context of ambipolar drift and $\mathbf{w}$ not assumed to be incompressible [10, 53]. As it is known that the effects Lorentz force do in fact play an important role in a plasma, the assumed form of the ambipolar drift component of the flow may be regarded as a naïve modification to the overall flow, providing an instructive non-linear toy model [10]. For simplicity, the form $a = \tau/\rho$ may be adopted, where τ is some

correlation time that is assumed to be phenomenologically-inert and smaller than the Alfvén time, and ρ the standard fluid density [10]. The evolution equation for M_L then complicates slightly, by the addition of a fourth-order magnetic correlation term due to the non-linearity (this term is denoted by $K(r,t)$ in the evolution equation for M_L) [10, 53], and may be written as:

$$\frac{\partial M_L}{\partial t} = \frac{2}{r^4}\frac{\partial}{\partial r}\left(r^4\eta_T(r)\frac{\partial M_L}{\partial r}\right) - 2M_L\left(\frac{\mathrm{d}^2 T_L}{\mathrm{d}r^2} + \frac{4}{r}\frac{\mathrm{d}T_L}{\mathrm{d}r}\right) + K(r,t) \tag{5.78}$$

$$K(r,t) = M_L(0,t)\frac{4a}{r^4}\frac{\partial}{\partial r}\left(r^4\frac{\partial M_L}{\partial r}\right). \tag{5.79}$$

A further important change now occurs in the turbulent diffusivity, $\eta_T(r)$. When there was no non-linear ambipolar component assumed in the flow, $\eta_T(r)$ contained the normal magnetic diffusivity, η. Now, however, this diffusivity is replaced by a time-dependent, ambipolar diffusion term, η_D, which is itself a function of η and $M_L(0,t)$ and may be expressed as [10]:

$$\eta_D(t) = \eta + 2aM_L(0,t), \tag{5.80}$$

meaning that η_T is now a function of both time *and* space. The saturation mechanism for the dynamo is hidden within this new ambipolar diffusivity. The effects of the Lorentz force on the fluid have effectively introduced yet *another* diffusivity between the field and flow to the model and, due to its time-dependence, it is also continually growing. The growth of this ambipolar diffusion may be seen as a form of impedance, causing the dynamo to saturate once a critical value of this diffusion has been reached [10].

Simple as this model may be, it serves to highlight two important points regarding the saturated state of the SSD: firstly, this saturated state may not necessarily depend on any microscopic parameters (e.g. η) when one is far away from the resistive scale and, secondly, that the saturated SSD may possibly share similar marginal eigenmode (i.e. when $R_m = R_{\mathrm{crit}}$) properties with its Kinematic counterpart [10].

5.6.3.2 Another Simple Ambipolar Modification: Incompressible Flow

Previously, we noted that the ambipolar component, $\mathbf{w}$, was not assumed to be incompressible. What would happen, then, if we made this assumption? Once more, we adopt the decomposition of the flow, $\mathbf{v}$, given in Equations (5.76), but now take the ambipolar component, $\mathbf{w}$, to have the form [10, 54]:

$$\mathbf{w} = a\left(\mathbf{B}\cdot\nabla\mathbf{B} - \nabla p\right), \tag{5.81}$$

where a is as before and p is some perturbed pressure which includes a magnetic contribution [54]. As per the assumption above, $\mathbf{w}$ also now obeys the incompressible condition $\nabla\cdot\mathbf{w} = 0$. The evolution equation for M_L now turns into an integro-differential equation which is generally not easily analysed by any means. However, if one considers the two regimes where $r \ll l$ and $r \gg l$, where $l(t)$ is some time-varying length-scale over which M_L is assumed to be peaked [10, 54], then the $K(r,t)$ term in Equation (5.78) may then be written as [10, 54]:

$$K(r,t) = M_L(0,t)\frac{2a}{r^4}\frac{\partial}{\partial r}\left(r^4\frac{\partial M_L}{\partial r}\right) + \int_0^8 \frac{\mathrm{d}u}{u}\left(\frac{\mathrm{d}M_L}{\mathrm{d}r}\right)^2 \quad r \ll l \tag{5.82}$$

$$K(r,t) = -\frac{2\eta_{HD}}{r^4}\frac{\partial}{\partial r}\left\{r^4\frac{\partial}{\partial r}\left[\frac{1}{r^4}\frac{\partial}{\partial r}\left(r^4\frac{\partial M_L}{\partial r}\right)\right]\right\} \quad r \gg l, \tag{5.83}$$

where η_{HD} is some non-linear hyperdiffusion that is defined through [54]

$$\eta_{HD} = \frac{2a}{5}\int_0^\infty r M_L(r,t)\mathrm{d}r. \tag{5.84}$$

It is clear that in both regimes of r, $K(r,t)$ is proportional to $M_L(0,t)$, which serves as a damping coefficient in the damping of M_L [54]. In the regime of $r \ll l$, saturation of the SSD occurs due to the inclusion of some non-linear diffusion term that grows with time and in the regime of $r \gg l$, saturation of the SSD occurs due to the inclusion of a non-linear hyperdiffusion term that grows with time [54]. In both cases, it is apparent that saturation occurs due to the effects of extra diffusion between the field and the flow, meaning that saturation will occur regardless of whether or not $\mathbf{w}$ is regarded as incompressible or not [10, 54].

5.7 Simulations

In the following section we present the results of several short simulations that were conducted in order to illustrate some of the concepts introduced in the previous sections.

We consider simulation of the Roberts Flow Dynamo, non-helical, forced, turbulence and finally a short example on helical, forced, turbulence. For all simulations, we restrict our interests solely to

the effects of a varying magnetic Reynolds number on the onset of dynamo action, whilst in the latter turbulence simulations, we also examine the effects of a varying magnetic Prandtl number on the onset of dynamo action. For the turbulence simulations, we also plot the one-dimensional energy spectra for the magnetic- and kinetic energies and briefly comment on some of their features in relation to the small-scale dynamo theory. Finally, we consider some of the energy spectra obtained from the magnetogenesis simulations conducted in Chapter 4 and make brief comment on their structure in relation to the long-term temporal behaviour of the magnetic field strength.

For the runs that ensue, we define the magnetic Reynolds and Prandtl numbers here for the sake of convenience:

$$R_m = \frac{v_{rms}}{\eta L} \qquad R_m = \frac{v_{rms}}{\eta k_f} \qquad P_m = \frac{\nu}{\eta}. \tag{5.85}$$

Here, the magnetic Reynolds number has been defined in two different ways, using the simulation box length, L, or forcing wavenumber, k_f, respectively; v_{rms} is the average rms velocity that is obtained from following the temporal evolution of the corresponding quantity during the simulation. These variants shall be used in the simulations for the kinematic dynamo and turbulence sections respectively. Also to be used in the latter section will be the **magnetic Prandtl number**, P_m, which is simply the ratio of the kinematic viscosity and magnetic diffusivity, and is used to characterise dynamo action to a certain extent [10].

A summary of key simulation parameters for this section may be found in Table 5.1

5.7.1 The Roberts Flow Kinematic Dynamo: Results and Discussion

The reader is to note that the simulation for this dynamo is based on the sample `kin-dynamo`, which is provided with the standard PENCIL CODE samples.

As mentioned before, the Roberts Flow dynamo is a kinematic dynamo that belongs to the slow dynamo family. A common feature of all kinematic dynamos is that they select the fastest-growing mode in a particular solution to the Induction Equations, which then causes the magnetic field strength to grow exponentially. As the dynamo is slow, however, it is also heavily dependent on the effects of magnetic diffusion in order to operate properly.

For the purposes of this simulation, we sought only to change the value of the magnetic diffusivity, thus changing the value of the associated magnetic Reynolds number, and examine its effects on the growth of some prescribed magnetic field. The prescribed field used in all cases here was random

Run	η	ν	P_m	R_m	k_f	Box Size	F_0	A_0
R1	10^{-1}			1.59		64^3		10^{-11}
R2	9×10^{-1}			0.18				
R3	10^{-2}			15.92				
R4	10^{-4}			1591.55				
NHT1	2×10^{-3}	2×10^{-2}	10	23.27	3	32^3	0.07	10^{-12}
NHT2	2×10^{-4}		100	201.91				
NHT3	2×10^{-3}		10	89.15	1			
NHT4				40.3	2			
HT1	2×10^{-3}		10	21.58	3			
HT2	2×10^{-4}		100	201.82				

Table 5.1: Simulation parameters for the dynamo runs. Runs in the R-group concentrated on the Roberts Flow Dynamo, whilst those in the NHT- and HT-groups concentrated on non-helically- and helically-forced turbulence respectively. Black cells indicate simulation parameters that were irrelevant within the particular group, whilst a grey cell indicates that the value appearing immediately above it was not changed for that particular run.

Gaussian noise, with an arbitrarily-chosen amplitude of 10^{-11}, on a computational box of dimensions $2\pi \times 2\pi \times 2\pi$ with 64^3 mesh points. Results of this simulation are presented in Figures 5.7, 5.8 and 5.9.

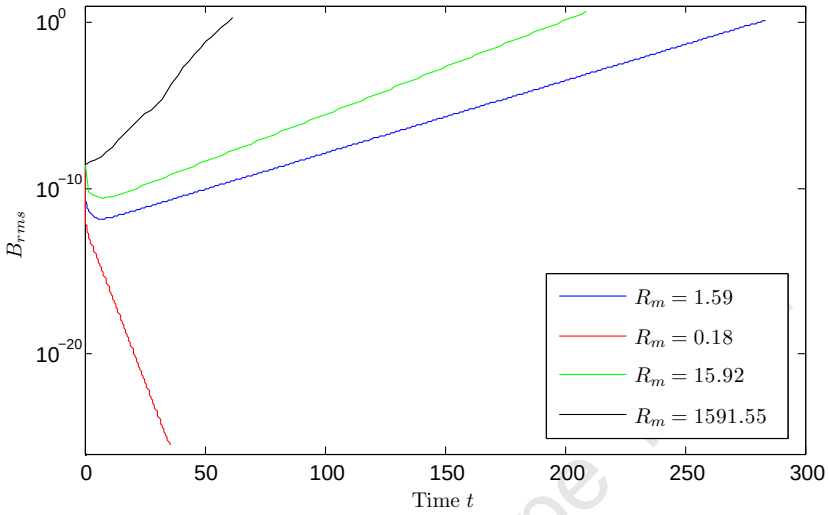

Figure 5.7: Full time-evolution of B_{rms} for various choices of the magnetic Reynolds number, R_m. Respect of the constraint $R_m > 1$ for dynamo action is clearly displayed.

The first run was done at a value of $R_m \sim 1.59$, which is fairly close to unity. As this value obeys the constraint that $R_m > 1$ for dynamo action, however, we should expect to see the field being amplified after some finite time. Examining the corresponding plot in Figure 5.7, we see that this is indeed true – the initial field is indeed amplified after some finite time. The remaining values of $R_m > 1$ each also show this same feature, in agreement with the theory. When we set $R_m < 1$, however, the initial field appears to decay monotonically in strength, again in agreement with the theory. Physically, this situation would correspond to too much diffusion present in the system, which renders the dynamo inoperable.

In all of the plots displayed in Figure 5.7, except from the runs with $R_m < 1$, it is evident that the field initially decays monotonically to some global minimum, after which the exponential growth begins. This behaviour is not obvious for the $R_m = 1591.55$ run, but was also observed. As explained before, this behaviour is to be expected because the dynamo is slow, thus some diffusion is needed to propagate the field within the system *before* the flow begins to amplify it. Mathematically, this field diffusion time would correspond to the time it takes for the fastest-growing mode in the eigensolution to be selected and then dominate over the others.

Examining the energy spectra (Figure 5.8) reveals that over the course of the run, both of the

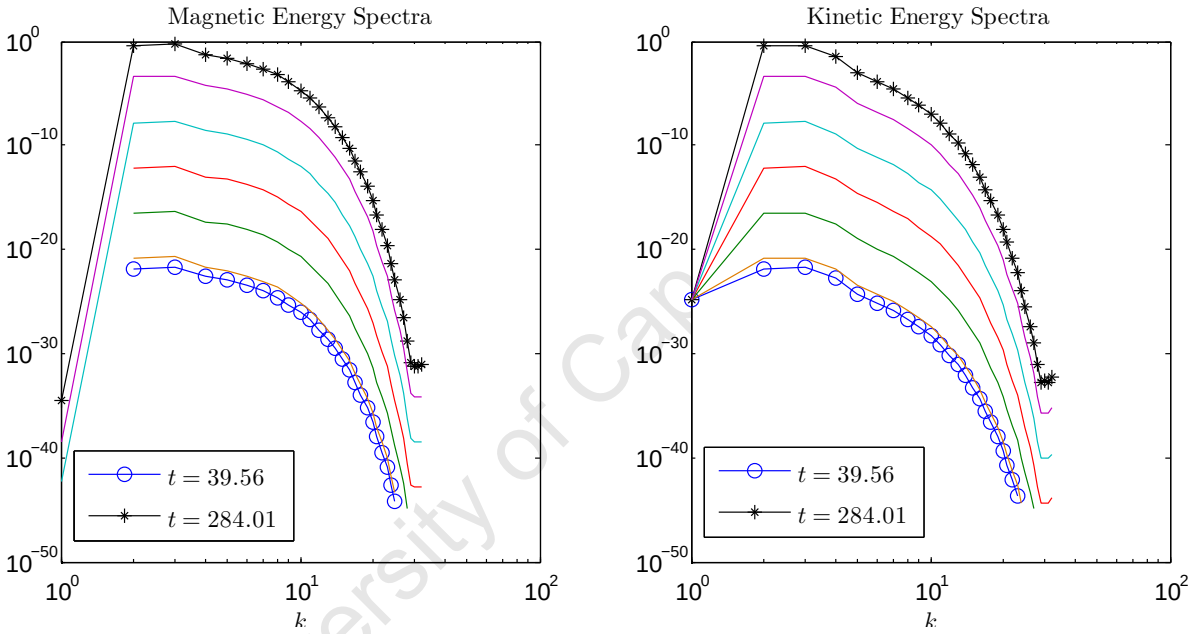

Figure 5.8: Magnetic and kinetic energy spectra corresponding to run R1. It is clear that the spectra all grow at the same rate during the kinematic phase. All other spectra, save for those that have been labelled, have been taken at times $t = 50, 100, 150$ *and* 200 *respectively. Spectra for the remaining runs, with the exception of run R2, show identical qualitative behaviour.*

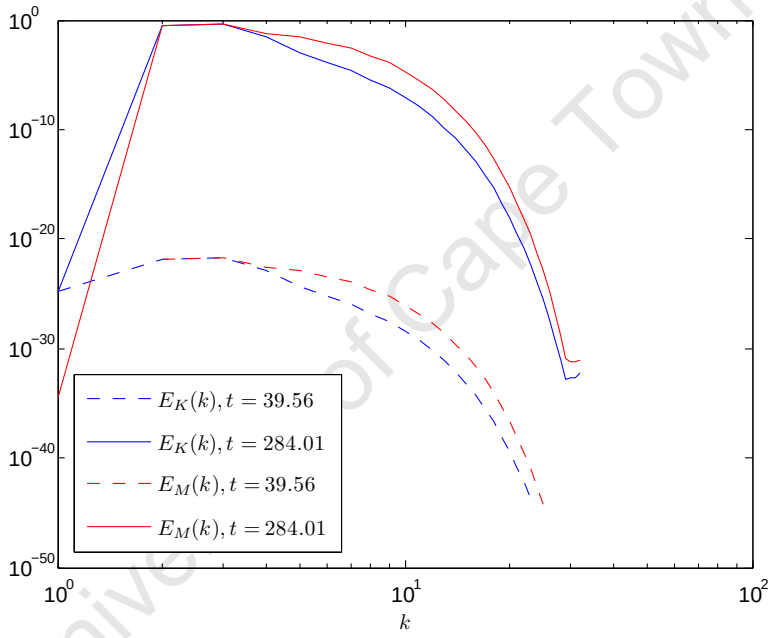

Figure 5.9: Magnetic and kinetic energy spectra corresponding to run R1. It is clear that for wavenumbers $k \geq 2$ the magnetic spectral energy is much greater than the kinetic spectral energy.

magnetic- and kinetic spectral energies appear to grow at a constant rate, which is characteristic of the kinematic dynamo, as well as the kinematic phase of a non-linear run [22]. Figure 5.9 shows that the magnetic spectral energy exceeds its kinetic counterpart at all wavenumbers $k \geq 2$, which indicates a conversion of kinetic energy into magnetic energy, as per the expectations of the energetic discussed previously.

A last feature to note here is that the field strength will continue to grow exponentially, without bound, due to the fact that there is nothing else present within the system that could cause the dynamo to stop working. This is of course due to the way the simulation has been set up.

5.7.2 Non-helical, Forced Turbulence: Results and Discussion

The reader should note that these simulations are based on the sample `helical-MHDturb`, which is provided with the standard PENCIL CODE samples, as well as the helical turbulence simulation teaching example, as provided by Brandenburg.[6]

5.7.2.1 A Note on Forcing Functions

The primary objective for this set of simulations is to investigate the effects of non-helical turbulence on dynamo action. For simulation purposes, the turbulence that is present within the simulations is forced and enters through a numerical forcing term present in the Navier-Stokes Equations. This is similar to the case of the numerical forcing used for the magnetogenesis simulations in Chapter 4. The forcing used in the simulation takes the following functional form [8, 22]:

$$\mathbf{f}(\mathbf{x},t) = \Re\left\{ f_0 c_s \sqrt{\frac{kc_s}{\tau}} \mathbf{f}_{\mathbf{k}(t)} \exp\left[j\mathbf{k}(t)\cdot\mathbf{x} + j\varphi(t)\right] \right\}. \tag{5.86}$$

Here, $\mathbf{k}(t) = (k_x(t), k_y(t), k_z(t))$ is a three-dimensional, time-dependent wavevector with magnitude k, f_0, a non-dimensional forcing amplitude, $\varphi(t)$, a random, time-dependent phase that obeys the constraint $-\pi < \varphi < \pi$ and τ, the standard time-step, as determined by the code [8, 22]; all other symbols retain their usual meanings. Because the wavevector and random phase are both time-dependent, and change at every time step, the forcing function may be regarded as delta-correlated in

[6] This exercise may be accessed at the following URL: `http://www.nordita.org/~brandenb/teach/PencilCode/HelicalDynamos.html`.

time (the velocity field is, unfortunately, not) [22]. For the forcing to be non-helical, it may be shown that the eigenfunctions, $\mathbf{f}_{\mathbf{k}(t)}$, take on the simple form given by [22]:

$$\mathbf{f}_{\mathbf{k}(t)} = \frac{\mathbf{k} \times \mathbf{e}}{\sqrt{\mathbf{k}^2 - (\mathbf{k} \cdot \mathbf{e})^2}}, \tag{5.87}$$

where $\mathbf{e}$ is some arbitrary unit vector that does not have the same direction as $\mathbf{k}$ [22]. Note that these eigenfunctions are themselves unit vectors [22]. The forcing function usually forces the velocity field around a certain average forcing wavenumber, k_f, [22] which can be changed by the user before runtime, by making use of pre-made files containing data relevant to the forcing wavenumber the user wishes to use.

5.7.2.2 Non-helical Results and Discussion

Dynamo action is once more investigated via the adjusting of R_m, the magnetic Prandtl number, P_m, and the average forcing wavenumber, k_f, all in the presence of the non-helical forcing described above. The prescribed field used in all cases here is once more random Gaussian noise, with an arbitrarily-chosen amplitude of 10^{-12}, on a computational box of dimensions $2\pi \times 2\pi \times 2\pi$ with 32^3 mesh points. Results of this simulation are presented in Figures 5.10, 5.8 and 5.9.

Examining all of the panels in Figure 5.10, it is evident that the velocity field strength remains relatively constant throughout the entire simulation run. In panels 1 and 2, the magnetic field strength is seen to initially undergo a monotonic decay to a global minimum, before entering an exponential growth phase and then finally levelling out to a relatively constant strength in a finite amount of time – the saturation phase. The same behaviour is seen in panel 4. Although the initial decay is not obvious, it is observed nonetheless.

The features described above, before the magnetic field saturates, are reminiscent of the behaviour observed in the kinematic dynamo simulations discussed previously. Indeed, the phase before saturation may in fact be regarded as a kinematic phase. Here, the effects of magnetic diffusion are once more crucial for the initial operation of the dynamo.

It is also apparent that as the average forcing wavenumber is increased, whilst holding P_m constant, that the field takes much longer to enter the kinematic and saturation phases (panels 1 and 2). Examining panel 3, where $k_f = 3$, the field strength does not appear to grow anymore – it decays monotonically instead, and continues to do so for the duration of the run. By reasoning of the re-

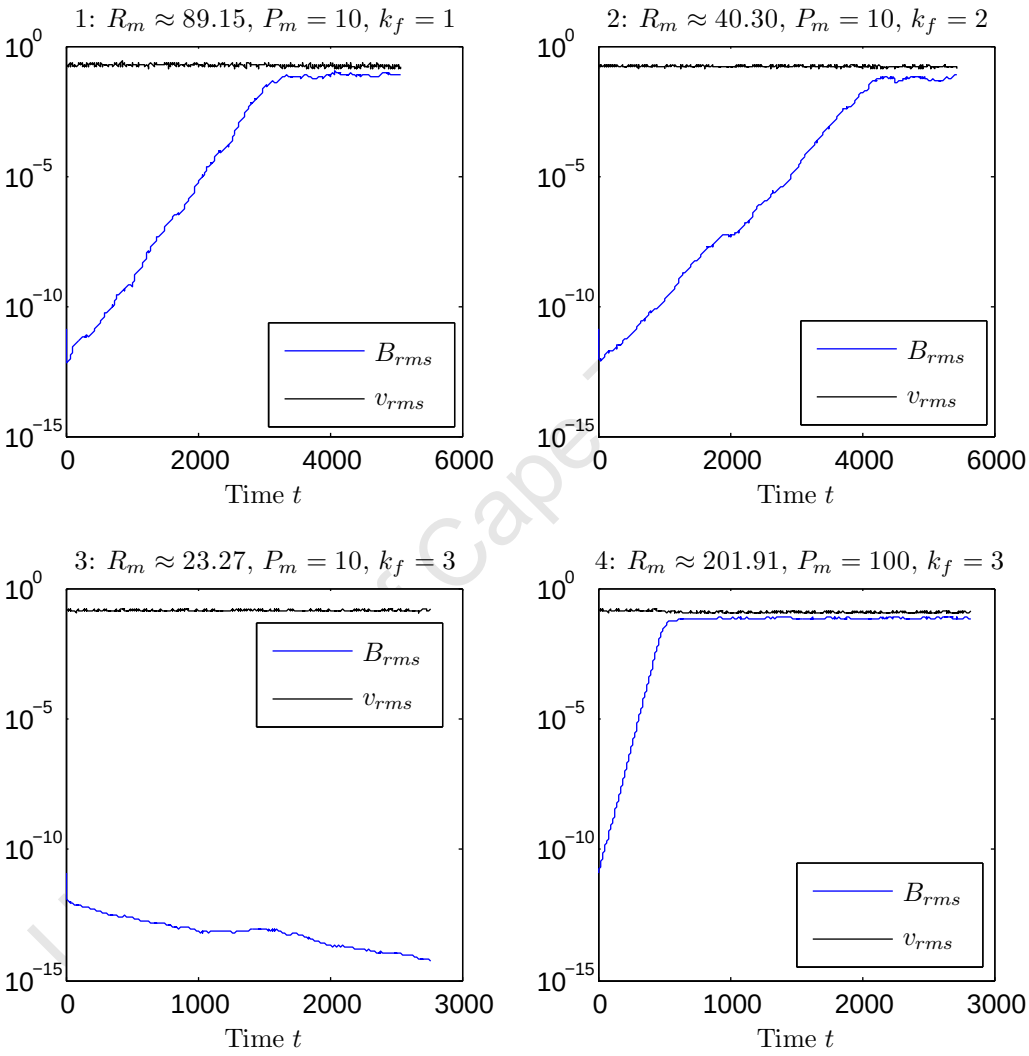

Figure 5.10: Full time-evolution of B_{rms} and v_{rms} for various choices of the forcing wavenumber, k_f. As can be seen in panels 1, 2 and 4, the magnetic field grows exponentially and then saturates after a given time. In panel 3, the field decays instead.

sults discussed in Section 5.6, it is then apparent that R_m is[7] below the previously-alluded-to critical threshold, $R_{m,\text{crit}}$, above which the dynamo is able to operate. Comparing panels 2 and 3, it is evident that the critical value lies in the range $23.27 \leq R_{m,\text{crit}} \leq 40.30$ for our choices of η and ν.

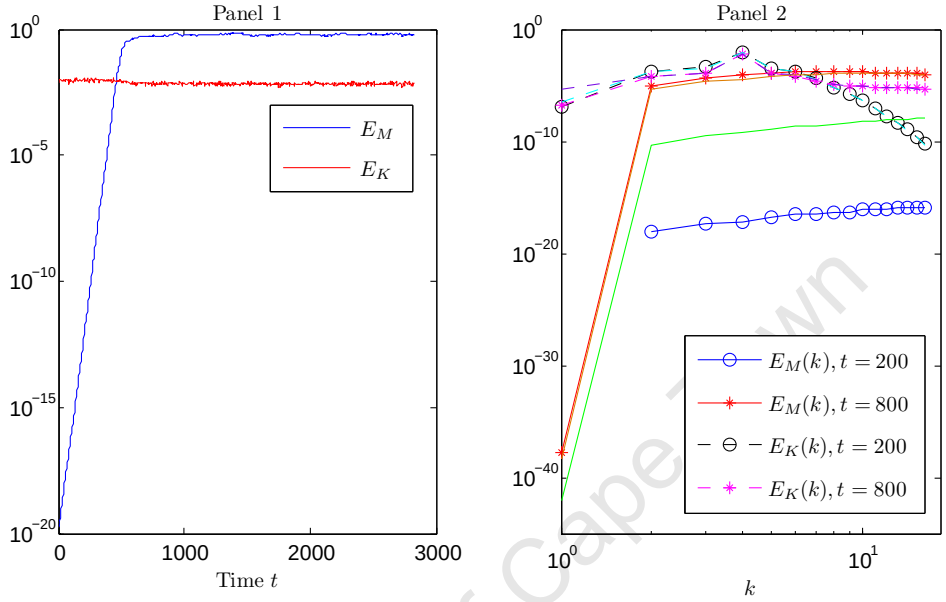

Figure 5.11: Temporal evolution of the magnetic- and kinetic energies, as well as their related spectra, corresponding to panel 4 of Figure 5.10. The magnetic energy is observed to grow larger than the kinetic energy, whilst the corresponding magnetic energy spectrum also appears to be larger than its kinetic counterpart at wavenumbers $k \geq 5$. Note how the kinetic energy spectrum is peaked about the forcing wavenumber, k_f.

The temporal evolution of the magnetic- and kinetic energies, as well as their related spectra displayed, are displayed in Figure 5.11 correspond to the evolution described in panel 4 of Figure 5.10. All of the other spectra, as well as their associated temporal energy evolutions, save for the case presented in panel 3 of Figure 5.10, are qualitatively similar to the case presented. The magnetic energy is observed to outgrow the kinetic energy around time $t \sim 450$, eventually slowing down and levelling out to a relatively constant value, indicative of the field's saturation. This outgrowth can be attributed to the kinematic phase of the simulation. Examining the associated energy spectra in panel 2 of Figure 5.11, the existence of the kinematic phase is once more confirmed, due to the magnetic energy spectra appearing to grow at a constant rate, again overtaking the its kinetic counterpart at wavenumbers $k \geq 5$ as the saturation phase sets in.

[7]Recall that we have defined the magnetic Reynolds number in terms of k_f for these simulations.

The dominance of the magnetic energy spectrum over the kinetic energy spectrum within a certain range of the higher wavenumbers is a typical feature of the dynamo's saturation behaviour in this case [22]. Examining the wavenumbers $k = 2$ and 4, it also appears that the magnetic energy spectrum is growing towards its kinetic counterpart, but its growth rate is not large enough in order to allow an overtake. This could be due to kinetic energy not being converted into magnetic energy at a fast enough rate at these wavenumbers, or because these wavenumbers lie so close to the forcing wavenumber, $k_f = 3$, where the kinetic energy spectrum is constantly peaked; kinetic energy could then be being transferred from this wavenumber to its immediate neighbours at a greater rate than that at which the kinetic energy is being converted into magnetic energy. Noting that the kinetic energy spectrum decreases overall, whilst the magnetic energy spectrum grows overall, suggests that energy is once more changing reservoirs as the dynamo operates, regardless of the forcing present.

5.7.2.3 Digression: The Helical Case

We now make some comments about dynamo action in the presence of helical, forced turbulence. As we consider this as an interesting and complementary digression, the discussion of results is kept brief.

It is known that helicity is an important, but not necessary, factor when investigating dynamo action in the presence of turbulence, as it lowers the critical magnetic Reynolds number required for dynamo action to set in [10]. In the case of forced turbulence, we only then require that the forcing function itself be helical. The eigenfunction given by Expression (5.87) changes to the form [8]:

$$\mathbf{f}_{\mathbf{k}(t)} = \frac{j\mathbf{k} \times (\mathbf{k} \times \mathbf{e}) - \upsilon k(\mathbf{k} \times \mathbf{e})}{\sqrt{1+\upsilon^2}\mathbf{k}^2\sqrt{1-\left(\frac{\mathbf{k}\cdot\mathbf{e}}{\mathbf{k}^2}\right)^2}}, \tag{5.88}$$

where υ is a free parameter and all other symbols retain their original meanings [8]. Note that when one makes the choice $\upsilon = 0$, Expression (5.87) is recovered. For the following results, we have set $\upsilon = 1$. The results are presented in Figure 5.12.

Examining Figure 5.12, the difference made by the helical forcing function is immediately obvious. Compared to panel 3 of Figure 5.10, the magnetic field present in panel 1 of Figure 5.12 now also grows, instead of decaying. This is perhaps the strongest difference. It is clear, then, that a helical forcing function reduces the critical magnetic Reynolds number that is required for dynamo action to commence [10]. The usual kinematic phase as seen before is also present for both fields. Another stark difference to be noted here is that the resultant saturated magnetic fields produced are much stronger

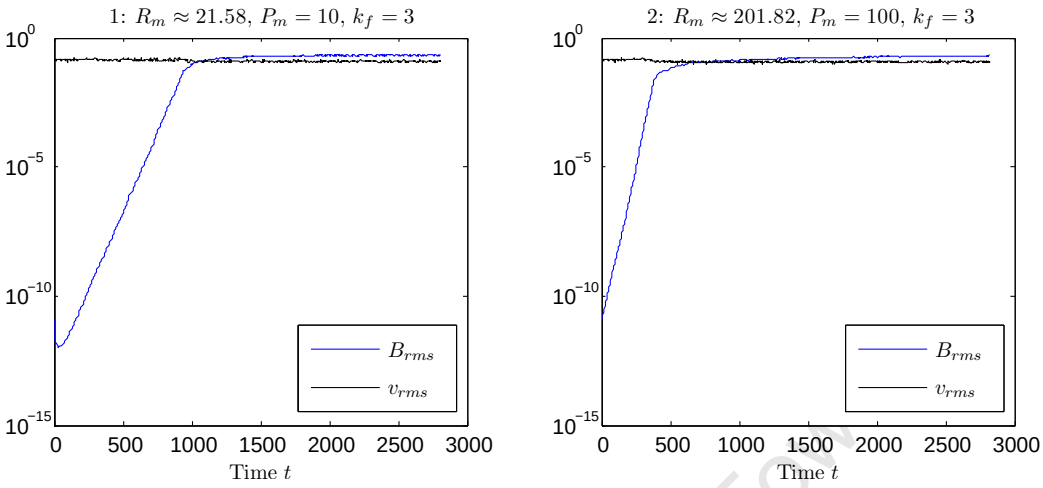

Figure 5.12: Full time-evolution of B_{rms} and v_{rms} for different values of P_m and R_m. As can be seen in both panels, the magnetic field grows exponentially and then saturates after a given time.

than their non-helically-forced counterparts, even outgrowing the strength of the velocity field in a finite time. Increasing the value of P_m causes the saturation phase to occur increasingly earlier. Thus, we can conclude that helical forcing in a turbulence simulation does lead to magnetic fields that are much stronger than their non-helically-forced counterparts, due to its presence lowering the critical magnetic Reynolds number required for dynamo action.

5.7.3 Magnetogenesis, Redux: Results and Discussion

We close this section by re-examining the curious temporal behaviour of B_{rms}, as observed in the simulations conducted in Chapter 4. Results are presented in Figures 5.13, 5.14, 5.15 and 5.16.

During the initial stages of field growth, it is assumed that the battery term played the dominant role of letting the field strength grow until the effects of diffusion became significant. Examining the plots in Figure 5.13, it can be seen that the kinetic energy decreases immediately as the magnetic energy increases, indicating that an energy transfer between the two reservoirs is taking place. This picture may indeed hold true throughout the entire run, though the kinetic energy itself also appears to grow, bearing the same qualitative features as its magnetic counterpart. The results would then

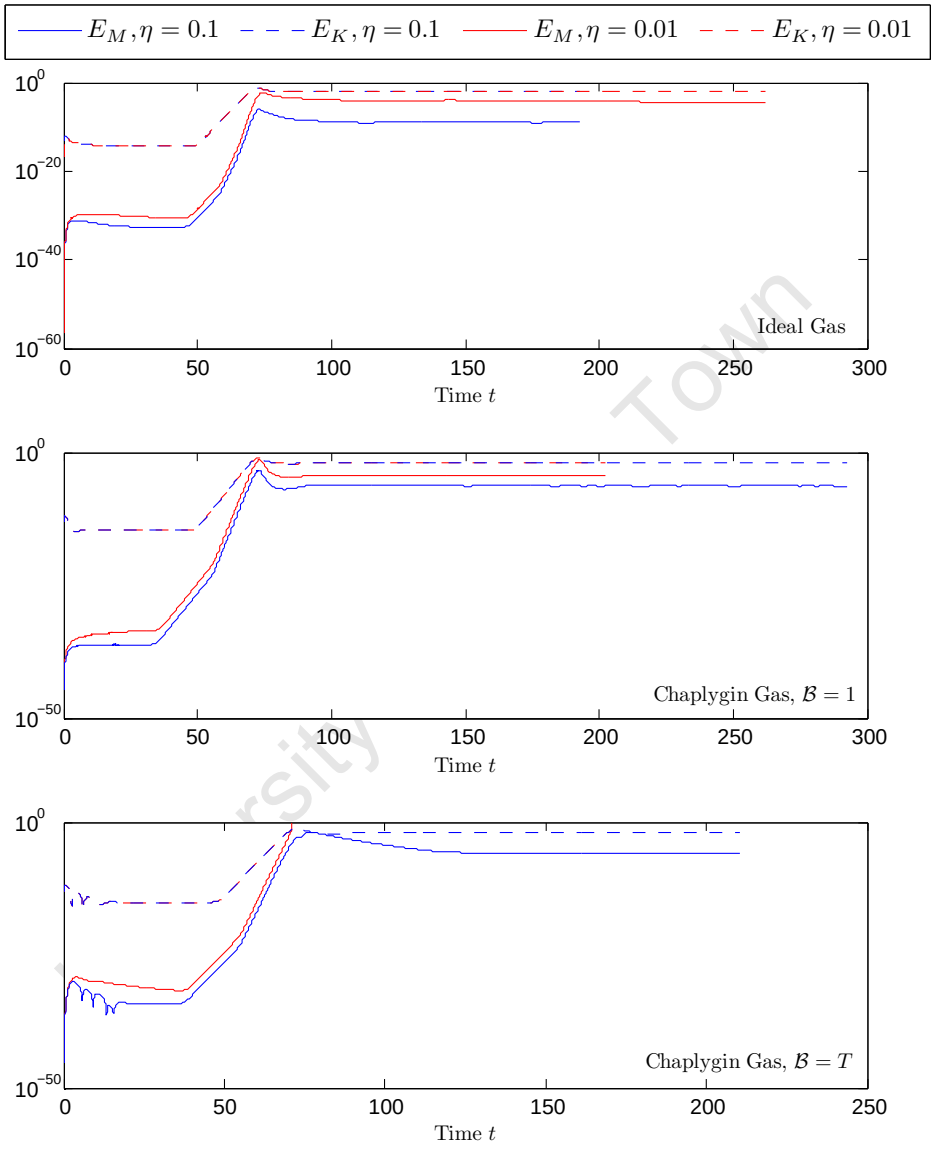

Figure 5.13: Full time-evolution of the magnetic- and kinetic energies, E_M and E_K, for the various magneto-genesis EoS simulations conducted in Chapter 4.

suggest that whilst kinetic energy is indeed being converted into magnetic energy, the kinetic energy reservoir is being replenished by some other source present in the system. A possible explanation for this could be the presence of the forcing term from the Navier-Stokes Equations. As the kinetic energy always appears to be greater than the magnetic energy, it would be reasonable to assume that the corresponding reservoir is being replenished at a rate faster than that at which the conversion to magnetic energy is occurring. Evident from all cases is also that magnetic energy may be being re-converted into kinetic energy and then being dissipated in some way, or being dissipated by some other means, causing the decrease after the global maximum.

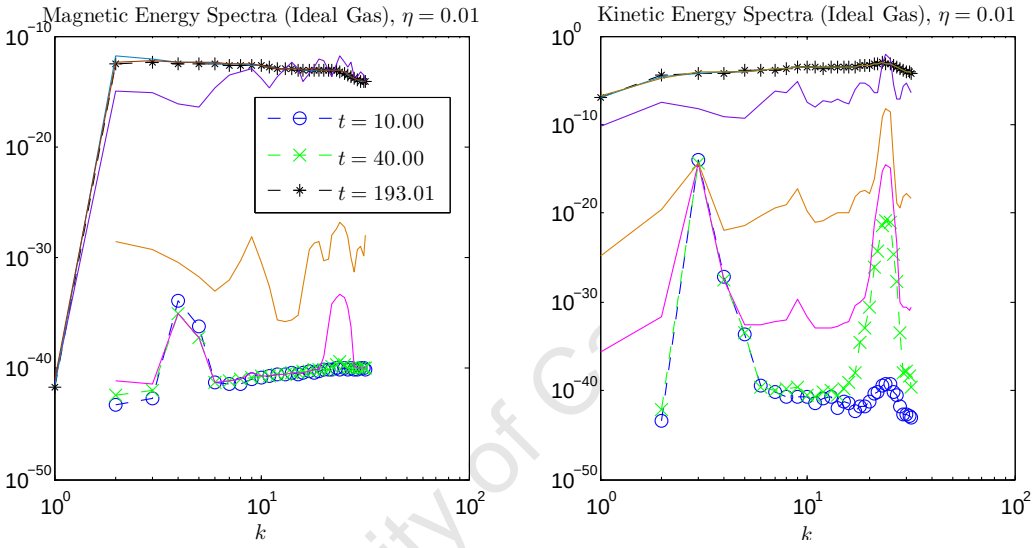

Figure 5.14: Magnetic and kinetic energy spectra corresponding to magnetogenesis run 3I. During the kinematic phase, both spectra appear to develop sharp peaks at the higher and lower wavenumbers, which gradually shrink as the spectra grow. Magnetic spectral energy is highest at $t = 70$, from whence it starts decreasing slightly. Spectra for the remaining runs in this group show identical qualitative behaviour.

Examining the corresponding energy spectra in Figures 5.14, 5.15 and 5.16, it is interesting to note that each of the kinetic energy spectra appear to have sharp peaks at wavenumbers $k = 3$ and $k = 24$, which appear to decline as the spectra grow. In the magnetic energy spectrum, this double-peak pattern is only displayed by both of the Ideal and $\mathcal{B} = T$ Chaplygin EoSs at wavenumbers $k = 4$ and $k = 24$ before the exponential growth phase begins, with the former exhibiting a very shallow peak at the higher wavenumber; the $\mathcal{B} = 1$ Chaplygin EoS also displays a sharp peak at the higher wavenumber. Despite these diminishing features, however, no dissipation range is observed in any of the spectra presented.

As the exponential growth phase commences, the energy measured at the various wavenumbers in

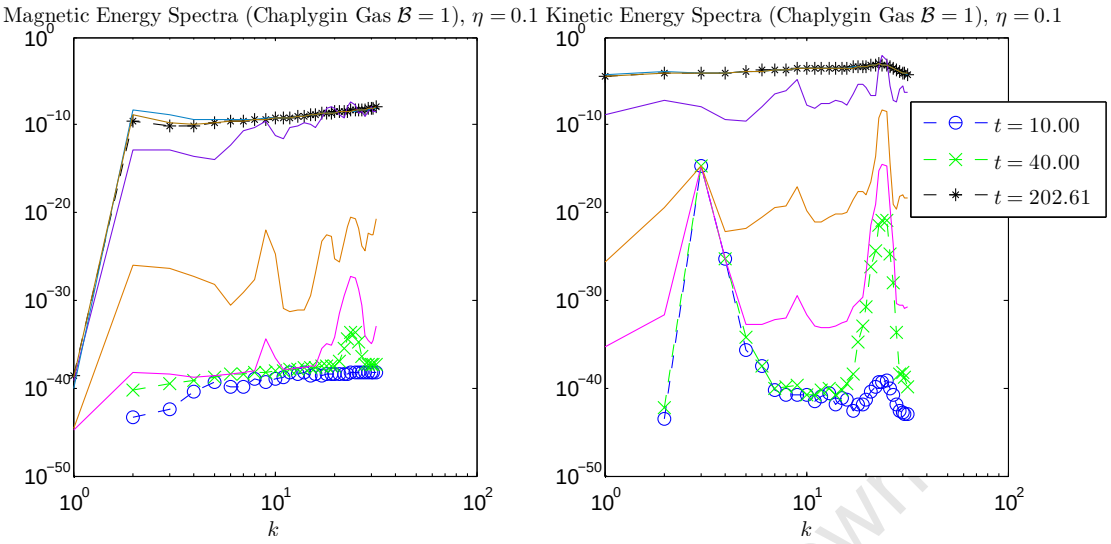

Figure 5.15: Magnetic and kinetic energy spectra corresponding to magnetogenesis run 1C1. During the kinematic phase, both spectra again appear to develop sharp peaks at the higher and lower wavenumbers, which gradually shrink as they grow. Magnetic spectral energy is highest at $t = 70$, from whence it starts decreasing slightly. Spectra for the remaining runs in this group show identical qualitative behaviour.

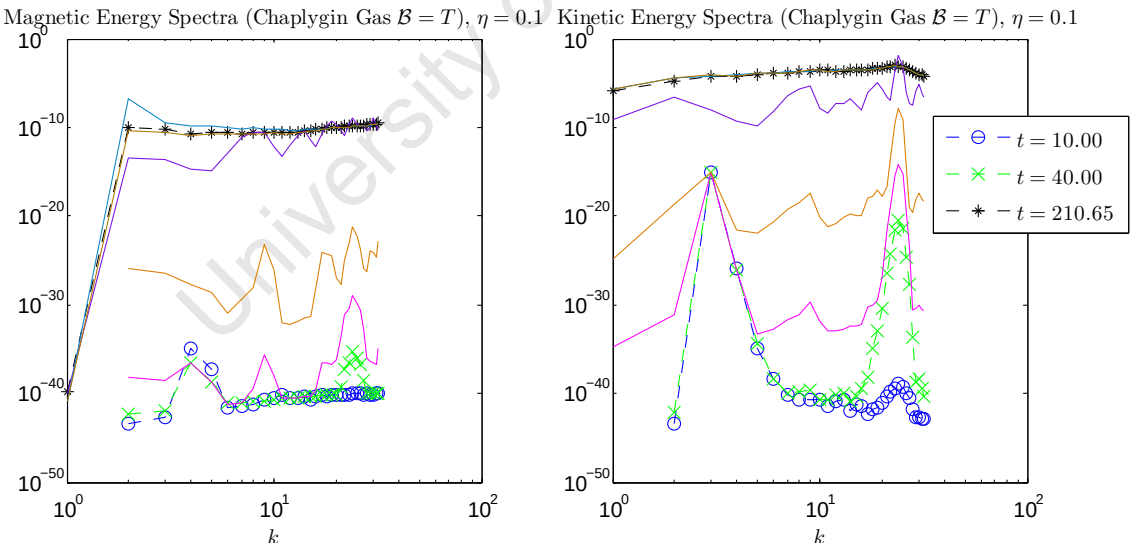

Figure 5.16: Magnetic and kinetic energy spectra corresponding to magnetogenesis run 2CT. During the kinematic phase, both spectra again appear to develop sharp peaks at the higher and lower wavenumbers, which gradually shrink as they grow. Magnetic spectral energy is highest at $t = 70$, from whence it starts decreasing slightly. Spectra for the remaining runs in this group show identical qualitative behaviour.

both spectra appears to grow in an "uneven" fashion. While the (twin) peaks displayed before the exponential growth phase appear to diminish, new peaks seem to form at the wavenumber $k = 10$ in all cases, suggesting that energy is being transferred here from the higher and lower wavenumbers. From the kinetic side, it is again apparent that as the $k = 24$ peak diminishes, the magnetic spectral energy at the same wavenumber appears to grow, possibly indicating once more that energy conversion is taking place, as expected.

In the final configuration, magnetic spectral energy appears to peak at wavenumber $k = 3$ for the Ideal Gas and $k = 32$ for the two Chaplygin gases, whilst kinetic spectral energy peaks at wavenumber $k = 24$ for all cases. Magnetic spectral energy appears to be greatest at the lower wavenumbers at time $t = 70$, which occurs around the time that B_{rms} reaches its global maximum. Beyond this time, the spectral energy at these wavenumbers decays toward the final, lower, configuration, whilst the spectral energy at the higher wavenumbers remains relatively constant at and after the time that the global maximum has been reached. Similar behaviour is observed for the kinetic energy spectrum, though the spectral energy change appears to be small across all wavenumbers.

Judging from the final configurations of the magnetic- and kinetic energy spectra for all of the EoS cases, it would appear that some sort of "steady state" has indeed been reached, as conversion rates between the two energies appear to become almost negligibly small. From this, it is expected that neither B_{rms} nor v_{rms} will grow in strength any longer, but will instead continue to persist at the same strengths to which they have grown. We may identify the exponential growth phase experienced by the magnetic field as some sort of "kinematic" phase with two distinct exponential growth rates (Figure 5.13 displays this clearly for all cases). Exponential decay after the global maximum is attributed to the effects of diffusion from the point-of-view of the equations, but may also be attributed to dissipation of magnetic energy by some means when considering the relevant energy spectra and the flow of energy in the system.

The results then suggest that dynamo action *may* be occurring only during the exponential growth phase. The dynamo in operation would most probably be kinematic and slow, having first relied on the effects of diffusion to damp the field strength after initial growth via the battery term. If this dynamo exists, then the decreasing conversion rate from kinetic- to magnetic energy would probably have caused it to saturate once the "kinematic" phase had ended, allowing the effects of diffusion to weaken the field strength slightly before letting the it enter the "steady-state". The behaviour observed in all of the spectra warrants further investigation using larger values of one or both of the viscosity and magnetic diffusion. The value of either of one of these parameters could possibly explain the reason for the "blowup" observed in run 3CT, as well as the absence of a dissipation range in all of the spectra presented.

5.8 Closing Points

In this chapter, we discussed the kinematic and small-scale dynamos, concentrating specifically on their roles in the amplification of magnetic fields.

The kinetic- and magnetic energy equations were introduced and their relationship to each other via the Lorentz force was briefly discussed. It was pointed out that kinetic energy is converted into magnetic energy via relevant physical processes specific to the system under consideration, and that an increase in magnetic energy leads to a decrease of kinetic energy within the system.

The Free Decay and Perfect Conductor limits of the Induction Equations were introduced. In the former case, it was shown that all magnetic fields suffer inevitable decay to zero on the resistive timescale, whilst in the latter case, it was shown that magnetic field lines are frozen into the fluid – an important property underlying the most basic workings of any dynamo. The magnetic Reynolds number was also introduced and its relationship to the onset of dynamo action was discussed. It was found that $R_m > 1$, nominally, for dynamo action to take place.

Restrictions on the types of fields that may be sustained by dynamo action, and the flows that may sustain them, were considered via the Cowling- and Zel'dovich Antidynamo theorems. In particular, it was noted that dynamo action can only occur in a flow that is fully three-dimensional, and that an axially-symmetric field cannot be sustained by an axially-symmetric flow.

We then introduced the Zel'dovich Stretch-Twist-Fold Dynamo, which describes how many dynamos are thought to operate. The dynamo algorithm was discussed in some detail, with mention also being made of some of its shortfalls. It was also noted that this dynamo could possibly be a qualitative example of a fast dynamo.

The kinematic dynamo problem was formally stated. Here, growing solutions are sought from the Induction Equations so that magnetic fields may be amplified and avoid resistive decay. The Roberts Cell Flow Dynamo was considered as a simple example of a kinematic dynamo that compliments both of the antidynamo theorems well. A formal definition of the flow used by this dynamo was given and the amplification mechanism was discussed.

Small-scale, non-helical, turbulent dynamos were introduced; the Kazantsev Dynamo was chosen as the example to be studied. It was found that this dynamo arose from splitting the magnetic- and velocity fields into mean-field and fluctuating parts, and then assuming that the fluctuating part of the velocity field could be represented by a turbulent velocity field that exhibited special statistical properties. The Kazantsev Equation was derived and it was shown that it may be reduced to a flavour of the non-linear Schrödinger Equation, from whence dynamo action could set on, provided that the

potential in the latter equation was sufficiently negative in some range. The Fourier Transform of the Kazantsev Equation was also considered, which provided a means of studying the temporal behaviour of the magnetic field by considering the behaviour of a magnetic energy spectrum rather than the field itself. This provided a simpler analytical alternative to solving the already complex Kazantsev Equation.

Saturation of the small-scale dynamo in the form of an artificial ambipolar drift term added to the total velocity field was discussed. It was found that, regardless of the assumptions of compressibility or incompressibility made on the new term, the dynamo will saturate – or stop working – due to the inclusion of an extra diffusion between the field and the flow, aside from the magnetic diffusion already present.

Finally, the results from the dynamo simulations conducted were presented and discussed. Dependence on the value of R_m for the onset of dynamo action was confirmed for the Roberts Flow Dynamo, non-helical forced turbulence and helical forced turbulence simulations. In the forced turbulence simulations, it was found that the magnetic field saturated after a given amount of time if dynamo action set in and that magnetic fields formed via helical forced turbulence were much stronger than their non-helical forced turbulence counterparts. The importance of a helical forcing function for the amplification of magnetic fields was also demonstrated and it was found that the value of the critical R_m was lowered greatly when a helical forcing function was used, as opposed to a non-helical forcing function. The section was closed by re-examining the behaviour observed in the evolution of B_{rms} in the magnetogenesis runs. Conversion of kinetic energy to magnetic energy was suggested by inspection of the relevant energy spectra, though this energy conversion rate appeared to decrease after the global maximum of B_{rms} was attained at the end of its exponential growth phase. It was concluded that kinematic dynamo action had caused the exponential growth phase, and that the field had indeed probably reached a "steady state", due to the decreasing rate of conversion of kinetic energy to magnetic energy.

Chapter 6

The Last Conclusion

Sì, Principessa, ascoltami!
Tu, che di gel sei cinta,
da tanta fiamma vinta
lamerai anche tu!
Prima di questa aurora,
io chiudo stanca gli occhi,
perché egli vinca ancora...
Per non vederlo più!

— Liù, *Turandot*, G. Puccini (1858 – 1924)

6.1 Final Closing Points

As we have already concluded each chapter in some detail previously, we present in the following a brief summary of the most important points covered in the preceding chapters of this dissertation.

6.1.1 Dissertation, Redux

In this dissertation we addressed the problems of generating magnetic fields from absolute zero initial conditions and the dependence of the onset of dynamo action on the magnetic Reynolds- and Prandtl numbers intrinsic to the system under consideration. These were investigated by means of numerical simulations done using the PENCIL CODE, which is a high-order finite difference magnetohydrodynamical code.

Basic results of the theories of Fluid Dynamics and Electromagnetism were recovered in order to build a set of Magnetohydrodynamical equations which were used in the simulations conducted for this dissertation. It was noted that the equations of Magnetohydrodynamics could be derived by the marriage of the equations of Fluid Dynamics to those of Electrodynamics, but are formally derived from the Boltzmann Equation of Particle Kinetic Theory. The concepts of kinetic and magnetic helicity, as well as several important points in the Theory of Turbulence were also discussed.

The PENCIL CODE was introduced and short discussions of the use of physical units to interpret simulation results and the numerical methods employed by the code were presented. This portion of the dissertation also saw the first round of numerical simulations presented. In particular, simulations conducted on the free decay limit of the Induction Equations demonstrated that any initial field given would eventually decay over time, regardless of its amplitude. It was found that changing the value of the magnetic diffusivity strongly affected the initial field's decay rate.

The General Ohm's Law was derived from the two-fluid approximation of the equations of motion for a fluid consisting of two distinct particle species. It was noted how the thermal battery term arose as a consequence of the approximation used. The Chaplygin Gas, defined by an exotic equation of state, was also introduced and discussed briefly. The Induction Equations with the thermal battery term were then derived. Simulations focussed on magnetogenesis via the thermal battery term, alternately using the Ideal- and Chaplygin Gas equations of state to model the relationship between pressure and density. Temporal evolution behaviour and strengths of the resulting magnetic fields were assessed and commented on.

Dynamo theory was considered in some detail. The equations of magnetic- and kinetic energy which

describe the energetics involved in the dynamo process were derived. Also considered in some detail were the Perfect Conductor and Free Decay limits of the Induction Equations, the origins of the magnetic Reynolds number and the antidynamo theorems. The Zel'dovich Stretch-Twist-Fold dynamo and the Roberts Flow Dynamo were also discussed as examples of fast and kinematic dynamos respectively. The small-scale, turbulent dynamo and Kazantsev Theory were discussed, and it was shown how the Kazantsev Equation may be reduced to a non-linear Schrödinger Equation in order to characterise the onset of dynamo action. Fourier analysis of the Kazantsev Equation was also discussed in some detail, demonstrating an alternative method of studying the temporal evolution and behaviour of the magnetic field. Simulations focussed on studying the onset of dynamo action when the magnetic Reynolds- and Prandtl numbers are varied; the Roberts Flow dynamo was simulated for the kinematic case and dynamo action due to non-helical and helical forcing function was investigated for the remaining simulations. Finally, the possibility of dynamo action in the magnetogenesis simulations was investigated.

6.1.2 Extensions to Future Work

The fields of Magnetogenesis and Turbulent Dynamo Theory are all as yet extremely vast, leaving much to be studied: in this dissertation, we have merely "scratched the surface" of both of these fields. Further work in the field of Magnetogenesis would potentially include a departure from the simple thermal battery to consider other mechanisms that allow for the generation of magnetic fields from absolute zero initial conditions. Magnetogenesis using the scale-factor dependent form of the Induction Equations could also be considered as a link to studying the origins of magnetic fields on cosmological scales.

Further work in the field of Dynamo Theory would involve a departure from small-scale dynamos, into the more complex large-scale dynamos. These dynamos obey the so-called **mean field** evolution equations, which describe the temporal evolution of the mean field components of the magnetic- and velocity fields. The effects of magnetic helicity on the evolution of the magnetic field and the efficiency of dynamo action would also serve as interesting compliments to study of both the large- and small-scale dynamos. Consideration can also be given to other terms that enter the Induction Equations via the General Ohm's Law and their effects on the evolution of the magnetic field can be assessed; an example of this would be the term describing Hall's Effect, which was previously neglected in Chapter 4. Interaction of the large- and small-scale dynamos via the inverse cascade of magnetic energy can also be investigated. Finally, comparisons of results obtained by the theory of Magnetohydrodynamics may also be made to other theories, for example, Hall Magnetohydrodynamics (Hall MHD) or Electron Magnetohydrodynamics (eMHD).

★

6.2 Acknowledgements

I firstly wish to acknowledge my supervisor, Dr Bob Osano, for his constant support and advice for the duration of my master's studies – I could not have asked for a better mentor. I also wish to acknowledge Prof. Axel Brandenburg of the Nordic Institute for Theoretical Physics (NORDITA) for his assistance in adapting the PENCIL CODE to include the use of a thermal battery term, as well as advice in regards to questions I had asked. My gratitude also goes to the rest of the members of the PENCIL CODE discussion group, especially Mr Philippe-A. Bourdin, for their advice and input in regards to questions I had asked. My acknowledgements also go to Dr Henri Laurie and Dr Nora Alexeeva for helpful discussions on the implementations of various numerical methods. My thanks also go to Dr Obinna Umeh and Mr Sean February for their useful advice on various Cosmology-related concepts. Lastly, I also wish to convey my acknowledgement and thanks to Mr Jaco Brandsen for helpful discussions on the Theory of Turbulence and Computational Fluid Dynamics. Finally, I would also like to acknowledge the funding support, in the form of a scholarship, from the National Research Foundation (NRF) of South Africa, administered by the Postgraduate Funding Office of the University of Cape Town.

★

Bibliography

[1] BABCOCK, H. W. The Topology of the Sun's Magnetic Field and the 22-Year Cycle. *Astrophysical Journal 133* (1961).

[2] BARASHENKOV, I. V. Advanced Mathematical Methods II, 2011. Unpublished lecture notes.

[3] BATCHELOR, G. K. On the Spontaneous Magnetic Field in a Conducting Liquid in Turbulent Motion. *Proceedings of the Royal Society of London. Series A, Mathematical and Physical Sciences 201*, 1066 (1950).

[4] BENTO, M. C., BERTOLAMI, O., AND SEN, A. A. Generalized Chaplygin Gas, Accelerated Expansion, and Dark-Energy-Matter Unification. *Physical Review D 66*, 4 (2002). arXiv:gr-qc/0202064.

[5] BIERMANN, L. Über den Ursprung der Magnetfelder auf Sternen und im interstellaren Raum. *Zeitschrift Naturforschung Teil A 5* (1950).

[6] BILIĆ, N., TUPPER, G. B., AND VIOLLIER, R. D. Cosmological Tachyon Condensation. *Physical Review D 80*, 2 (2009). arXiv:gr-qc/0809.0375.

[7] BRANDENBURG, A. *Computational Aspects of Astrophysical MHD and Turbulence*. 2003.

[8] BRANDENBURG, A., DOBLER, W., ET AL. The PENCIL Code: A High-Order MPI code for MHD Turbulence; User's and Reference Manual, 2013. Obtained at the following URL: `http://www.nordita.org/pencil-code/doc/manual.pdf`.

[9] BRANDENBURG, A., JENNINGS, R. L., NORDLUND, Å., RIEUTORD, M., STEIN, R. F., AND TUOMINEN, I. Magnetic Structures in a Dynamo Simulation. *Journal of Fluid Mechanics 306* (1996).

[10] BRANDENBURG, A., AND SUBRAMANIAN, K. Astrophysical Magnetic Fields and Nonlinear Dynamo Theory. *Physics Reports 417* (2005).

[11] CHAPLYGIN, S. On Gas Jets. *Scientific Memoirs, Moscow University 1*, 1 (1904). Also, NACA Technical Memorandum 1063 (1944). URL: http://archive.org/details/nasa_techdoc_20030066368.

[12] CHARBONNEAU, P. Decay and amplification of magnetic fields. In *Solar and Stellar Dynamos*, vol. 39 of *Saas-Fee Advanced Courses*. Springer Berlin Heidelberg, 2013.

[13] CONTOPOULOS, I., KAZANAS, D., AND CHRISTODOULOU, D. M. The Cosmic Battery Revisited. *Astrophysical Journal 652* (2006). arXiv:astro-ph/0608701.

[14] COWLING, T. G. The Magnetic Field of Sunspots. *Monthly Notices of the Royal Astronomical Society 94* (1933).

[15] DOI, K., AND SUSA, H. Generation of a Seed Magnetic Field around First Stars: The Biermann Battery Effect. *Astrophysical Journal 741* (2011). arXiv:astro-ph.CO/1108.4504.

[16] FRESCURA, F. Astrophysical Fluid Mechanics, 2011. Unpublished lecture notes.

[17] GNEDIN, N. Y., FERRARA, A., AND ZWEIBEL, E. G. Generation of the Primordial Magnetic Fields during Cosmological Reionization. *Astrophysical Journal 539* (2000). arXiv:astro-ph/0001066.

[18] GOEDBLOED, J. P., AND POEDTS, S. *Principles of Magnetohydrodynamics, with Applications to Laboratory and Astrophysical Plasmas*. Cambridge University Press, 2004, ch. 1-4.

[19] GORINI, V., KAMENSHCHIK, A., MOSCHELLA, U., AND PASQUIER, V. The Chaplygin Gas as a Model for Dark Energy. *"ArXiv Astrophysics e-prints"* (2004). arXiv:gr-qc/0403062.

[20] GRIFFITHS, D. J. *Introduction to Electrodynamics*, 3 ed. Benjamin Cummings, 1998.

[21] HANAYAMA, H., TAKAHASHI, K., KOTAKE, K., OGURI, M., ICHIKI, K., AND OHNO, H. Biermann Mechanism in Primordial Supernova Remnants and Seed Magnetic Fields. *Astronomische Nachrichten 327* (2006). arXiv:astro-ph/0510855.

[22] HAUGEN, N. E., BRANDENBURG, A., AND DOBLER, W. Simulations of Nonhelical Hydromagnetic Turbulence. *Physical Review E 70*, 1 (2004). arXiv:astro-ph/0307059.

[23] HERZENBERG, A. Geomagnetic Dynamos. *Royal Society of London Philosophical Transactions Series A 250* (1958).

[24] JACKSON, J. D. *Classical Electrodynamics*, 3 ed. Wiley, 1998.

[25] JONES, C. A. Dynamo theory, 2007. Unpublished. Obtained at the following URL: http://www1.maths.leeds.ac.uk/~cajones/LesHouches.html.

[26] KAHNIASHVILI, T., BRANDENBURG, A., CAMPANELLI, L., RATRA, B., AND TEVZADZE, A. G. Evolution of inflation-generated magnetic field through phase transitions. *Physical Review D 86*, 10 (2012). arXiv:astro-ph.CO/1206.2428.

[27] KAMENSHCHIK, A., MOSCHELLA, U., AND PASQUIER, V. An Alternative to Quintessence. *Physics Letters B 511* (2001). arXiv:gr-qc/0103004.

[28] KAZANTSEV, A. P. Enhancement of a Magnetic Field by a Conducting Fluid. *Soviet Journal of Experimental and Theoretical Physics 26* (1968).

[29] KRAICHNAN, R. H., AND NAGARAJAN, S. Growth of Turbulent Magnetic Fields. *Physics of Fluids 10* (1967).

[30] KULSRUD, R. M., AND ANDERSON, S. W. The Spectrum of Random Magnetic Fields in the Mean Field Dynamo Theory of the Galactic Magnetic Field. *Astrophysical Journal 396* (1992).

[31] KULSRUD, R. M., CEN, R., OSTRIKER, J. P., AND RYU, D. The Protogalactic Origin for Cosmic Magnetic Fields. *Astrophysical Journal 480* (1997). arXiv:astro-ph/9607141.

[32] LANDAU, L. D., AND LIFSHITZ, E. M. *Fluid Mechanics, Second Edition: Volume 6 (Course of Theoretical Physics)*, 2 ed. Course of theoretical physics by L. D. Landau and E. M. Lifshitz, Vol. 6. Butterworth-Heinemann, 1987.

[33] LEIGHTON, R. B. A Magneto-Kinematic Model of the Solar Cycle. *Astrophysical Journal 156* (1969).

[34] LELE, S. K. Compact Finite Difference Schemes with Spectral-like Resolution. *Journal of Computational Physics 103* (1992).

[35] LOMAX, H., PULLIAM, T. H., AND ZINGG, D. W. *Fundamentals of Computational Fluid Dynamics*. Springer Verlag, 1999.

[36] MARON, J., AND BLACKMAN, E. G. Effect of Fractional Kinetic Helicity on Turbulent Magnetic Dynamo Spectra. *Astrophysical Journal Letters 566* (2002).

[37] MESTEL, L., AND ROXBURGH, I. W. On the Thermal Generation of Toroidal Magnetic Fields in Rotating Stars. *Astrophysical Journal 136* (1962).

[38] MOFFATT, H. K. *Magnetic Field Generation in Electrically Conducting Fluids*. Cambridge University Press, 1978, ch. 6.

[39] MOLCHANOV, S. A., RUZMAĬKIN, A. A., AND SOKOLOV, D. D. The Kinematic Dynamo in a Random Flux. *Uspekhi Fizicheskikh Nauk 145* (1985).

[40] MOLCHANOV, S. A., RUZMAĬKIN, A. A., AND SOKOLOV, D. D. Short-correlated Random Flow as a Fast Dynamo. *Soviet Physics Doklady 32* (1987).

[41] PARKER, E. N. Hydromagnetic Dynamo Models. *Astrophysical Journal 122* (1955).

[42] POPE, S. B. *Turbulent Flows*. Cambridge University Press, 2000, ch. 6.

[43] ROBERTS, G. O. Spatially Periodic Dynamos. *Philosophical Transactions of the Royal Society of London. Series A, Mathematical and Physical Sciences 266*, 1179 (1970).

[44] ROBERTS, G. O. Dynamo Action of Fluid Motions with Two-Dimensional Periodicity. *Philosophical Transactions of the Royal Society of London. Series A, Mathematical and Physical Sciences 271*, 1216 (1972).

[45] SCHEKOCHIHIN, A. A., COWLEY, S. C., HAMMETT, G. W., MARON, J. L., AND MCWILLIAMS, J. C. A Model of Nonlinear Evolution and Saturation of the Turbulent MHD Dynamo. *New Journal of Physics 4* (2002). arXiv:astro-ph/0207503.

[46] SCHEKOCHIHIN, A. A., COWLEY, S. C., HAMMETT, G. W., MARON, J. L., AND MCWILLIAMS, J. C. The Nonlinear Small-scale Dynamo and Isotropic MHD Turbulence. *ArXiv Astrophysics e-prints* (2002). arXiv:astro-ph/0207151.

[47] SCHEKOCHIHIN, A. A., HAUGEN, N. E. L., BRANDENBURG, A., COWLEY, S. C., MARON, J. L., AND MCWILLIAMS, J. C. The Onset of a Small-scale Turbulent Dynamo at Low Magnetic Prandtl Numbers. *Astrophysical Journal Letters 625* (2005). arXiv:astro-ph/0412594.

[48] SCHEKOCHIHIN, A. A., MARON, J. L., COWLEY, S. C., AND MCWILLIAMS, J. C. The Small-scale Structure of Magnetohydrodynamic Turbulence with Large Magnetic Prandtl Numbers. *Astrophysical Journal 576* (2002). arXiv:astro-ph/0203219.

[49] SCHLEICHER, D. R. G., LATIF, M., SCHOBER, J., SCHMIDT, W., BOVINO, S., FEDERRATH, C., NIEMEYER, J., BANERJEE, R., AND KLESSEN, R. S. Magnetic Fields During High Redshift Structure Formation. *ArXiv Astrophysics e-prints* (2012). arXiv:astro-ph.CO/1211.4356.

[50] SCHOBER, J., SCHLEICHER, D., FEDERRATH, C., GLOVER, S., KLESSEN, R. S., AND BANERJEE, R. The Small-scale Dynamo and Non-ideal Magnetohydrodynamics in Primordial Star Formation. *Astrophysical Journal 754* (2012). arXiv:astro-ph.CO/1204.0658.

[51] SPITZER, L. *The Physics of Fully Ionized Gases*. Interscience Publishers, Inc., 1956, ch. 2.

[52] SUBRAMANIAN, K. Dynamics of Fluctuating Magnetic Fields in Turbulent Dynamos Incorporating Ambipolar Drifts. *ArXiv Astrophysics e-prints* (1997). arXiv:astro-ph/9708216.

[53] SUBRAMANIAN, K. Unified Treatment of Small- and Large-Scale Dynamos in Helical Turbulence. *Physical Review Letters 83* (1999). arXiv:astro-ph/9908280.

[54] SUBRAMANIAN, K. Hyperdiffusion in Nonlinear Large- and Small-Scale Turbulent Dynamos. *Physical Review Letters 90*, 24 (2003). arXiv:astro-ph/0303015.

[55] SUBRAMANIAN, K. Magnetizing the universe. *ArXiv Astrophysics e-prints* (2008).

[56] SUBRAMANIAN, K., NARASIMHA, D., AND CHITRE, S. M. Thermal Generation of Cosmological Seed Magnetic Fields in Ionization Fronts. *Monthly Notices of the Royal Astronomical Society 271* (1994).

[57] VAINSHTEIN, S. I., AND ZEL'DOVICH, YA. B. Origin of Magnetic Fields in Astrophysics (Turbulent "Dynamo" Mechanisms). *Physics-Uspekhi 15*, 2 (1972).

[58] WIDROW, L. M. Origin of Galactic and Extragalactic Magnetic Fields. *Reviews of Modern Physics 74* (2002). arXiv:astro-ph/0207240.

[59] WILLIAMSON, J. H. Low-Storage Runge-Kutta Schemes. *Journal of Computational Physics 35* (1980).

[60] ZEL'DOVICH, YA. B. The Magnetic Field in the Two-dimensional Motion of a Conducting Turbulent Fluid. *Zhurnal Eksperimentalnoi i Teoreticheskoi Fiziki 31* (1956).

[61] ZEL'DOVICH, YA. B., AND RUZMAĬKIN, A. A. Magnetic Field of a Conducting Fluid in Two-dimensional Motion. *Zhurnal Eksperimentalnoi i Teoreticheskoi Fiziki 78* (1980).

List of Figures

List of Tables

Listings

Appendix A

Other Introductory Results, Revisited

If you look at any great fashion photograph out of context, it will tell you just as much about what's going on in the world as a headline in The New York Times.

— Anna Wintour (1949 –)

In this Appendix we present some additional introductory results which are meant to compliment those already presented in Section 2.1 of Chapter 2. The reader is reminded once more that all of the following derivations are done within a non-relativistic frame-of-reference. Note also that results presented in this section have been based largely on reference [16] and, to some extent, reference [32].

A.1 Deriving Euler's Equation for Fluid Flow

We now turn to the derivation of Euler's Equation for fluid-flow. Some assumptions must be taken into account [16]:

1. The fluid-flow is frictionless.
2. The fluid-flow is inviscid.
3. The fluid obeys the Equation of Motion of an *ideal fluid*.

A.1.1 The Equation of Motion for a General Fluid

Consider a small fluid element in the Lagrangian co-ordinate system. Suppose that it has a mass δm and occupies a volume δV at a certain time t. We may then express δm as

$$\delta m = \varrho \delta V, \tag{A.1}$$

where ϱ is the fluid density. To the first order in its Taylor Series expansion, the contact force δF^i_{cont} on the fluid element is given by

$$\delta F^i_{\text{cont}} = \partial_j \sigma^{ij} \delta V, \tag{A.2}$$

using the shorthand notation $\partial_j \equiv \partial/\partial x_j$, and the total gravitational force on the element is given by

$$\delta F^i_{\text{grav}} = \delta m g^i. \tag{A.3}$$

And so,

$$\delta F^i_{\text{tot}} = \delta F^i_{\text{grav}} + \delta F^i_{\text{cont}} = \delta m a^i \tag{A.4}$$

by Newton's Second Law of Motion. Noting that the acceleration field is in fact only the rate-of-change of the velocity field, noting the mass-density relationship established in Expression (A.1), and bearing in mind the Superposition Principle, we may then express Expression (A.4) as

$$\delta m \frac{\mathrm{D}v^i}{\mathrm{D}t} = \delta m g^i + \partial_j \sigma^{ij} \delta V. \tag{A.5}$$

Simplification yields our first result: the **Equation of Motion for a General Fluid**, given as

$$\boxed{\varrho \frac{\mathrm{D}v^i}{\mathrm{D}t} = \partial_j \sigma^{ij} + \varrho g^i + \varrho f^i,} \tag{A.6}$$

where the term ϱf^i is included to emphasise that other forces, which may be present, have not been considered in the derivation, but can be included without loss of generality. In terms of force-per-unit-mass, Equations (A.6) read

$$\boxed{\frac{\mathrm{D}v^i}{\mathrm{D}t} = \frac{1}{\varrho}\partial_j \sigma^{ij} + g^i + f^i,} \tag{A.7}$$

and their vector version,

$$\boxed{\frac{\mathrm{D}\mathbf{v}}{\mathrm{D}t} = \frac{1}{\varrho}\nabla \cdot \tilde{\boldsymbol{\sigma}} + \mathbf{g} + \mathbf{f}.} \tag{A.8}$$

A.1.2 Euler's Equation

Before, we stated that in deriving Euler's Equation, we would assume that the fluid-flow under consideration is frictionless. Mathematically, this would correspond to making some special demands on the stress tensor, σ^{ij}.

Generally, we would write this tensor as

$$\sigma^{ij} = -p\delta^{ij} + \tau^{ij}, \tag{A.9}$$

where the first tensor term involves the scalar pressure, p, and Krönecker Delta Symbol and the second tensor term, τ^{ij}, represents the action of viscosity on the fluid. These terms are discussed in some more detail later on. The assumption of an inviscid fluid allows us to set $\tau^{ij} = 0$ immediately, leaving behind a stress tensor of the form

$$\sigma^{ij} = -p\delta^{ij}. \tag{A.10}$$

Substituting this form of the stress tensor into Equations (A.7) and simplifying the result gives the tensorial form of **Euler's Equation**:

$$\boxed{\frac{\mathrm{D}v^i}{\mathrm{D}t} = -\frac{1}{\varrho}\partial^i p + g^i + f^i.} \tag{A.11}$$

Alternatively, this equation may be written as

$$\boxed{\frac{\mathrm{D}\mathbf{v}}{\mathrm{D}t} = -\frac{1}{\varrho}\nabla p + \mathbf{g} + \mathbf{f}.} \tag{A.12}$$

As both of these forms are equivalent, we shall make use of them interchangeably.

It is important to note that Euler's Equation is satisfied by ideal fluids, as no real fluids are completely inviscid. In our derivation, we have only considered collisional and gravitational forces acting on the fluid elements, only introducing the presence of other "external" forces via a unified term $\mathbf{f}$ at the very end. This would not, and should not, change the derivation if they were to be included at the offset; we only excluded them for simplicity.

A.2 More on the Stress Tensor, σ^{ij}

The stress tensor, σ^{ij} can generally be written as the sum of two constituent tensors which arise from physics. The first part concerns the *average velocity* of the fluid particles; that is, $\mathbf{v}(\mathbf{x}, t)$, the velocity field of the continuum that the fluid is described in. The second part concerns the *difference between the velocity of any given fluid particle and the fluid element's average velocity* – the so-called **thermal velocity**. This velocity is reflected implicitly in the hydrostatic pressure and fluid temperature parameters in the continuum formalism.

When a fluid is at rest, hydrostatic pressure is present as a stress. In physical terms, we would say that the force-per-unit-area (i.e. the *pressure*, p) that is exerted by the fluid, on a surface, is always both perpendicular to the surface *and* independent of the surface's orientation or attitude. In mathematical terms, we would say the following:

$$\Sigma^i = \sigma^{ij} n_j, \tag{A.13}$$

where n_j denotes a unit normal to the surface. This is true for *all* unit normals n^i. Also, note that

$$\begin{aligned} \Sigma^i &= -p\delta^{ij} n_j \\ &= -pn^i. \\ \Rightarrow \sigma^{ij} &= -p\delta^{ij}, \end{aligned} \tag{A.14}$$

where the minus-sign tells us that this force acts in the direction opposite to the surface normal (i.e. it is a compressive force). Thus, σ^{ij} has the form given by equation (A.14) for a fluid **at rest**.

Since the fluid molecules are perpetually in **thermal motion**, regardless of whether the fluid is actually in motion or not, hydrostatic pressure develops as a result of this. When the fluid is in motion, additional stresses may develop as a result of viscosity. Taking this into account, we may then express the stress tensor as the sum of two constituent parts as before:

$$\sigma^{ij} = -p\delta^{ij} + \tau^{ij}.$$

The first term is due to the aforementioned hydrostatic pressure and the thermal motion of the fluid particles. It is *always* present, regardless of whether or not the fluid is in motion or if the velocity field has gradients. The second term is due to viscous stresses present in the fluid and is *only* present (i.e. non-zero) when the velocity field has gradients.

A.2.1 Newtonian Fluids and their General Equation of Motion

We turn our consideration now to τ^{ij}, the **viscous stress tensor**. Note again that this tensor is only non-zero when the velocity field has gradients. The gradients present in the velocity field directly result in deformations in the fluid. Considering the case where these deformations rates are small, we may expand τ^{ij} in a Taylor Series:

$$\tau^{ij} = \tau^{ij}(0) + \frac{\partial \tau^{ij}}{\partial e_{mn}}(0)e_{mn} + \frac{1}{2}\frac{\partial^2 \tau^{ij}}{\partial e_{mn} e_{rs}}(0)e_{mn}e_{rs} + \ldots, \tag{A.15}$$

where we have asserted that $\tau^{ij} = \tau^{ij}(e_{11}, e_{12}, \ldots, e_{33})$ in general (here, e_{ij}'s are the strain rates), and that the first term goes to zero immediately due to the viscous stress vanishing when the deformation rate vanishes. As the derivatives of τ^{ij} evaluated at zero are simply constants, we may then write the expansion above as

$$\tau^{ij} = Y^{ijmn}e_{mn} + \frac{1}{2}Y^{ijmnrs}e_{mn}e_{rs} + \ldots. \tag{A.16}$$

For our purposes, we shall stop at the first-order term, which is the defining property of **Newtonian Fluids**. Thus,

$$\boxed{\tau^{ij} = Y^{ijrs}e_{rs};\ \ e_{rs} = \frac{1}{2}(\partial_r v_s + \partial_s v_r).} \tag{A.17}$$

It can be shown that Y^{ijrs} is symmetric on the indices s and r and also has the form

$$Y^{ijrs} = \alpha g^{ij}g^{rs} + \beta\left(g^{ir}g^{js} + g^{is}g^{jr}\right), \tag{A.18}$$

where g^{ij} and its other counterparts represent the **metric tensor**, and α and β are coefficients which shall be determined shortly. But how shall we interpret them? Consider the following application of the defining property of a Newtonian Fluid:

$$\begin{aligned}
\tau^{ij} &= Y^{ijrs}e_{rs} \\
&= \frac{1}{2}\left[\alpha g^{ij}g^{rs} + \beta\left(g^{ir}g^{js} + g^{is}g^{jr}\right)\right](\partial_r v_s + \partial_s v_r) \\
&= \frac{1}{2}\alpha g^{ij}\left(g^{rs}\partial_r v_s + g^{rs}\partial_s v_r\right) + \frac{1}{2}\beta g^{ij}\left(g^{ir}g^{js} + g^{is}g^{jr}\right)\left(g^{rs}\partial_r v_s + g^{rs}\partial_s v_r\right) \\
&= \alpha\left(\nabla\cdot\mathbf{v}\right)g^{ij} + \beta\left(\partial^i v^j + \partial^j v^i\right).
\end{aligned} \tag{A.19}$$

Some more work tells us that $\beta = \mu$, the **coefficient of viscosity**, and that $\alpha = \lambda$, the **coefficient of bulk viscosity**. We may thus finally express the viscous stress tensor as

$$\boxed{\tau^{ij} = \lambda\left(\nabla\cdot\mathbf{v}\right)g^{ij} + \mu\left(\partial^i v^j + \partial^j v^i\right),} \tag{A.20}$$

and the stress tensor for a Newtonian Fluid then follows as

$$\boxed{\sigma^{ij} = -p\delta^{ij} + \lambda\left(\nabla\cdot\mathbf{v}\right)g^{ij} + \mu\left(\partial^i v^j + \partial^j v^i\right).} \tag{A.21}$$

Recall the definition of the Equation of Motion for a General Fluid:

$$\varrho\frac{\mathrm{D}v^i}{\mathrm{D}t} = \partial_j\sigma^{ij} + \varrho g^i + \varrho f^i.$$

Substituting into the above equation the expression for the stress tensor given by Expression (A.21), and doing the differentiation, yields us our final result for this section:

$$\boxed{\varrho\frac{\mathrm{D}v^i}{\mathrm{D}t} = -\partial^i p + (\lambda+\mu)\partial^i\left(\nabla\cdot\mathbf{v}\right) + \mu\nabla^2 v^i + \left(\partial^i\lambda\right)\left(\nabla\cdot\mathbf{v}\right) + \left(\partial_j\mu\right)\left(\partial^i v^j + \partial^j v^i\right) + \varrho g^i + \varrho f^i,} \tag{A.22}$$

which is the **Equation of Motion for an Isotropic Newtonian Fluid**.